

## **THE HIGH-THROUGHPUT MICRO-ADHESION TESTER**

THE HIGH-THROUGHPUT MICRO-ADHESION TESTER

By

ANDREA COLLIS, B. ENG

A Thesis

Submitted to the School of Graduate Studies

in Partial Fulfilment of the Requirements

for the Degree

Master of Applied Science

McMaster University

© Copyright by Andrea Collis, February 2005

**MASTER OF APPLIED SCIENCE(2005)**  
**(Chemical Engineering)**

**McMaster University**  
**Hamilton, Ontario**

**TITLE:           The High-Throughput Micro-Adhesion Tester**

**AUTHOR:       Andrea Collis, B. Eng (McMaster University)**

**SUPERVISOR: Dr. R. H. Pelton and Dr. K. Dalnoki-Veress**

**NUMBER OF PAGES:     x, 102**

## ABSTRACT

The high-throughput micro-adhesion tester (HMAT) was constructed to test the adhesive strength of polymers. The design criteria included the ability to rapidly test many different samples in a serial format, and a probe design that would compliment this objective by being easy to place and pull from the samples and easy to mass produce. The HMAT was able to perform 48 adhesion tests at about 30s per test for a total of 24 min. The final probes were made from a capillary tube with a small metal cap on the top for ease of lifting. They are easy to make and easy to place and pull from the custom probe box. The probe box was designed to hold the probes upright while the polymer is drying and during the test while not interfering with the test itself. Tests on PDMS show reasonable repeatability with the standard deviation being about 20% of the mean value. Since the HMAT is meant to be used for primary screening, the accuracy of the measurements is not as critical as it would be for later tests.

## ACKNOWLEDGMENTS

I would like to start by thanking Dr. Pelton and Dr. Dalnoki-Veress for all of their guidance and support without which this thesis would not have been possible. Paul Gatt was also invaluable for building, and in some cases, designing parts. He was very helpful and patient even when I would come into the workshop for the umpteenth time to get him to make ‘just one small change’. I would also like to thank Adam for helping me get all of the hardware connected properly as well as Mike, Andrew, Marie-Josee, Jess, John, Joanna, and Michelle for their friendship throughout this project. Thanks to the Chemical Engineering Department. And finally, thanks to my family and Dave for their unwavering support.

ABSTRACT	iii
ACKNOWLEDGEMENTS	iv
TABLE OF CONTENTS	v
LIST OF FIGURES	vii
LIST OF TABLES	x
1 Adhesion	1
1.1 Molecular Adhesion	3
1.2 Theories	4
1.2.1 Hertz Theory	4
1.2.2 JKR Theory	5
1.3 Adhesion on Larger Scales	8
2 High Throughput Materials	11
2.1 The value of High Throughput Screening	11
2.2 How High Throughput Screening is implemented	11
2.3 A Brief History	12
2.4 Current Uses	13
2.5 Sample Preparation	14
2.5.1 Rapid Serial	14
2.5.2 Simultaneous Library	15
2.6 Testing	16
2.6.1 Rapid Serial	16
2.6.2 Simultaneous Testing	18
2.7 Data Collection	19
3 Experimental	20
3.1 Objective	20
3.2 Materials	21
3.3 PVAm Preparation	21
3.4 Hardware	22
3.4.1 The Instron	22
3.4.2 Parts List	23
3.4.3 Calibration of Load Cell	24
3.4.4 Software	25
3.5 Procedure	25
4 Results and Discussion	26
4.1 Preliminary Experiments	26
4.1.1 Using PVA	26
4.1.2 Bead Punching Tests	30
4.1.3 Using PDMS	32
4.2 Experiments on the High-Throughput Micro-Adhesion Tester	37
4.2.1 The High-Throughput Micro-Adhesion Tester (HMAT)	37
4.2.2 The Glass Rods	42

4.2.3 The capillary Tubes	49
4.2.4 The final tests	51
5 Conclusion	53
APPENDIX A – LabView Program	56
APPENDIX B.1 – Probes	96
APPENDIX B.2 – Hooks	100

## List of Figures

Figure 1 – A schematic demonstrating surface tension	1
Figure 2 – The separation of two different materials	2
Figure 3 – A schematic of the geometry used in the Hertz equation <sup>3</sup>	4
Figure 4 – The Hertz equation over a large range of $F_5$	5
Figure 5 – A schematic of the Hertzian and JKR contact area <sup>4</sup>	6
Figure 6 – The energy balance approach. (a) shows the load-displacement relationship for the contacting samples, and (b) shows the stress distribution corresponding to the points in (a) <sup>4</sup>	7
Figure 7 – The stress-strain curves for elastic and brittle failure	10
Figure 8 – A typical scheme for combinatorial research <sup>7</sup>	12
Figure 9 – A set of masks that could be used in a quaternary masking scheme <sup>12</sup>	15
Figure 10 – An example of a split synthesis procedure. The number of compounds produced from this particular scheme would be 144. <sup>20</sup>	16
Figure 11 – The experimental set-up of Sormana and Meredith’s impact apparatus. <sup>21</sup>	17
Figure 12 – The current experimental set-up of the NIST MCAT test bed. <sup>24</sup>	19
Figure 13 – A schematic of the Instron Universal tester	22
Figure 14 – The 96 well plate secured to the Instron. Here two well plates are used to hold the probes more upright, but the original configuration used only one well late.	23
Figure 15 – Calibration for the 100 g load cell	25
Figure 16 – The first tests done on the Instron using PVAm (a) at two different polymer concentrations and (b) different pull speeds. The experiments shown in graph (a) were done using 1 drop of solution and were pulled at 25 mm/min. The error bars represent the standard deviation of 7 and 10 samples for the 1 and 2 polymer concentrations solutions respectively. The experiments shown in graph (b) were done using 1 drop of 1 polymer concentrations solution.	28
Figure 17 – A schematic of (a) the bottom of a glass bead after a test, (b) a glass bead sitting in a well and (c) a picture of the bottom of a bead after it has been pulled. Because of the conical geometry of the wells, the polymer left a ‘ring’ of material.	29
Figure 18 – The second configuration on the Instron. The plate was turned upside-down and the glass beads were poked out from the bottom of the wells.	30
Figure 19 – The second tests done on the Instron using PVA (a) at two different polymer concentrations and (b) different pull speeds. The experiments shown in graph (a) were done using 1 drop of solution and were pushed at 25 mm/min. The error bars are the standard deviation of 4 and 8 samples for the 1 and 2 wt % solutions respectively. The experiments shown in graph (b) were done using 1 drop of 1 polymer concentrations solution. The error bars are the standard deviation of 4 samples for both data points.	31
Figure 20 – The next tests done on the Instron using PDMS (a) with different viscosities and (b) different pull speeds. The experiments shown in graph (a) were done using 0.45 mg PDMS and were pulled at 100 mm/min. The error bars are the standard deviation of 6, 6, 5 and 6 samples for the increasing viscosities. The experiments	

shown in graph (b) were done using 0.45 mg PDMS. The error bars are the standard deviation of 5 and 6 samples for the 10 and 50 pull speeds respectively.	33
Figure 21 – The next tests done on the Instron using PDMS with (a) different viscosities and (b) different amounts of polymer. The experiments shown in graph (a) were done using 0.75 mg PDMS and were pulled at 25 mm/min. The error bars are the standard deviation of 5 samples for both data points. The experiments shown in graph (b) were done using 1.25 mg PDMS and were pulled at 25 mm/min. The error bars are the standard deviation of 5 for the 15 $\mu$ l samples, 3 for the 25 $\mu$ l samples, and 4 for the 20 $\mu$ l samples.	35
Figure 22 – The tests done on the Instron using PDMS and the capillary tube probes with different viscosities. These experiments were done using 2.5 mg PDMS and were pulled at 25 mm/min. The error bars are the standard deviation of 3 samples for both data points.	36
Figure 23 – A schematic of the HMAT. (a) A front view and (b) a side view	39
Figure 24 – The HMAT	40
Figure 25 – The probe box	40
Figure 26 – The probe lifter	41
Figure 27 – The user interface	42
Figure 28 – The well plate holder	43
Figure 29 – The first tests done on the HMAT. (a) Load curves taken from the HMAT where curves 2-6 were at 1M cs and curves 7-11 were at 100,000 cs and (b) the maximum load at different viscosities. The experiments shown in graph (a) were done using 0.6 mg PDMS. The experiments shown in graph (b) were done using 0.6 mg PDMS. The error bars are the standard deviation of 5 and 4 samples for the 10,000 and 100,000 viscosities respectively.	44
Figure 30 – Tests done on the HMAT using # 4 probes showing the maximum load at different viscosities and a logarithmic trend line. These experiments were done using 0.35 mg PDMS and were pulled at 0.3 mm/s. The error bars are the standard deviation of 6 samples for all of the data points.	45
Figure 31 – Tests done on the HMAT using # 4 probes showing the maximum load at different pull-off speeds. These experiments were done using 0.325 mg of 1M cs PDMS. The error bars are the standard deviation of 6 samples for all of the data points.	46
Figure 32 – Tests done on the HMAT using # 4 probes showing the maximum load using different amounts of polymer. These experiments were done using 1M cs PDMS and were pulled at 0.4 mm/s. The error bars are the standard deviation of 3 samples for all of the data points.	46
Figure 33 – Tests done on the HMAT using # 6 probes. (a) Load curves taken from the adhesion apparatus and (b) the maximum load at different viscosities. The experiments shown in graphs (a) and (b) were done using 0.6 mg of PDMS. The error bars are the standard deviation of 6 samples for both data points.	48
Figure 34 – Load curves for the first capillary tube experiments on the HMAT. These experiments were done using 0.575 mg of 1M cs PDMS.	50
Figure 35 – Tests done on the HMAT using # 7 probes showing the maximum load at different viscosities. These experiments were done using 0.15 mg PDMS and were	

pulled at 0.3 mm/s. The error bars are the standard deviation of 2, 4, 4 and 5 samples for the increasing viscosities.	51
Figure 36 – Tests done on the HMAT using the final probes showing the maximum load at different viscosities. These experiments were done using 0.25 mg PDMS and were pulled at 0.3 mm/s. The error bars are the standard deviation of 5 samples for both data points	52
Figure 37 – Tests done on the HMAT using the final probes showing the maximum load at different viscosities. These experiments were done using 0.375 mg PDMS and were pulled at 0.3 mm/s. The error bars are the standard deviation of 7, 8, 7, 5, 7 and 7 samples for the increasing viscosities.	52
Figure B.1.1 – Probe #1 – The first probes. They were made using a 5 mm diameter glass bead with a plastic tab glued onto them	97
Figure B.1.2 – Probe #2 – The 5 mm glass beads on their own	97
Figure B.1.3 – Probe #3. 5 mm diameter glass rods with a rounded tip	98
Figure B.1.4 – Probe #4. 5 mm diameter glass rods with a rounded tip and a wire loop glued to the top	98
Figure B.1.5 – Probe #5. 1.75 mm diameter capillary tubes with one closed end and the other end bent to form a hook	98
Figure B.1.6 – Probe #6. 5 mm diameter glass rods with a rounded tip and suture string tied across the top	99
Figure B.1.7 – Probe #7. Capillary tube with a small piece of glass glued perpendicular to the tube in a ‘t’ shape.	99
Figure B.1.8 – Probe #8. The final form of the probe. A capillary tube with a flat head glued to the top for easy lifting	99
Figure B.2.1 – The first set-up on the Instron. Probe #1 is placed in the well and the clamp on the Instron is used to pull it out	100
Figure B.2.2 – Probe #3 also utilized the existing clamp for the experiment	101
Figure B.2.3 – A hook used to perpendicularly lift probes # 4, 5 and 6.	101
Figure B.2.4 – The fork shaped hook used for probe #7.	101
Figure B.2.5 – The final form of the probe lifter	102

## **List of Tables**

Table 1 – The parts required to build the adhesion apparatus

23

## 1 Adhesion

An adhesive can be defined as “a linear or branched amorphous polymer above its  $T_g$ .”<sup>1</sup> The theory involves the notion that the material must be able to flow to fill holes created by molecular roughness and essentially ‘grip’ the two surfaces that are to be adhered. However, adhesion starts with surface tension. The concept of surface tension can be understood by looking at the schematic in Figure 1. Molecules attract each other. Interior molecules have a net force of zero as they are surrounded by similar molecules, which exert the same force. Molecules at the surface are not completely surrounded and this results in a net force down into the liquid. This is what creates surface tension ( $\gamma$ ).<sup>2</sup> Surface tension is related to adhesion in the following way: If two materials A and B are separated (Figure 2) two things occur. First, the surface between the materials is destroyed and second two new interfaces are created with material A and air, and material B and air. The energy of the surfaces when they are in contact is called *interfacial tension* while the energy of any material and air is referred to as *surface tension*.

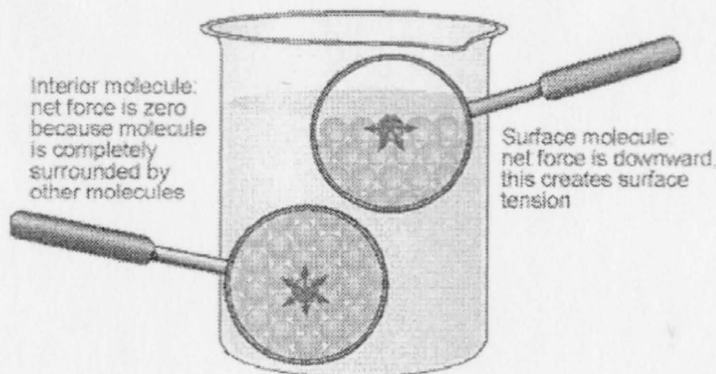
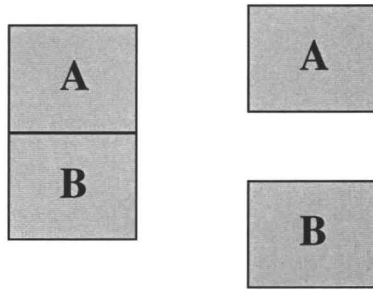


Figure 1 – A schematic demonstrating surface tension<sup>2</sup>



**Figure 2 – The separation of two different materials**

Surface tension is a form of energy. It is defined thermodynamically as the partial derivation of Gibbs free energy with respect to surface area.<sup>2</sup>

$$\gamma = \left( \frac{\partial G}{\partial A} \right)_{TP} \quad (1)$$

Surface tension is also a force and as such a liquid can exert a pulling force on a solid as it is lowered into it. One of the methods of measuring surface tension utilizes this phenomenon. In the DuNouy method, a ring is lowered into the liquid and the force required to lift it up again is measured. The surface tension is then determined by the following equation:<sup>2</sup>

$$\gamma = \frac{F_{\max}}{4\pi R f_{HJ}} \quad (2)$$

where  $F_{\max}$  is the maximum force,  $R$  is the radius and  $f_{HJ}$  is a correction factor.

The thermodynamic work of adhesion is also related to the Gibbs free energy through the following equation:<sup>2</sup>

$$\Delta G = W_{AB} = \gamma_A + \gamma_B - \gamma_{AB} \quad (3)$$

where  $W$  is the work of adhesion, and  $A$  and  $B$  signify two different materials. According to this equation, the work of adhesion is simply a function of the surface and interfacial tensions. Or, it is the work required to destroy the interface between the two materials while creating two new surfaces. The work of adhesion can be measured by contact mechanics methods. These are now described.

### **1.1 Molecular Adhesion**

Hertz was the first to analyze the contact between two spheres and in 1882 he developed an equation to predict the contact area based on the applied force. The major assumptions he made were that the spheres were perfectly elastic, there was no friction, the experiment was reversible, and that there was no adhesive force acting between the spheres.<sup>3</sup> In 1971 Johnson, Kendall and Roberts developed a more accurate equation that now allowed the spheres to exhibit adhesion.<sup>4</sup>

Using the JKR method, the surface energy of a solid can be determined. JKR measurements are useful because the surface energy of materials is an important material property. This parameter is easy to measure for a liquid and there are many different ways to obtain this value. For example, the pendant drop method can be used. However, none of the methods that work for liquids can be used to determine the surface energy of a solid. The Hertz and JKR theories are discussed below.

## 1.2 Theories

### 1.2.1 Hertz Theory

Hertz noticed a black spot appeared where the two spheres touched and suggested that this black spot corresponded with the adhesive contact of the spheres. He found that it would increase in diameter with the cube root of the load,  $F$ . The final relationship he found between the radius of contact and applied force was<sup>4</sup>

$$a^3 = \left(\frac{3\pi}{4}\right)(k_1 + k_2) \left(\frac{R_1 R_2}{R_1 + R_2}\right) F \quad (4)$$

where  $a$  is the radius of the contact spot,  $F$  is the applied force,  $R_i$  is the radius of sphere  $i$ ,

$k_i = \frac{1 - \nu_i^2}{\pi E_i}$ ,  $\nu$  is Poisson's ratio and  $E$  is the tensile modulus. Figure 3 shows the

geometry of the two spheres.

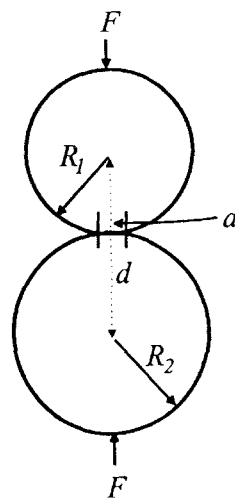
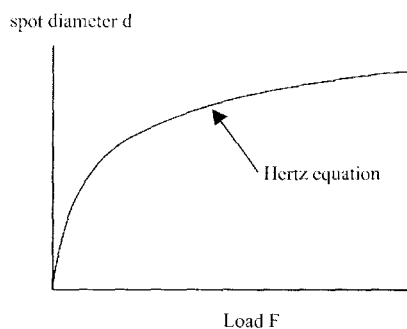


Figure 3 – A schematic of the geometry used in the Hertz equation<sup>3</sup>

The assumptions that Hertz made (mentioned above) led to the conclusion that the contact area would approach zero as the load approached zero (Figure 4).



**Figure 4 – The Hertz equation over a large range of  $F$ <sup>5</sup>**

The Hertz theory works for large loads, but in 1932 Bradley showed that the spheres are still deforming under zero load.<sup>5</sup> Therefore, there needed to be a modification to this theory.

### **1.2.2 JKR Theory**

In 1971 Johnson, Kendall and Roberts modified the Hertz theory. The main difference was that now adhesion was included. This meant that the growth of contact area under low loads was adhesion driven and that the final contact spot was an equilibrium between the force of adhesion and the elastic energy in the material. Their assumptions were very similar to Hertz' and included the assumptions that there was no friction, the spheres were perfectly elastic, the experiment was reversible, or in thermodynamic equilibrium, and that the force of adhesion was short-ranged and only acted inside the contact area.<sup>6,7</sup> Figure 5 shows the difference in profile between the Hertz and JKR theory. The dashed line is the contact profile the spheres would show in

the Hertzian regime and the solid line in the JKR profile. It can be seen that the contact area is larger when adhesion is involved.

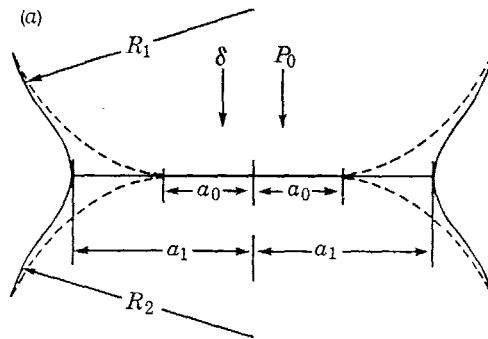


**Figure 5 – A schematic of the Hertzian and JKR contact area<sup>4</sup>**

In order to develop this new theory, Johnson et. al. used an energy balance approach. They calculated the total energy as

$$U_T = U_M + U_E + U_S \quad (5)^4$$

where  $U_M$  is the mechanical energy in the applied load,  $U_E$  is the elastic energy of the materials, and  $U_S$  is the loss in surface energy obtained by the joining of the two surfaces. The following thought experiment will illustrate the difference in forces between the two theories.

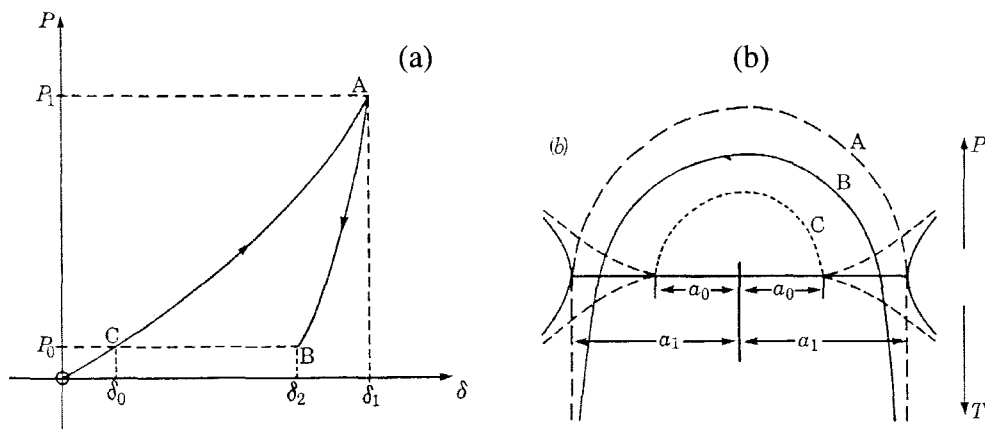


**Figure 6 – The energy balance approach. (a) shows the load-displacement relationship for the contacting samples, and (b) shows the stress distribution corresponding to the points in (a)<sup>4</sup>**

Figure 6 (a) shows three possible states: A, B, and C. B is the only real state while the other two are purely theoretical. At position C a load  $P_0$  is applied. The displacement of the spheres is  $\delta_0$  and the radius of contact is  $a_0$ . This is a Hertzian force as there is no force of adhesion and the force is entirely compressive (Figure 6 (b)). A load  $P_1$  is then applied and we get a new radius  $a_1$  and displacement  $\delta_1$ . However, we are still neglecting adhesion, therefore this is still a Hertzian force and is completely compressive. Finally, the load is relaxed back to  $P_0$  to get the experimentally determined state B. Since in reality there is adhesion the force profile looks different. There is still compression in the center, but the force has become tensile at the edge of the contact area.<sup>4</sup>

From this balance Johnson *et al.* were able to arrive at a new equation to describe the relationship between the contact radius and applied force, which now included the work of adhesion,  $W_A$ .

$$a^3 = \frac{R}{K} \left( F + 3W_A \pi R + \sqrt{6W_A \pi R F + (3W_A \pi R)^2} \right) \quad (6)^4$$

where  $K = \frac{4}{3\pi(k_1 + k_2)}$  and  $R = \frac{R_1 R_2}{R_1 + R_2}$ . The surface energy is related to the work of

adhesion through the equation  $W_A = 2\gamma_S$  if the two spheres are the same material.

During unloading the contact area does not decrease stably throughout the experiment.

At a certain point elastic instability sets in and the spheres will suddenly detach. For

contacting spheres this instability occurs when the radius of contact is at 63% of the

radius at zero load.<sup>8</sup> Unloading will begin when<sup>4</sup>

$$F = -\frac{3}{2} W_A \pi R \quad (7)$$

Johnson *et al.* obtained this relationship by looking at equation (3). If the force is

negative, then for the radius to be a real number,  $6W_A \pi R F \leq (3W_A \pi R)^2$ .

### **1.3 Adhesion on Larger Scales**

On an engineering scale, there are four categories of adhesion.<sup>9</sup>

#### 1) Mechanical Adhesion

The two surfaces physically interlock. The amorphous adhesive flows into the spaces created by the surface roughness, which causes the interlocking mechanism.

#### 2) Specific adhesion

Weak forces such as van der Waals and hydrogen bonding lead to secondary bonds between the substrate and the adhesive.

#### 3) Chemical Bonds

A reaction takes place and primary bonds are formed either between the substrate and adhesive, and/or within the adhesive itself. One common example is epoxy. The epoxy resin and hardener are mixed together and cross-links are formed within the adhesive as the glue dries.

#### 4) Surface interpenetration

This mechanism is driven by polymer diffusion. The polymer chains can slowly penetrate the substrate surface and so have a better ‘grip’ on the material.

When testing adhesives, one of the most important issues to know is when or how it will fail. There are two basic types of failure; adhesive and cohesive. Adhesive failure occurs between the adhesive and the substrate. In the ideal case adhesive failure is described by equation (3). Cohesive failure occurs within the adhesive itself and equation 3 reduces to  $W_A=2\gamma_A$ . However, the measured adhesion is often much larger than that calculated from equation (3). This is caused by energy losses due to inelastic deformation and energy dissipation.<sup>10</sup> Another possibility is that the adhesive is stronger than the materials it is holding together and the material itself fails.

Another way to categorize adhesive failure into two groups is to determine whether the failure is brittle or elastic (Figure 7). Brittle materials have no give and simply reach a maximum stress and then fail while elastic materials stretch first. Elastic materials can go through three stages before failure. First the material is pulled until it starts to deform at the elastic yield. Then the material deforms during the cold draw until it is no longer able to do so any more and enters the work hardening stage and then finally fails. Many polymers can be elastic or brittle depending on the conditions. If the

polymer is chilled or pulled at a fast rate, or if the polymer has become cross-linked the material will act like a brittle substance, and at warmer conditions and a slower rate of pulling the material will be more elastic.

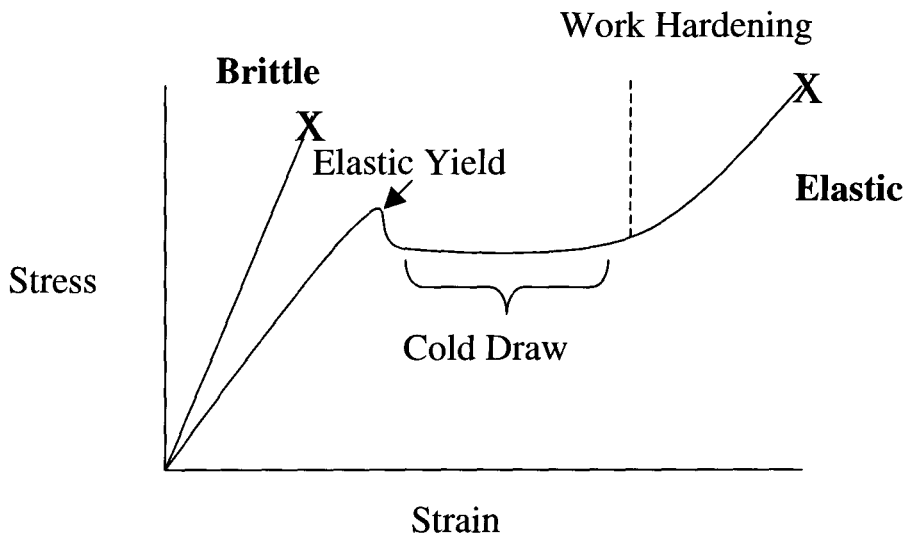


Figure 7 – The stress-strain curves for elastic and brittle failure<sup>11</sup>

Even though an adhesive will fail given enough force, the goal is to find the right adhesive for the job so that it can hold against the maximum force that the particular joint is likely to see.

Common tests for adhesion require a lot of material. One test can take a few grams of adhesive. Another difficulty is that each test can take minutes to hours to complete. One such test is the peel test. In this method, a layer of adhesive is pressed between two substrates. One can be rigid and the other flexible, or both can be flexible. The top substrate is then pulled apart from the bottom layer and the force is measured. The typical dimensions for these substrates are about 2.5 cm x 15 cm so a fair amount of adhesive is needed.

## **2 High Throughput Materials**

### ***2.1 The value of High Throughput Screening***

The number of undiscovered and untested materials, especially those with greater than two or three different atomic species, is limitless. Therefore, the discovery of new, and useful materials is tedious and time-consuming. The increasing use of high throughput testing methods is an attempt to make this search systematic and faster. Currently, our theoretical understanding does not allow us to predict the properties of new structures. Consequently the discovery of useful materials with specific properties using this method requires a lot of material to experiment with and many iterations in order to run the material through the number of tests needed. If experiments are carried out by the conventional one-at-a-time approach it can be very costly and time-consuming.<sup>12,13</sup> However, using combinatorial techniques many different properties on hundreds of samples can be tested in one day and the results easily compared.<sup>14,15</sup> The result of using the combinatorial approach is increased efficiency and reduced time-to-discovery.

### ***2.2 How High Throughput Screening is implemented***

The main purpose of high throughput screening is to determine which materials look promising and warrant a closer look. In general, Figure 8 shows a typical scheme used for high throughput research. Therefore, there are a few factors that should be taken into consideration when designing such experiments. The main debate in combinatorial research is the balance between speed and accuracy.<sup>16</sup> The purpose of these experiments

is to test a large number of materials at a very high rate using a small amount of material, but accuracy must be kept at a reasonable level so that the results are reliable. Ideally, a good high throughput testing apparatus should have the following characteristics: It should be able to analyse small samples, there should be minimal sample preparation required, rapid turnaround for sets of samples, and automated data acquisition. These requirements all help to speed up the whole process.<sup>17</sup> Once the first screen of materials has taken place, the initial large number of samples can be easily reduced to a smaller set that warrant a closer look with more accurate testing methods.

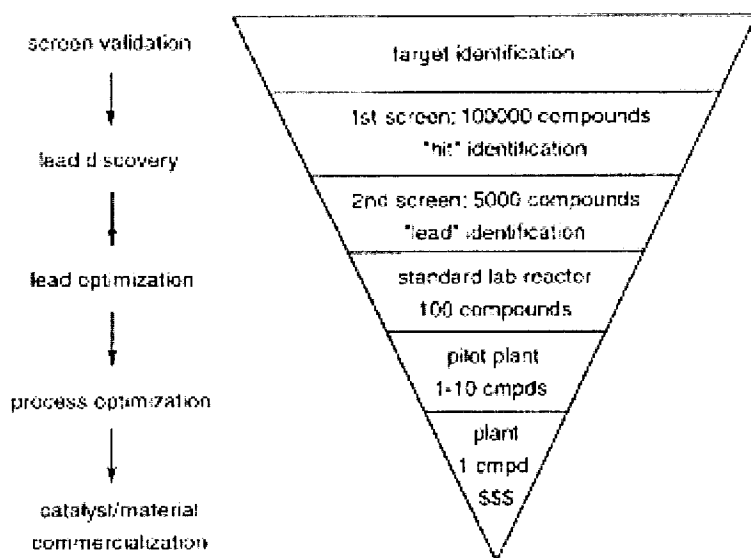


Figure 8 – A typical scheme for combinatorial research<sup>7</sup>

### **2.3 A Brief History**

The first example of high throughput science is attributed to Edison. In 1878, he tried over 1600 different materials in his search for a useful filament for the electric light bulb before determining that carbonized cotton thread in a vacuum was the best

choice.<sup>13,14</sup> In 1912 Ciamician, an Italian photochemist, manually set up hundreds of flasks on the roof of the University of Bologna in order to determine which of the chemicals placed within these flasks were photoactive.<sup>14</sup> These men used what would today be considered slow methods to find the ideal material, but they were systematic and faster than rigorously testing each sample. In modern times, the most prevalent use of high throughput chemistry is seen in pharmaceuticals. Biological materials are hard, if not impossible, to model given today's understanding of what makes drugs work and so trial-and-error methods are commonly used for the discovery of new drugs. Thus, high-throughput testing is immediately seen to be useful.

## ***2.4 Current Uses***

Although the discovery of the light bulb was the first to benefit from combinatorial science, it has been the pharmaceutical industry that has gained the most in terms of vast libraries of samples that can be quickly tested.<sup>13</sup> One example allows for more than 1600 combinations to be tested simultaneously.<sup>18</sup> Only in the last 10 years have other fields such as polymer research begun to explore the uses of high throughput testing. Polymer research is well suited for exploration by high throughput methods as there are several factors that can be varied during sample preparation such as the monomer, catalysts, processing methods and conditions that all affect the end properties as well as many parameters to investigate, including different rheological and material properties.<sup>14</sup>

There are a few categories that high throughput methods fall into. Firstly, it can be used in either the preparation step or the testing step. Within these two groups, the methods can be further categorized as being either rapid serial or simultaneous. Simultaneous high throughput methods are often referred to as combinatorial methods.

## **2.5 Sample Preparation**

### **2.5.1 Rapid Serial**

Samples are usually prepared one at a time in a lab. However, using new methods, they can be prepared very rapidly. In the area of mechanical testing of polymers, there are many examples of high throughput methods being put to use. In 2003, Potyrailo *et al.* reported the use of a combinatorial microextruder system that they had designed.<sup>19</sup> It is a co-rotating twin extruder that is able to produce strands of polymer 1-2 mm in diameter or films that are 5-12 mm wide and 0.3-1 mm thick. Because of its small size, 40-200 times less material is required for polymer generation than a typical extruder used in the study of polymer formulations. In order for the extruder to be deemed reliable, it must be able to consistently produce a continuous stream of well-mixed polymer. The high throughput microextruder system was able to do just this. It was run at 10 g/min for as long as 3 hours and produced consistent polymer and even had the ability to change the composition of the product within 30 s with good reproducibility (5-6% relative standard deviation of the fluorescence signal). Thus, many different small samples of polymer could be prepared quickly. The resulting samples were then put through weathering performance tests. The purpose of these tests was to investigate the effect of UV light on the polymer. Usually this kind of test requires thousands of hours to

adequately expose the polymer to outdoor conditions, so in order to speed up the adsorption of UV, which is an important factor in determining the outdoor lifetime of the material, a UV absorber was added to the polymer and it was exposed to very high UV levels (the equivalent of 30 suns).

### 2.5.2 Simultaneous Library

In this category, the goal is to make as many samples that can be prepared at once using as few steps as possible. In 1995 Xiang *et al.* described the synthesis of libraries of materials into thin films by using shadow masks. These masks allow material to be deposited in specific locations while preventing deposition at other location by simply covering these areas. Each new material was deposited by RF sputtering into patterns defined by these masks. Figure 9 shows a quaternary masking scheme where each mask is rotated 90° for 4 deposition steps per mask. The films are deposited in layers of different materials. This results in a total of  $4n$  deposition steps and up to  $4^n$  compositions, where  $n$  is the number of distinct masks.<sup>12</sup>

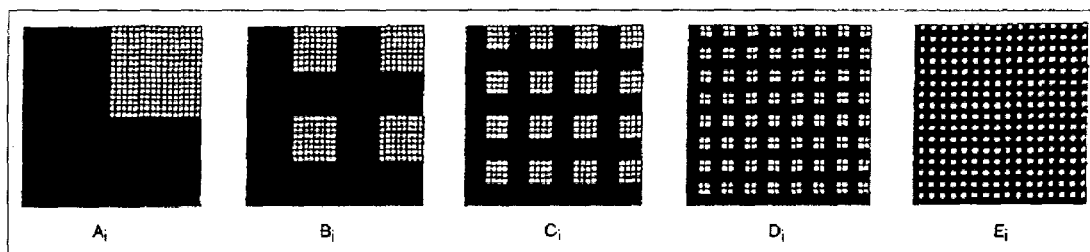


Figure 9 – A set of masks that could be used in a quaternary masking scheme<sup>12</sup>

Another way to prepare libraries of materials in as few steps as possible involves what is called split synthesis. The materials are typically synthesised on resin beads. In

1991, Lam *et al.* developed a useful method for building material libraries of peptides shown in Figure 10.<sup>20</sup> The resin beads are split into separate reaction vessels that each contain a different peptide and are allowed to react to completion. The beads are then pooled together to randomize the beads and split apart into separate vessels again to undergo another reaction. In this manner every possible combination will be in the final mixture in a minimum number of reactions.

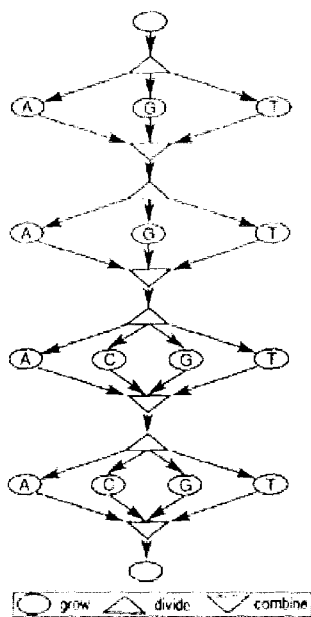


Figure 10 – An example of a split synthesis procedure. The number of compounds produced from this particular scheme would be 144.<sup>20</sup>

## 2.6 Testing

### 2.6.1 Rapid Serial

Testing is usually done one by one. The advantages of high throughput methods are that the tests can be preformed much faster and very little material is required. Some accuracy is often lost, but can be overcome after the first screening. Sormana and

Meredith designed a high throughput impact apparatus in 2003.<sup>21</sup> The set-up is shown in Figure 11. The sample film, which is  $25 \times 25$  mm, is secured between two steel plates which is in turn mounted onto a ball-bearing rail guide. The plates are perforated with holes 3 mm in diameter. The film is dropped onto the contact tip, which is attached to a force sensor. The data collected is used to provide information on a number of useful parameters including maximum impact force and impact energy of a material.

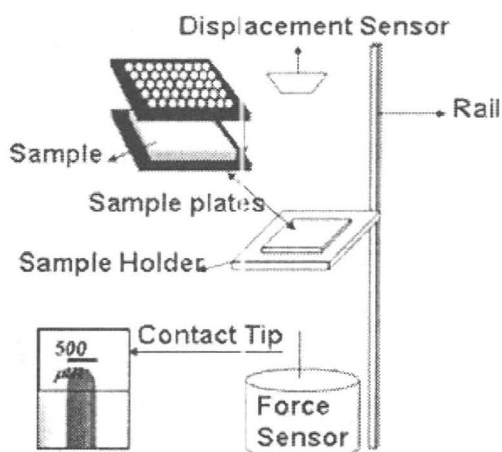


**Figure 11 – The experimental set-up of Sormana and Meredith's impact apparatus.<sup>21</sup>**

Another approach that involves more high-tech methods is described next. An atomic force microscope (AFM) is useful in the characterization of surfaces. The basic principle is that a sharp miniature probe scans the surface of a small amount of material while a laser detects the deflection of the probe. In 2003, Green described using a tip array to characterize the surface of a material with multiple chemicals during a single run.<sup>22</sup> Basically, the array of tips was treated such that there were three different chemistries and the sample had two different chemistries. Then, when the tips were used to scan the sample, each of the six possible combinations could be measured.

## 2.6.2 Simultaneous Testing

Many samples can also be tested at the same time. One of the main benefits of this method, besides the rapidity, is that all of the samples are under the same environmental conditions, thus these factors do not need to be considered when comparing results.<sup>18</sup> In 2003, Kossuth *et al.* developed an instrument to measure the mechanical properties of 96 thin films simultaneously.<sup>23</sup> The Parallel dynamic mechanical thermal analysis (DMTA<sup>TM</sup>) is able to measure such factors as modulus, spring constants, and failure strength by bringing an array of 96 pins into contact with the samples. These pins all have independent force sensors on their opposite end and can move in an oscillatory manner. The set-up also includes an environmental chamber so that the following parameters can be controlled: Temperature, temperature ramp rate and the frequency of oscillation. Since the DMTA is able to measure 96 sample sites simultaneously, many different samples can be tested for favourable properties, or many repeats can be run on a few samples to increase confidence in the data.

The National Institute of Standards and Technology (NIST) is currently working on a few projects that involve high throughput methods. One focuses on an adhesive evaluation.<sup>24</sup> The multi-lens combinatorial adhesion test (MCAT) that is being designed is based on the mechanics that Johnson, Kendall and Roberts (JKR) developed. The current form of the instrument is shown in Figure 12. It is able to perform several hundred to several thousand simultaneous tests by utilizing an array of hemispherical lenses that are attached to a vertical actuator. In this way, adhesion can be measured over a large space of a film, or a library of films. For each lens, both lens displacement and

contact area can be measured. In future configurations, the load seen by each lens could potentially be measured as well. The aim is to be able to test and map properties that are of interest including tack and viscoelasticity as a function of temperature and under different conditions.

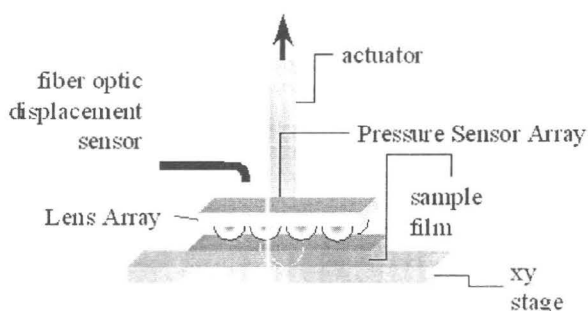


**Figure 12 – The current experimental set-up of the NIST MCAT test bed.<sup>24</sup>**

## **2.7 Data Collection**

With tests that can be done rapidly, the amount of data that is collected can be overwhelming. Thus, data is often automatically collected and stored on computer, and advanced statistics are used to interpret the results. Two related methods are called principle component analysis (PCA) and partial least squares (PLS) and can be used to determine the main influencing factors of a system of any dimension or number of variables. Tuchbreiter *et al.* shows the usefulness of PLS when screening for polymer properties.<sup>25</sup> They use test data sets obtained by more reliable experiments to create a model and then compare the new data to the model. Using PLS they show that their tests accurately predict the modulus, density and shore/hardness, but some improvement is needed in predicting ultimate tensile strength.

High throughput methods are being developed and used in many areas where speed and number of experiments is important. Theories on how to accurately predict properties such as chemical activity and polymer bonding strength are not yet reliable, hence the most thorough way to find a material with favourable properties is to test every possibility. Since this would take a prohibitively long time using conventional methods, this has not been possible in the past. High-throughput tests greatly reduce the time and effort needed to determine promising candidate materials.

## **3 Experimental**

### ***3.1 Objective***

The purpose of this project was to design a high-throughput apparatus to test the relative strength of small amounts polymer adhesives. The concept we used is the rapid serial approach to quickly test many samples one at a time. In this way many samples that are distinctly separated can be rapidly tested. The use of less than a gram of material per sample can be very useful especially when dealing with exotic materials where producing a lot of material is costly or time consuming. The major challenges were to design the probes and a way to hold the samples before and during testing. The probes had to be easy to place into and pull out of the samples and easy to make. It should also be easy to change their surface properties. The sample holder had to hold these probes upright at all times, yet it couldn't interfere with the actual test. In order to design the probes, preliminary tests were done on the Instron 4411 Universal Tester. Using a crude design for holding the samples in place, the different probes could be tested for

repeatability. Later, an adhesion apparatus was constructed and the best probe chosen from the first tests could be further refined, and the sample holder could now also be developed.

### **3.2 Materials**

For the first experiments, V-Bottom 96-well plates part # 2605 were purchased from Thermo Labsystems, 5 mm diameter glass beads were purchased from Quackenbush Company Inc. The polymers used were polyvinylamine (PVAm) from BASF (MW 34.6 KDaltons, HG 94.6 %) and polydimethylsiloxane (PDMS) (Viscosities of 5,000 cs with trimethylsiloxy terminations, 10,000 cs, 50,000 cs with silanol terminations, 60,000 cs with trimethylsiloxy terminations, 100,000 cs with vinyl dimethyl terminations and 1,000,000 cs with trimethylsiloxy terminations) from Petrarch Systems Inc. The PVAm was dissolved in distilled water and the PDMS was dissolved either in octamethylcyclotetrasiloxane (D4), Pentane, or Heptane.

### **3.3 PVAm Preparation**

The PVAm was purified in the following steps:

1. Dilute PVA to about 0.5% with distilled water
2. Put solution in dialysis tube
3. Place dialysis tube in water for 2-3 days
4. Empty contents into a flask
5. Mix a solution of dry ice and acetone and dunk flask into this mixture until it is frozen
6. Freeze dry
7. Scrape remaining solid

The PVA could then be dissolved in water and used in experiments.

### **3.4 Hardware**

#### **3.4.1 The Instron**

The early experiments were completed using an Instron 4411 Universal tester (Figure 13) with a 50 N load cell. For these tests, the well plate was secured with string to the bottom clamp and the top clamp was positioned to be able to clamp onto the top of the probe (Figure 14). As the top clamp was raised upwards, the load cell would measure the force needed to lift the probe and a force curve would be recorded and saved.

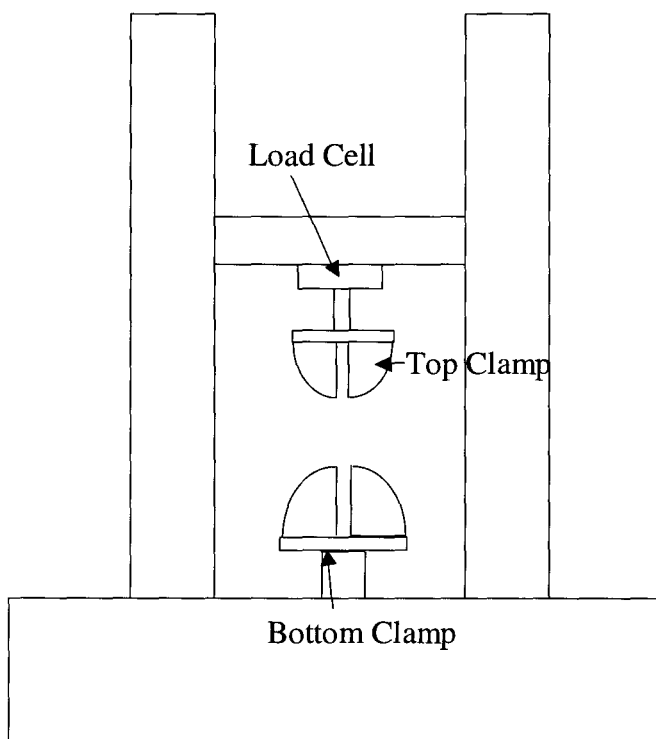


**Figure 13 – A schematic of the Instron Universal tester**

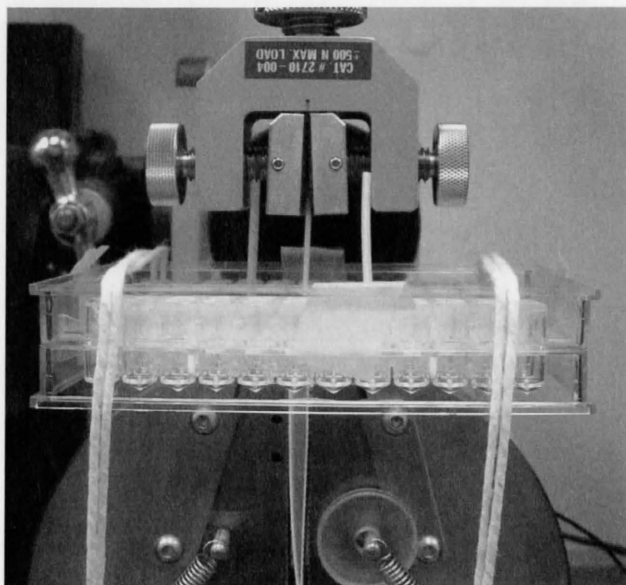


**Figure 14 – The 96 well plate secured to the Instron. Here two well plates are used to hold the probes more upright, but the original configuration used only one well plate.**

### 3.4.2 Parts List

The final apparatus is comprised of the following equipment listed in Table 1.

The design and construction of the apparatus will be described below.

**Table 1 – The parts required to build the adhesion apparatus**

Part	Supplier	Part Number	Other Information
150 mm Linear Translation Stage	Newport	ILS150CC	Y-Direction
100 mm Linear Translation Stage	Newport	ILS100CC	X-Direction
25 mm Linear Translation Stage	Newport	VP-25XA	Z-Direction
3 Axis Motion Controller	Newport	ESP300-111112	
100 g Load Cell	Transducer Techniques		
1000 g Load Cell	Transducer Techniques		
17" x 22" x 2.4" Optical Breadboard	Newport	EG-22-2-SP	

2 0.5 m Structural Rails	Newport	X95-0.5	
2 Clamping Carriages	Newport	CX95AS	
2 Mounting Bases	Newport	M-PBN16	
Precision Optical Rail	Newport	PRL-24	
Precision Rail Carrier	Newport	PRC-3	
L-shaped bracket	McMaster Machine Shop		
Probe Box	McMaster Machine Shop		Described below
Probe Lifter	McMaster Machine Shop		Described in Figure B.2.1 to Figure B.2.5
Probes	McMaster Machine Shop		Described in Figure B.1.1 to Figure B.1.8
PCI-GPIB	National Instruments	PCI-GPIB	
SCC-SG24	National Instruments	SCC-SG24	
SC-2345	National Instruments	SC-2345	
2 m 2X GPIB Cable	National Instruments	2 m 2X GPIB Cable	

### 3.4.3 Calibration of Load Cell

Before using, both load cells had to be calibrated. In order to do this, known weights were suspended from the load cell and the voltage was read. The data gave a linear correlation when graphed (Figure 15). This information could then be used in the LabView program to predict the force in grams.

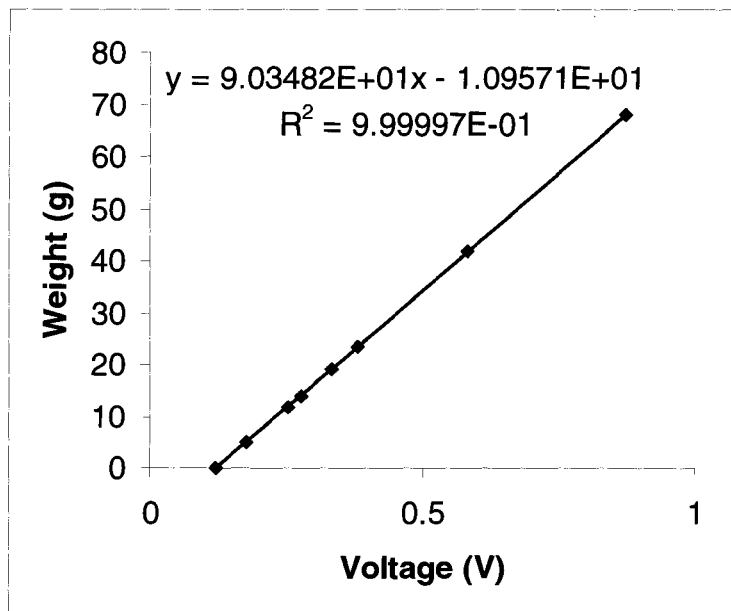


Figure 15 – Calibration for the 100 g load cell

### 3.4.4 Software

A program was written using LabView 7.0 in order to integrate the translations stages and the load cell (Appendix A).

### 3.5 Procedure

While the equipment changed over the course of these experiments, the procedure remained constant. Once all of the materials were prepared, which included having equipment ready and solutions mixed, the experiment could begin. A small amount of polymer solution, anywhere from 5  $\mu\text{l}$  to 75  $\mu\text{l}$  with the typical amount being about 10  $\mu\text{l}$ , was deposited into each of 8 to 15 wells at a time depending on the number of probes available. This was done using an eyedropper at first and subsequently a micropipette. The probes were placed in the wells and then allowed to sit long enough to ensure that the

solvent had evaporated, which was 2 hours to 12 hours depending on the solvent. Finally, the well plate could be taken to the tester and the probes could be pulled out and the adhesion force measured.

## **4 Results and Discussion**

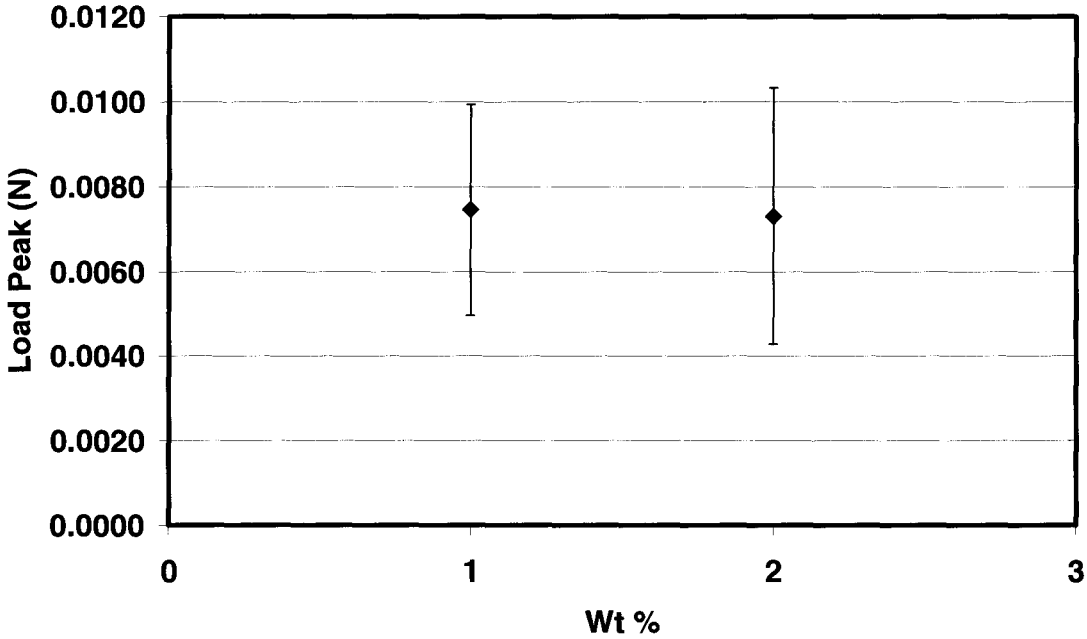
### ***4.1 Preliminary Experiments***

#### **4.1.1 Using PVA**

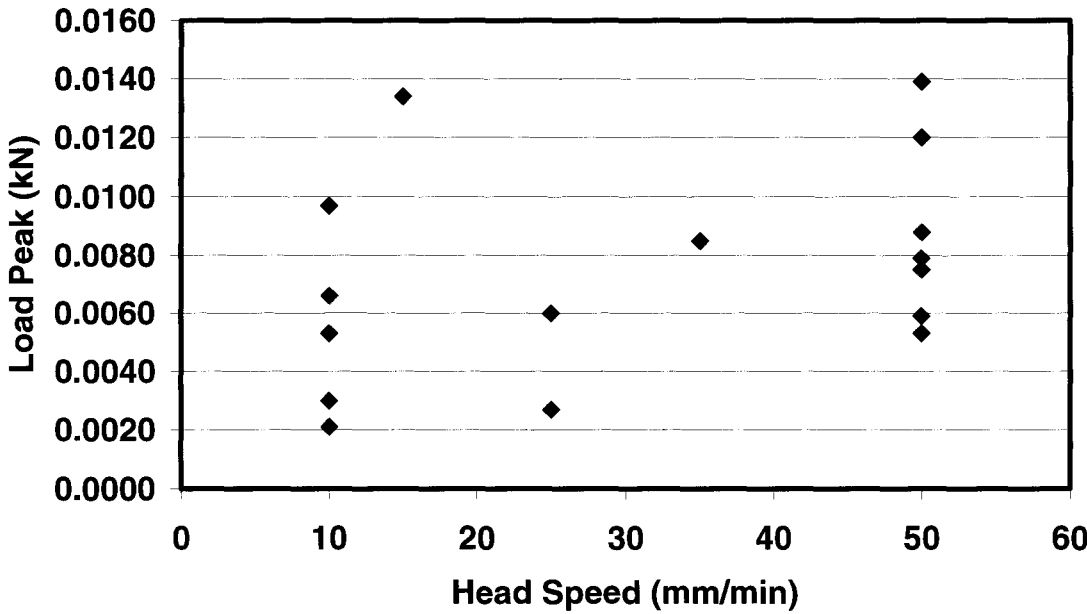
The purpose of the initial experiments was to evaluate potential sample probe geometries. Ideally, the probes should have the following characteristics: They should be easy to place in and pull out of the wells and should stay upright at all times. The geometry should be straightforward. It should be simple to make many probes that have the same characteristics, and it should be easy to change the surface properties of these probes. It was determined that glass was the best material to work with as it is common and the surface chemistry well known and it is non-deformable. In addition, a sphere was chosen as the probe tip because then the surface contact geometry on a v-shaped well is known.

The preliminary experiments were done manually on the Instron 4411 Universal Tester using probes made by gluing (using epoxy) a small glass bead (5 mm diameter) onto the end of a piece of plastic tie (Figure B.1.1 Appendix B.1). The first polymer tested was PVAm. The PVAm was diluted with distilled water to a concentration of 0.1 - 2 wt%. An eyedropper was then used to deposit 1 drop into each well. The probes were placed in these wells and the water allowed to evaporate. Once the samples were ready,

the well plate was secured to the Instron as shown in Figure 14. To test each sample, each well was in turn positioned beneath the load cell, the probe secured to the top clamp, and the test was performed. The maximum load was recorded and repeats were done on each data point. Figure 16 shows the results of the first tests. All error bars shown represent the standard deviation found using Excel. The number of measurements used in each error bar is stated in the figure caption. After the probes were pulled, it could be seen that the residue pattern left by the polymer on the bottom of the probes was a ring (Figure 17). This was expected due to the geometry. Since the probes were spherical and the bottoms of the wells were conical, capillary forces would draw the adhesive solution to the interface of these two surfaces. However, the actual pattern on the bottom of the glass beads was more of an oval shape indicating that the beads were not perfectly round.



(a)



(b)

Figure 16 – The first tests done on the Instron using PVAm (a) at two different polymer concentrations and (b) different pull speeds. The experiments shown in graph (a) were done using 1 drop of solution and were pulled at 25 mm/min. The error bars represent the standard deviation of 7 and 10 samples for the 1 and 2 polymer concentrations solutions respectively. The experiments shown in graph (b) were done using 1 drop of 1 polymer concentrations solution.

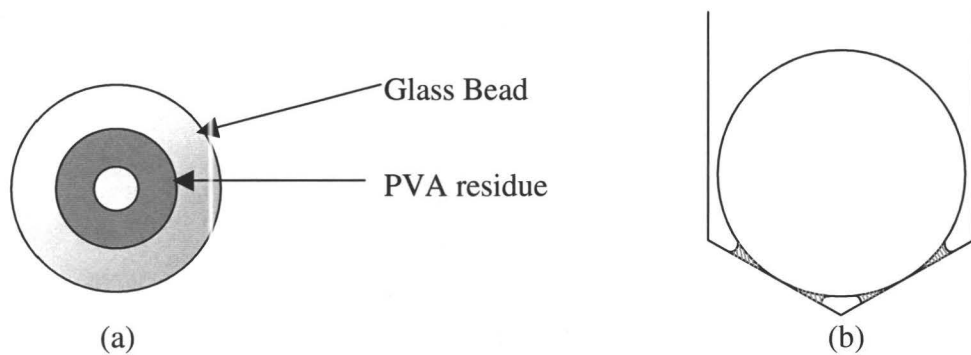


**Figure 17 – A schematic of (a) the bottom of a glass bead after a test, (b) a glass bead sitting in a well and (c) a picture of the bottom of a bead after it has been pulled. Because of the conical geometry of the wells, the polymer left a ‘ring’ of material.**

As can be seen from the standard deviations of the different measurements, there is no statistical difference between experiments. One of the problems that were encountered was that PVA is sensitive to humidity so that tests done on different days could give different results. On a few occasions, the polymer didn't fully dry before the test, so there was elastic failure instead of brittle failure. Another issue was that the forces involved were at the lower end of the load cell range and so the uncertainty in the readings may have been large enough to affect the force measurements. A third issue was that when the probes were drying it was difficult to keep them upright. Often, the probes would dry with a slight tilt and so they would not necessarily be pulled directly vertically.

#### **4.1.2 Bead Punching Tests**

Another preliminary experiment involved a different configuration. 1 mm holes were drilled into the wells of a well plate and the glass beads were poked out with a piece

of wire that was attached to the load cell (Figure 18). To try to increase accuracy, the polymer solution was deposited with a micropipette and using 20-30  $\mu\text{l}$ . Due to the high surface tension of water the drop could be deposited into the wells that had holes in them with no leaking. Figure 19 shows the results of these tests.

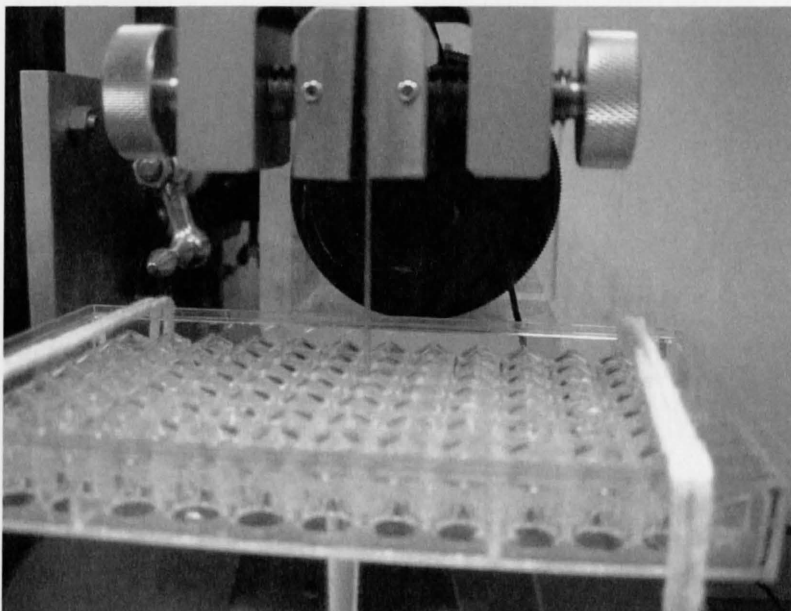


**Figure 18 – The second configuration on the Instron. The plate was turned upside-down and the glass beads were poked out from the bottom of the wells.**

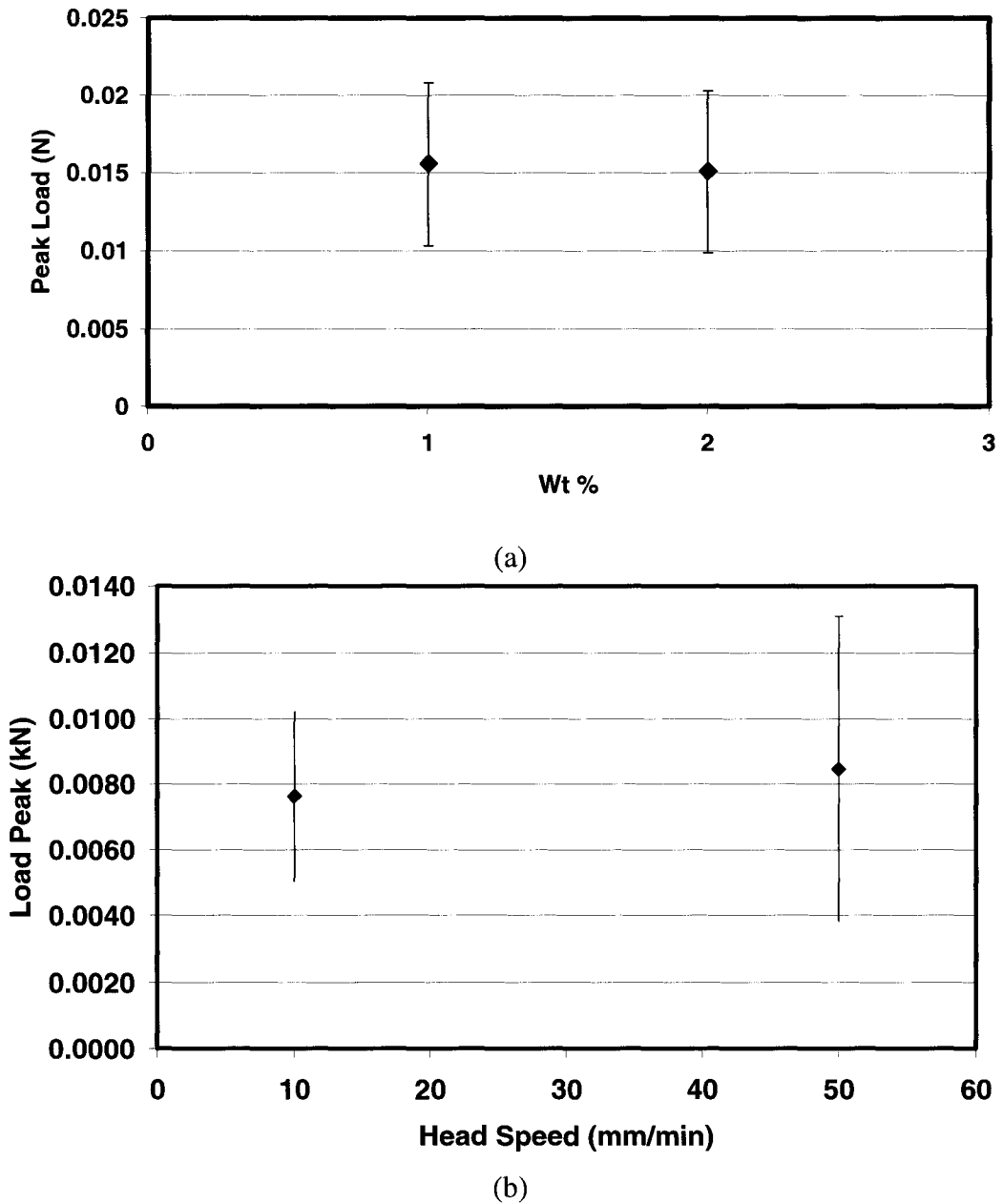
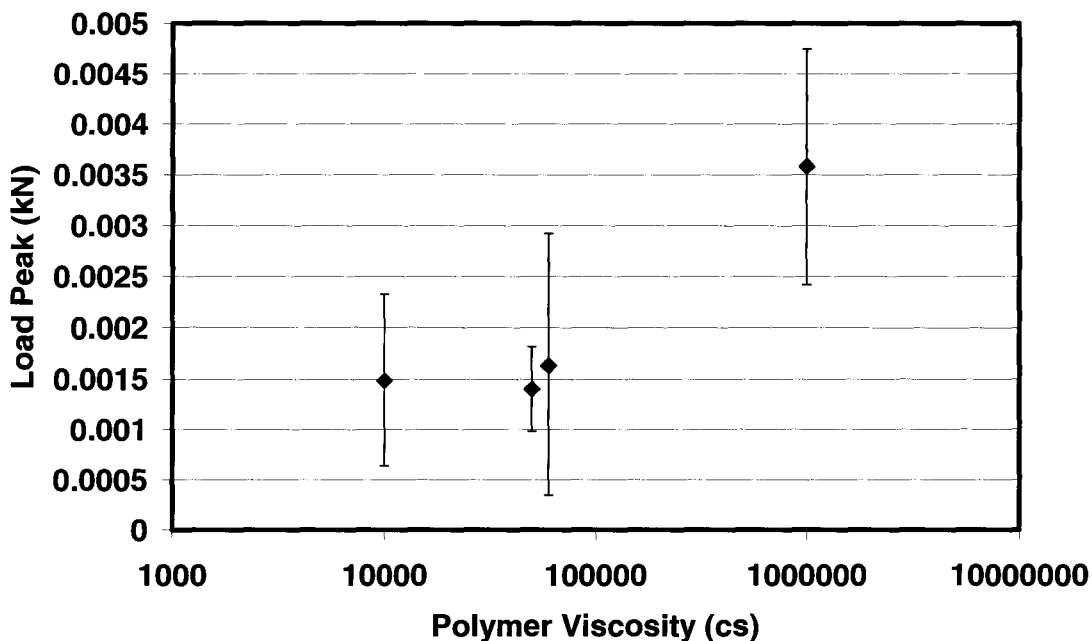


Figure 19 – The second tests done on the Instron using PVA (a) at two different polymer concentrations and (b) different pull speeds. The experiments shown in graph (a) were done using 1 drop of solution and were pushed at 25 mm/min. The error bars are the standard deviation of 4 and 8 samples for the 1 and 2 wt % solutions respectively. The experiments shown in graph (b) were done using 1 drop of 1 polymer concentrations solution. The error bars are the standard deviation of 4 samples for both data points.

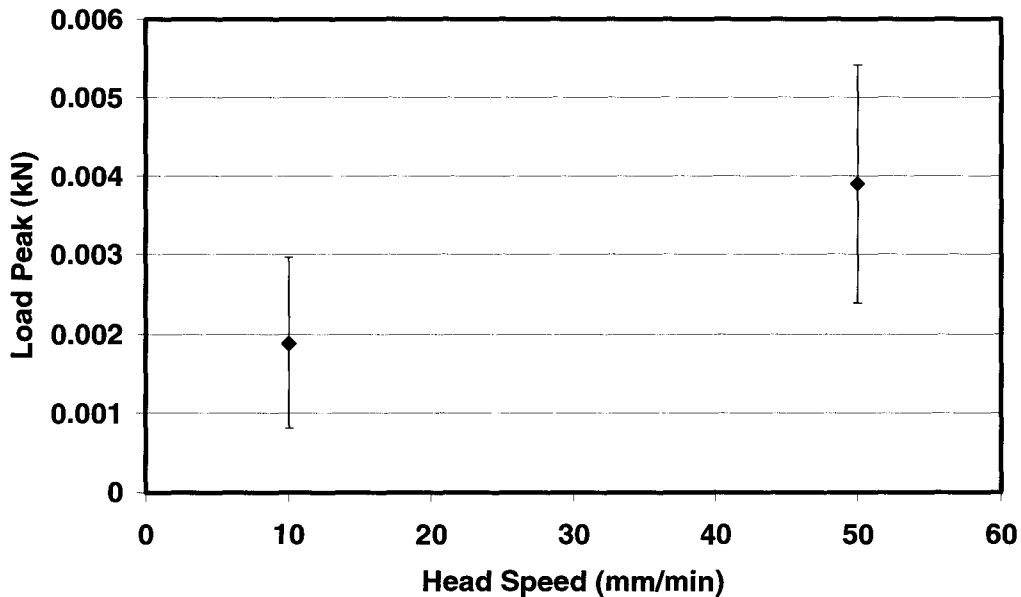
These tests proved to be just as inaccurate as the first tests. In addition, when this was later tried with PDMS dissolved in a liquid with a lower surface tension than water, the solution did not stay in the well.

### **4.1.3 Using PDMS**

PDMS was used with a few different viscosities dissolved in D4. Glass rods with a rounded tip were used for the probes with greater success (Figure B.1.3 Appendix A.1). The improvement was likely because the ends of the glass rods were more spherical than the glass beads, and the expected difference between readings was greater since there was a significant difference in the stickiness of the polymers with different viscosities as opposed to different amounts of PVAm. Also, in order to try to keep the probes upright while the polymer was drying a second well plate that had the bottom of the wells drilled out was placed on top of the original well plate and used to brace the probes. The top plate was turned upside-down so that the bracing wells would be as high as possible



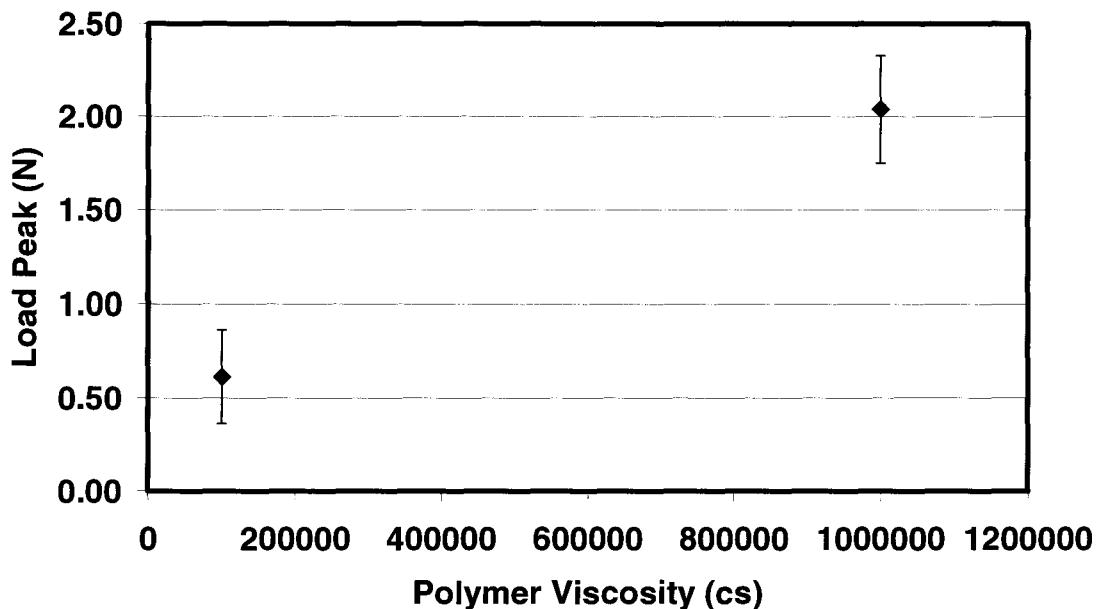
(a)



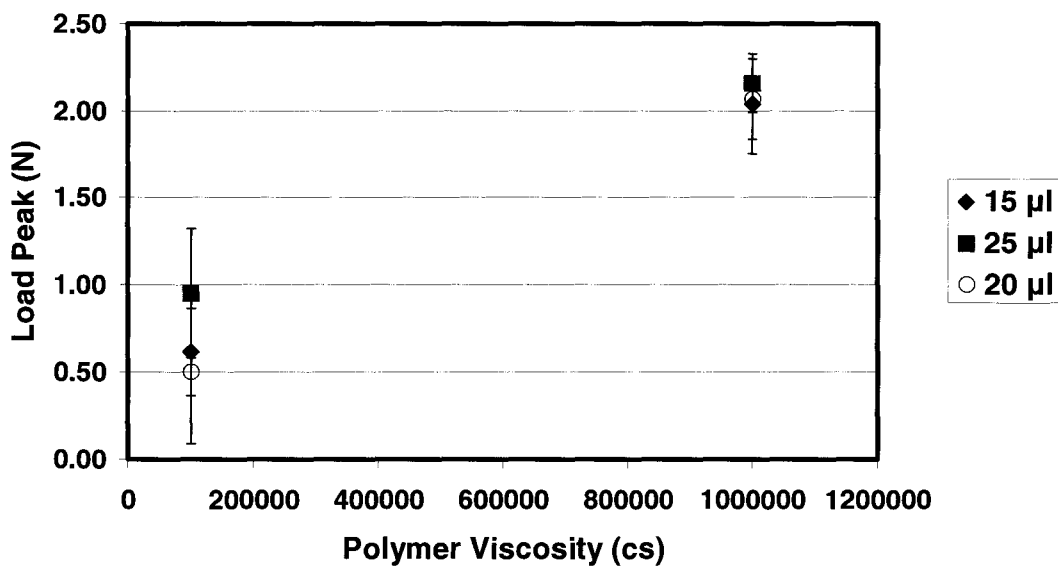
(b)

Figure 20 – The next tests done on the Instron using PDMS (a) with different viscosities and (b) different pull speeds. The experiments shown in graph (a) were done using 0.45 mg PDMS and were pulled at 100 mm/min. The error bars are the standard deviation of 6, 6, 5 and 6 samples for the increasing viscosities. The experiments shown in graph (b) were done using 0.45 mg PDMS. The error bars are the standard deviation of 5 and 6 samples for the 10 and 50 pull speeds respectively.

Figure 20 shows the results for these experiments. There is a slight statistical difference between the highest and lowest viscosities and the different pull speeds, but the standard deviation is still unacceptable. One problem that was encountered was that in trying to clamp onto the glass rods, the rods would be moved from their original position. In order to fix this, new probes were made by gluing a piece of wire to the glass rod to make a loop (Figure B.1.4 Appendix A.1) and suture string was tied to the loop and clamped to the load cell. Suture string was chosen because it does not stretch much when pulled. At this point heptane was used as the solvent because D4 took too long to evaporate. Figure 21 shows that the results are improving. There is now statistical difference between the pull-off force of the 1M and the 100,000 cs polymer. Different amounts of polymer ranging from 0.75-1.25 mg were tried, but there was no discernable difference in these measurements.



(a)



(b)

Figure 21 – The next tests done on the Instron using PDMS with (a) different viscosities and (b) different amounts of polymer. The experiments shown in graph (a) were done using 0.75 mg PDMS and were pulled at 25 mm/min. The error bars are the standard deviation of 5 samples for both data points. The experiments shown in graph (b) were done using 1.25 mg PDMS and were pulled at 25 mm/min. The error bars are the standard deviation of 5 for the 15 µl samples, 3 for the 25 µl samples, and 4 for the 20 µl samples.

Another type of probe was also made at this time (Figure B.1.5 Appendix A.1). It is a 1.75 mm diameter capillary tube with the open end bent over so that a piece of suture string could be tied to that end. This gives a much smaller surface for adhesion. The resulting measurements were not significantly different between the two different viscosities (Figure 22). This is most likely because of their very small size and weight such that the Instrons' load cell had difficulties detecting the force.

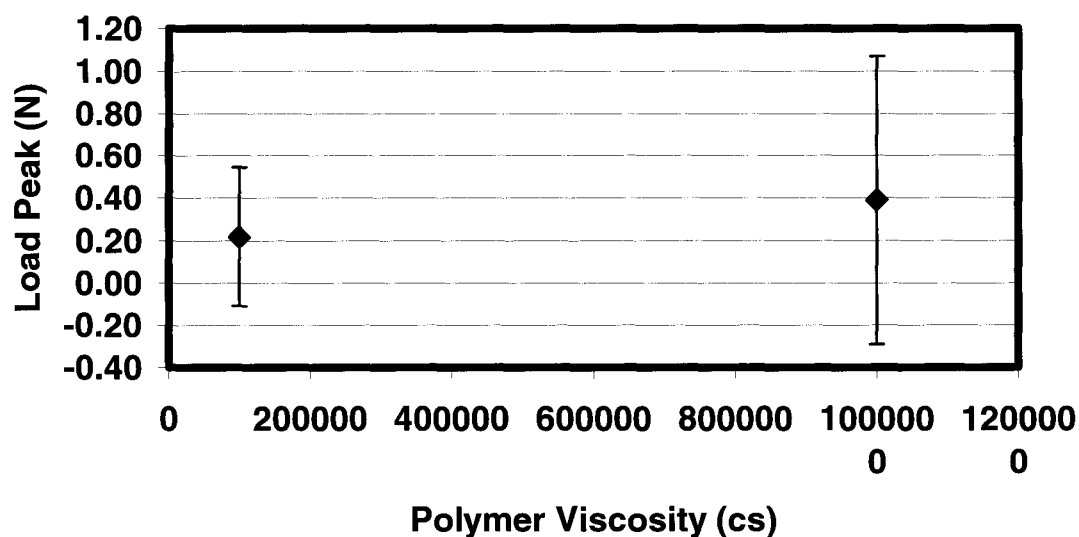


**Figure 22 – The tests done on the Instron using PDMS and the capillary tube probes with different viscosities. These experiments were done using 2.5 mg PDMS and were pulled at 25 mm/min. The error bars are the standard deviation of 3 samples for both data points.**

As a result of these initial experiments, it was determined that the 5mm glass rods held the most promise as they were easy to place and could be pulled directly vertically out of the wells. However they did take some effort to assemble. Also, we were not yet ready to completely abandon the probes bases on the capillary tubes.

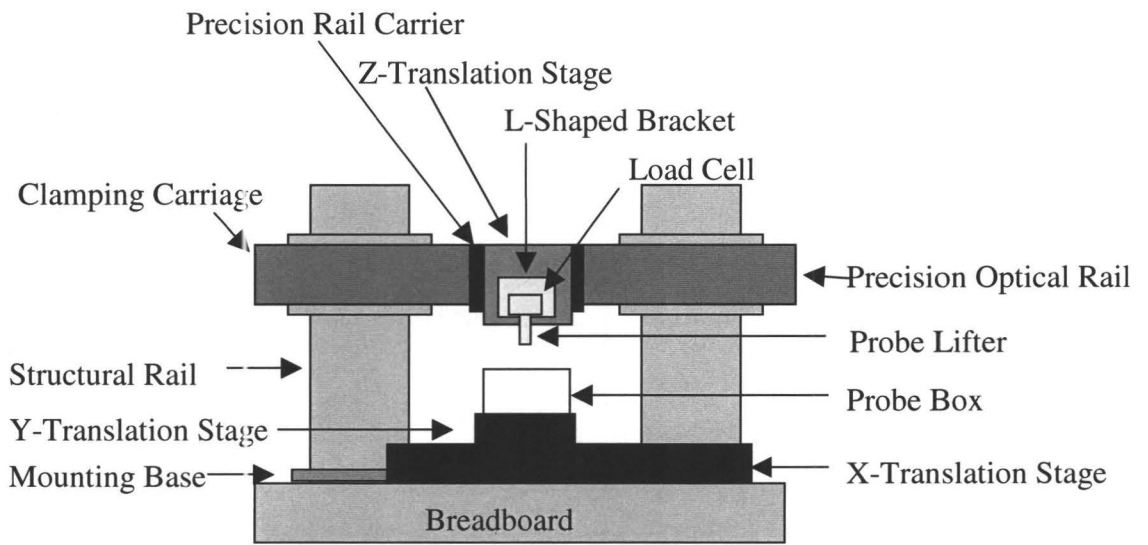
## ***4.2 Experiments on the High-Throughput Micro-Adhesion***

### ***Tester***

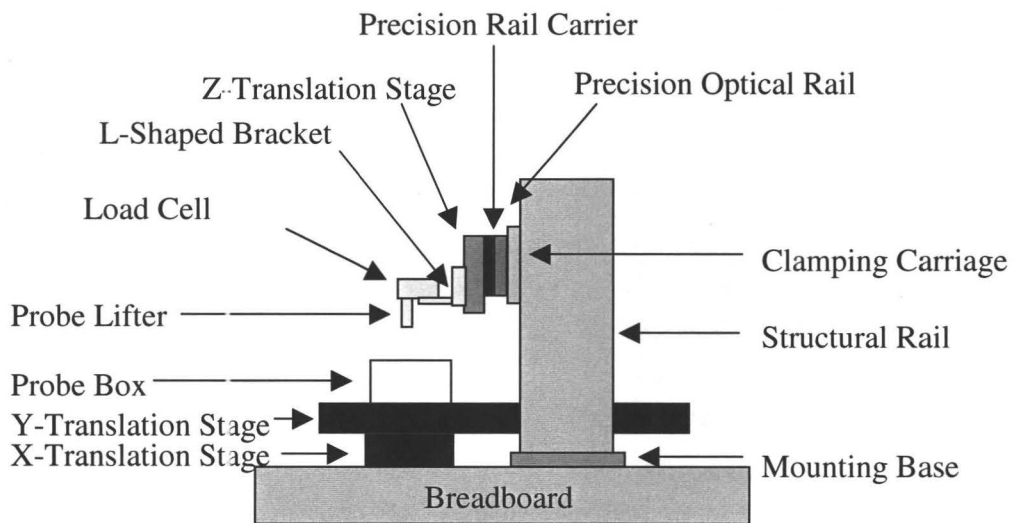
#### **4.2.1 The High-Throughput Micro-Adhesion Tester (HMAT)**

Once the preliminary experiments were completed and there was a general understanding of the adhesion apparatus design and its capabilities of, a device was constructed from the parts mentioned in Table 1. Figure 23 and Figure 24 show the completed adhesion tester. The structural rails are mounted on the mounting bases, which are in turn mounted at opposite ends of the optical table. The precision optical rail is attached to the structural rails via the clamping carriages and the precision rail carrier is clamped to this rail. The z-stage is attached to this carrier. The x-stage is mounted directly to the optical table while the y-stage is mounted perpendicularly to the x-stage. The probe box (Figure 25) sits atop the x and y translation stages. The probe box went through a few revisions that will be described before coming to this final form. The probe lifter (Figure 26) is attached to the load cell, which is in turn attached to the z translation stage via the L-shaped bracket. The probe lifter also went through a number of revisions described in the next few sections and in Appendix A.2. Thus, the probe lifter can be moved up and down while the load cell measures the force. When the force is measured, it includes the weight of the probe which should be subtracted from the data. However, in all cases the probe itself represented less than 1% of the measurement, so it was neglected. A LabView program was written in order to automate the following process:

- The probe box is moved so that the fork of the probe lifter is beneath the first probe cap.
- The z stage moves upwards until the probe lifter is touching the probe
- Once the fork touches the probe there is a delay of 10 seconds to let the polymer relax
- The probe is lifted out of its well and the force curve is recorded
- The probe is lowered again and the probe box positioned so that the next probe can be tested.
  - o Each test takes about 30 s
- This repeats until all sites have been tested
- The resulting data is saved into two text files showing the peak forces and the entire curves that can be opened using a spreadsheet program
- Using the current configuration, only every other row can be used because the probe lifter is too big to fit between each row



(a)



(b)

Figure 23 – A schematic of the HMAT. (a) A front view and (b) a side view

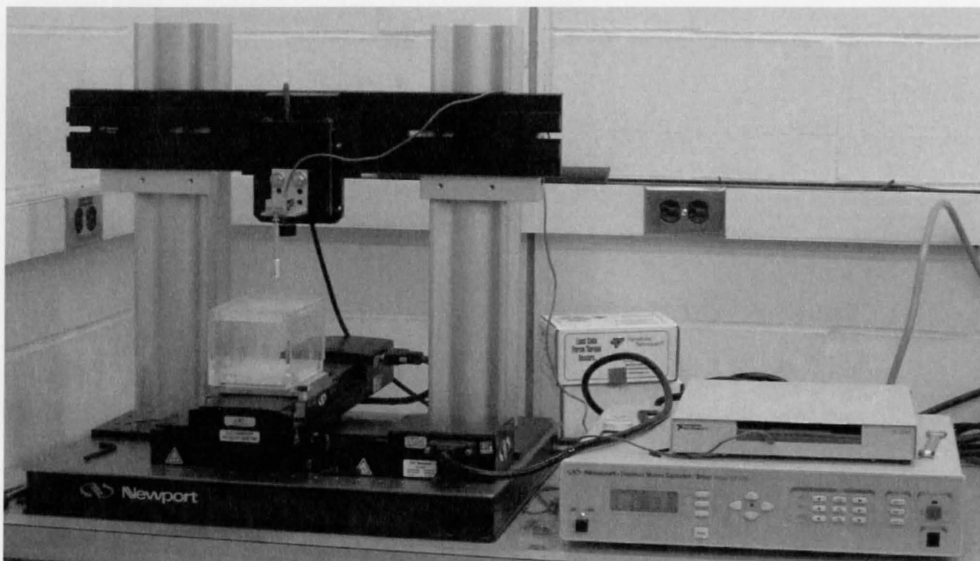


**Figure 24 – The HMAT**

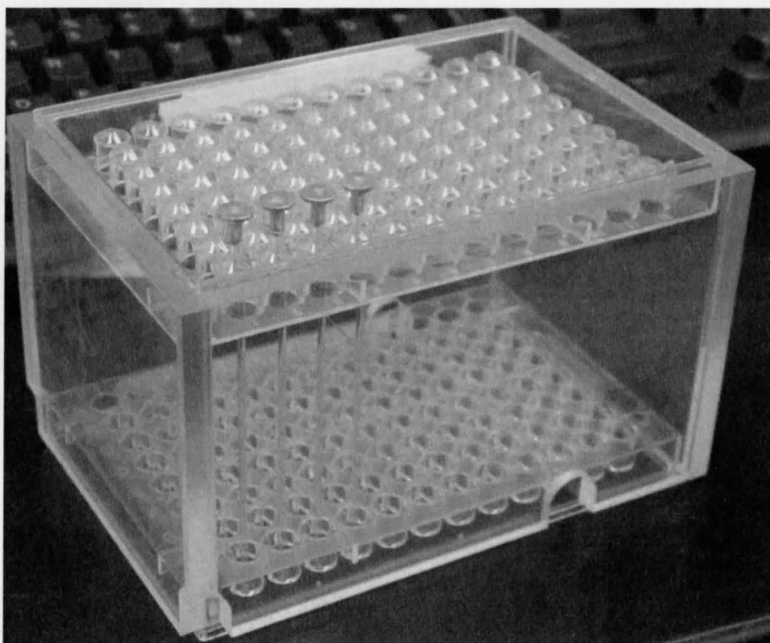


**Figure 25 – The probe box**

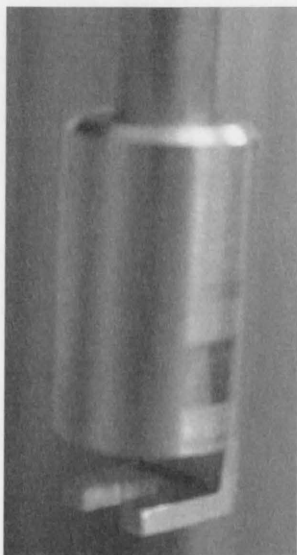


**Figure 26 – The probe lifter**

The user interface is shown in Figure 27. Here, the user can change the following parameters:

- Number of rows containing probes, the number of probes in each row and first row that contains probes
  - o The user is not required to use the entire well plate at a time, but can instead specify a smaller area to be tested
- Delay time
  - o This gives the polymer a chance to relax before testing begins
- Velocity that the probe is lifted out of each well
- The scan rate and the number of scans to read at one time
  - o These parameters effect how many points are on the force curve

The user also has control over the following:

- Homing
  - o Each time the translation stages are turned on they must be homed so that they can find the location of zero on their axis.
- Loading
  - o The probe box holder is moved so that it is most accessible
- Testing
  - o The user can start the test at their own convenience
- Stopping
  - o The user can stop the movement of the z-stage and continue with the test, or can stop the test altogether

The interface displays the following information:

- Current force curve
- Peak force readings for the current row
- Current z-position
- Final 3D surface plot for peak force readings

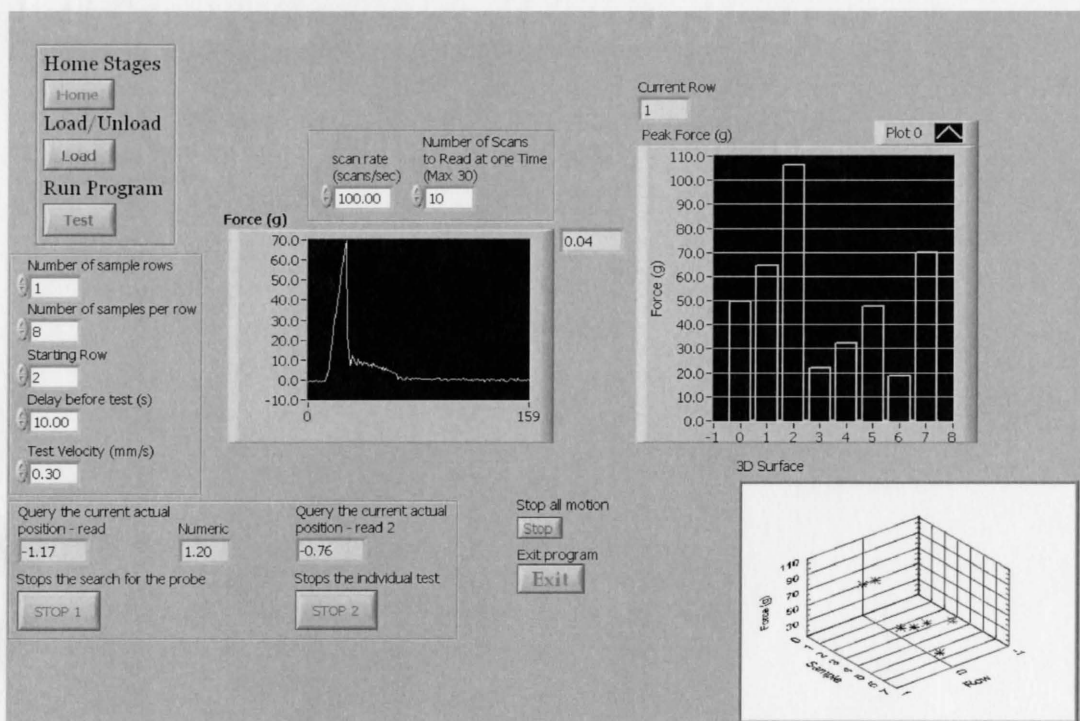
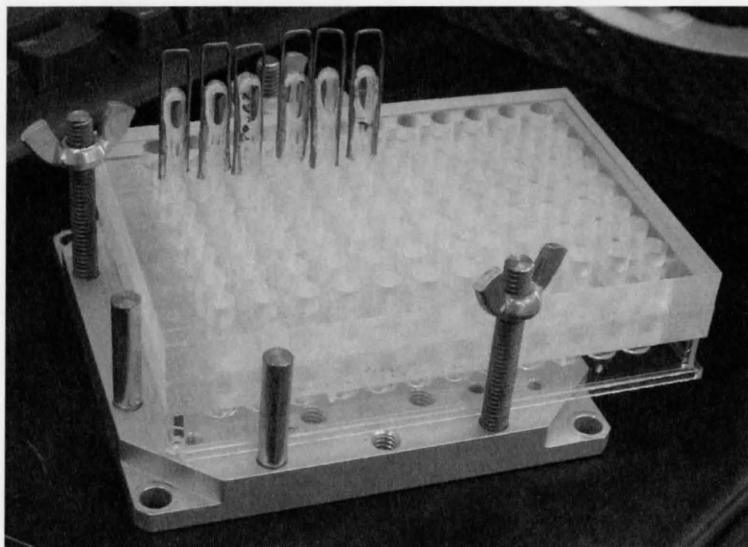


Figure 27 – The user interface

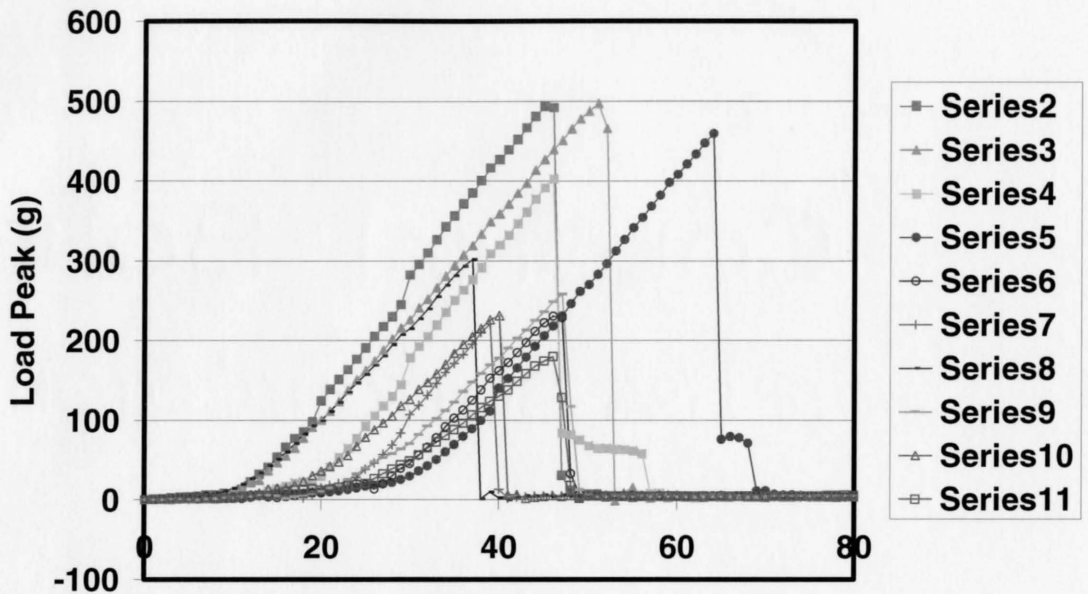
## 4.2.2 The Glass Rods

Probe # 4 was used for these experiments with a hook constructed out of a piece of wire (Figure B.2.3 Appendix A.2) so that the probes could be easily grabbed on to. A holder was constructed which included a plate cover to hold the probes upright at all times (Figure 28). The well plate and plate cover is held down by two screws and held against the side of the holder by another screw on the far side. The experiments done

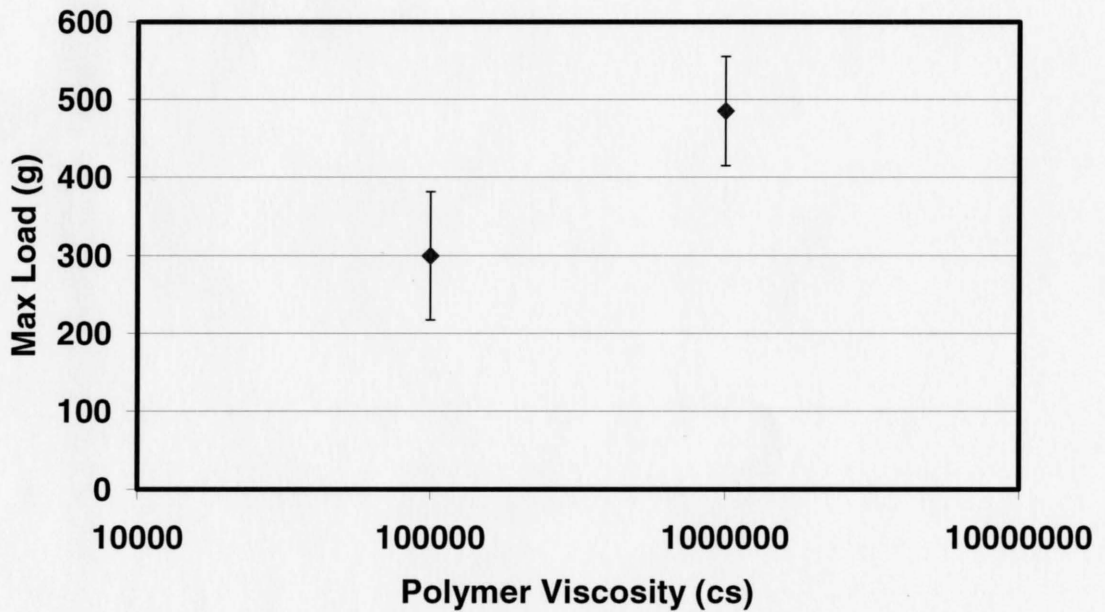
using the glass rods were promising from the start (Figure 29). The curves were straight with a lot of data points up to the pull-off point. Also, there is statistical difference between the two different viscosities. As testing continued, a strong logarithmic correlation was found between polymer viscosity and adhesion strength (Figure 30).



**Figure 28 – The well plate holder**



(a)



(b)

Figure 29 – The first tests done on the HMAT. (a) Load curves taken from the HMAT where curves 2-6 were at 1M cs and curves 7-11 were at 100,000 cs and (b) the maximum load at different viscosities. The experiments shown in graph (a) were done using 0.6 mg PDMS. The experiments shown in graph (b) were done using 0.6 mg PDMS. The error bars are the standard deviation of 5 and 4 samples for the 10,000 and 100,000 viscosities respectively.

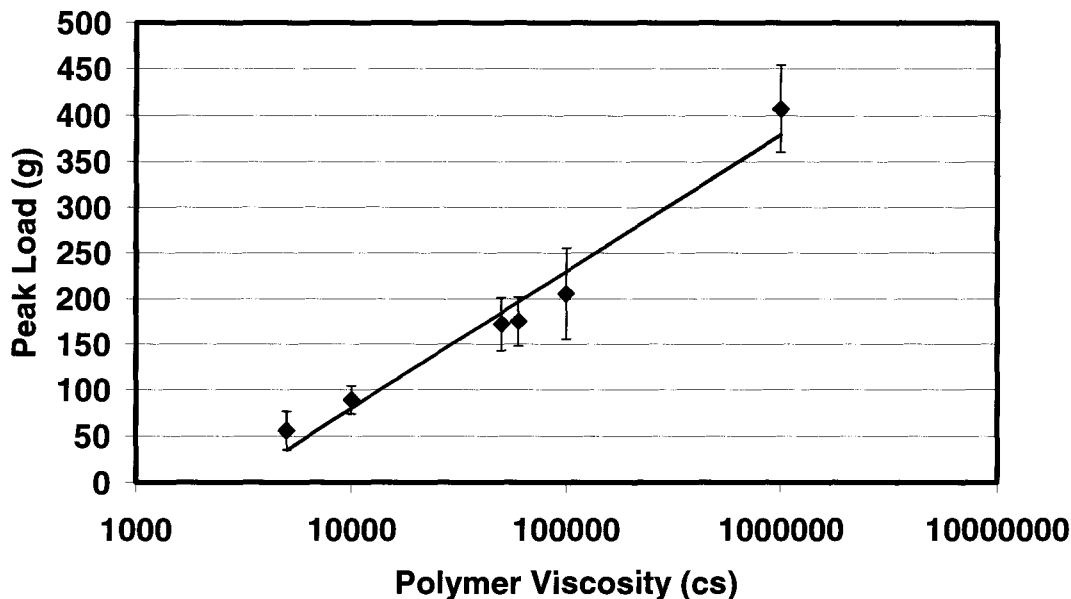


**Figure 30 – Tests done on the HMAT using # 4 probes showing the maximum load at different viscosities and a logarithmic trend line. These experiments were done using 0.35 mg PDMS and were pulled at 0.3 mm/s. The error bars are the standard deviation of 6 samples for all of the data points.**

Because the # 4 probes were so promising, other experiments were done using these probes. Figure 31 shows a comparison of different pull-off speeds. As expected, the faster the pull-off speed, the greater the adhesion strength. Also, it was found that as the pull-off speed was increased, the variation in the measurements also increased.

Figure 32 shows an experiment comparing different amounts of polymer in each well. The amount of polymer used doesn't seem to affect the adhesion strength as much as it affects the standard deviation of the measurements. In general, the greater the amount of polymer, the more variation is seen in the readings.

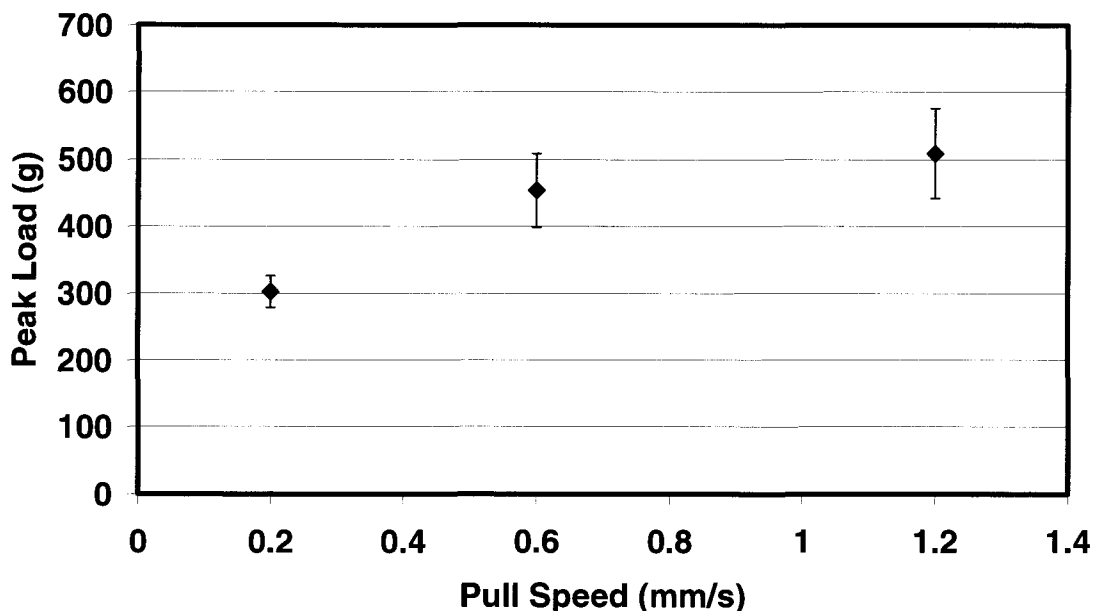


Figure 31 – Tests done on the HMAT using # 4 probes showing the maximum load at different pull-off speeds. These experiments were done using 0.325 mg of 1M cs PDMS. The error bars are the standard deviation of 6 samples for all of the data points.

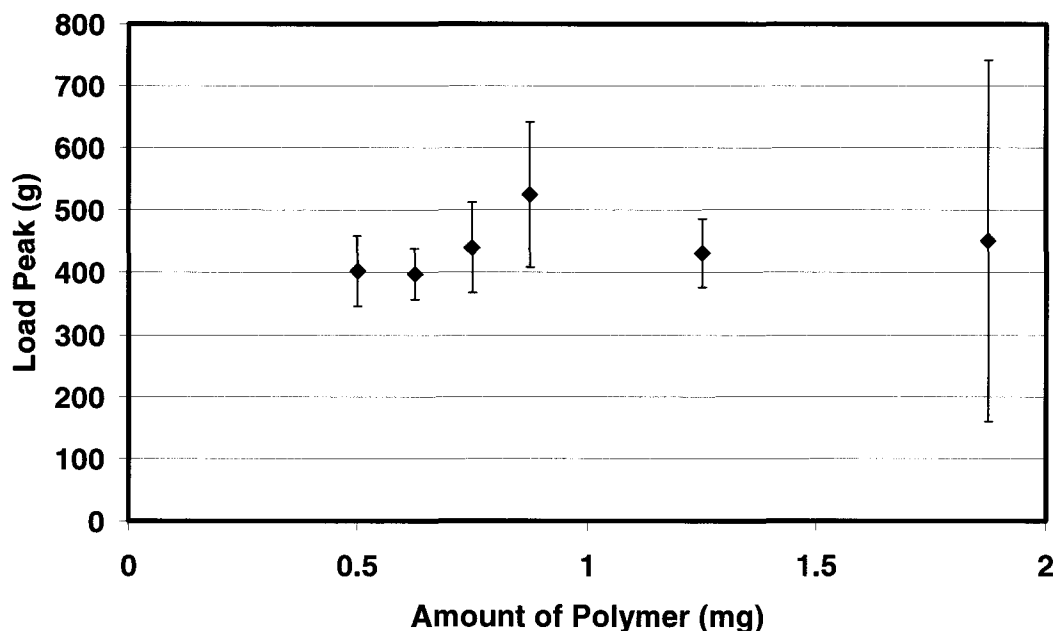
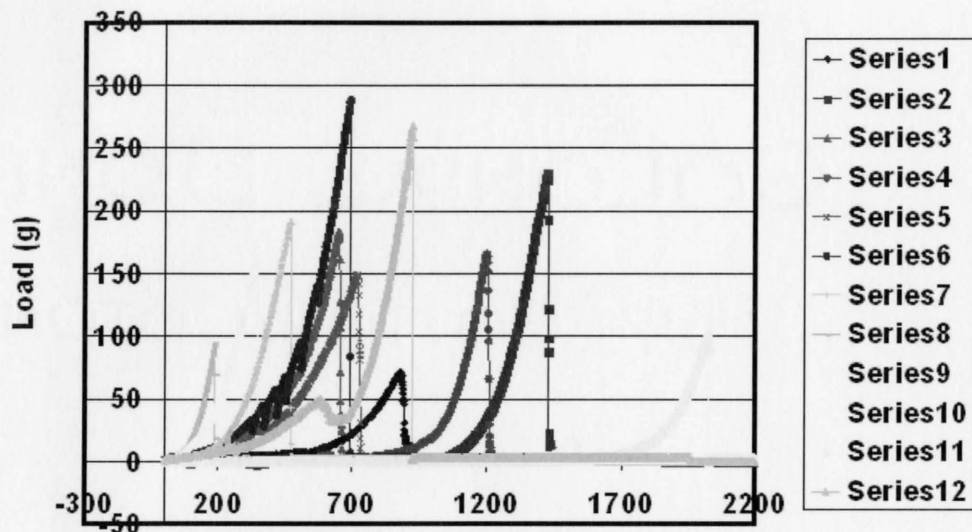


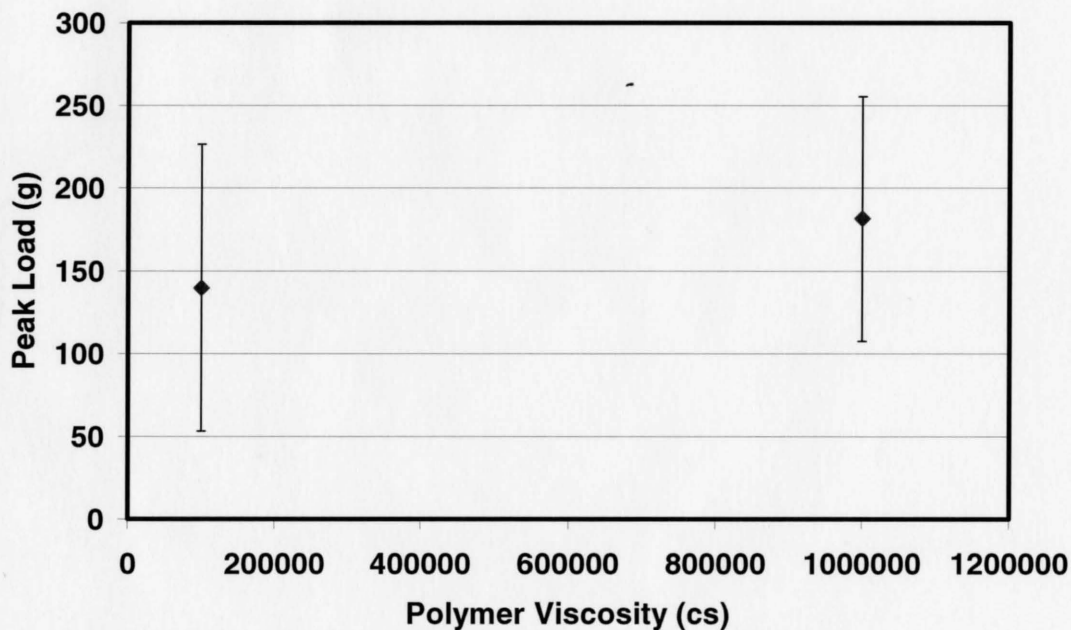
Figure 32 – Tests done on the HMAT using # 4 probes showing the maximum load using different amounts of polymer. These experiments were done using 1M cs PDMS and were pulled at 0.4 mm/s. The error bars are the standard deviation of 3 samples for all of the data points.

One of the possible problems with the probes with loops attached (probe #4) was that the point of contact between the hook and the loop would not necessarily be in the exact centre since both have a curved shape. Therefore, during testing the hook may slide before reaching a stable position or may not pull directly vertically. To try to solve this, another probe was constructed. Two posts were glued to the glass rods and suture string was tied across the top (Figure B.1.6 Appendix A.1).

Figure 33 shows the results from using the # 6 probes. Because the hook first has to draw the string taught, the curve approaches the maximum more gradually than it did when using the # 4 probes. The standard deviations are very large and there is no statistical difference between the two different polymer viscosities. Also, there were difficulties in trying to get the hook to catch the string as it would not necessarily be in the correct position directly above the probe, or the string would get caught on the hook when moving to the next sample.



(a)



(b)

Figure 33 – Tests done on the HMAT using # 6 probes. (a) Load curves taken from the adhesion apparatus and (b) the maximum load at different viscosities. The experiments shown in graphs (a) and (b) were done using 0.6 mg of PDMS. The error bars are the standard deviation of 6 samples for both data points.

### **4.2.3 The capillary Tubes**

The capillary tubes still showed promise as they had the most potential of meeting the design criteria, however they were unacceptable in their current form. Hence, further work was put into improving them. The data from the capillary tube probes in their initial form (Figure 34) were scattered and had a lot of sample-to-sample variation. This was due to a few reasons. First, these experiments were all done with the 1000 g load cell, so the measurements were at the very bottom of the instruments' range. For this reason, in future tests using the capillary tube probes the 100 g load cell was used. However, the main problem was with the probes themselves. Even though the plate cover for these tests had smaller holes for the smaller diameter probes, there was still some space for movement so that the probe would not rub against the cover during the test. This was enough movement so that the probes could tilt and move before and during the test. To try to solve this issue, in later tests the height of the plate cover was raised to allow the least possible deviation from vertical.

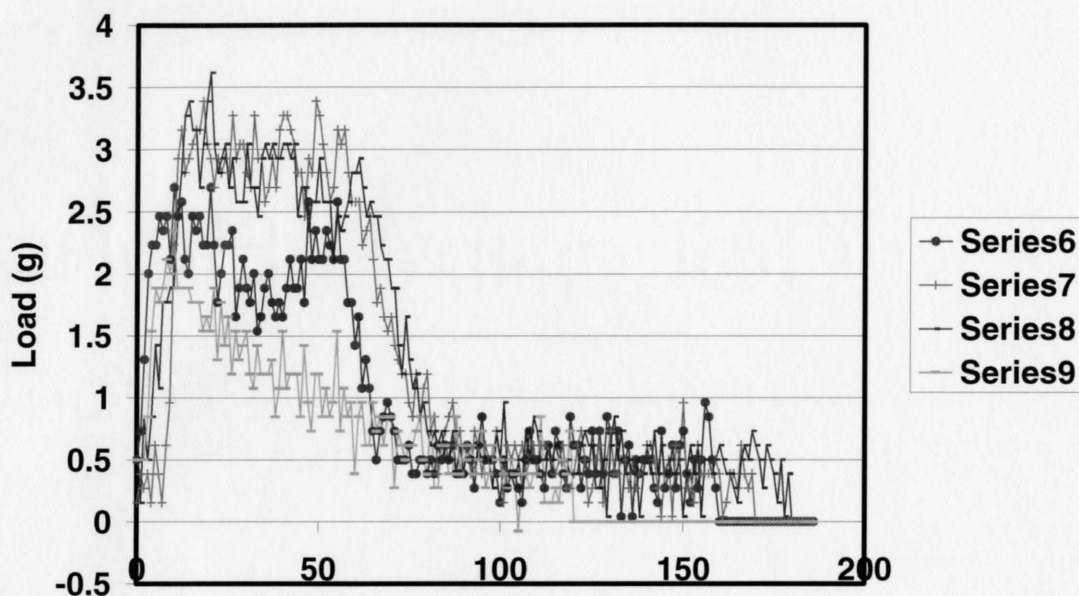


**Figure 34 – Load curves for the first capillary tube experiments on the HMAT. These experiments were done using 0.575 mg of 1M cs PDMS.**

In an effort to try to get the hook to pull normal to the well plate, probes # 7 were constructed (Figure B.1.7 Appendix A.1). They were made by gluing a smaller piece of glass to the capillary tubes to make a ‘t’ shaped probe. A new hook was constructed that was similar to a forklift (Figure B.2.4 Appendix A.2) that would lift the probe vertically by lifting both sides of the probe simultaneously. Results showed this probe type was promising (Figure 35). There is a trend with statistical significance except for the measurements at 100,000 cs. These ideas were used in the construction of the final form of the hook and probe.

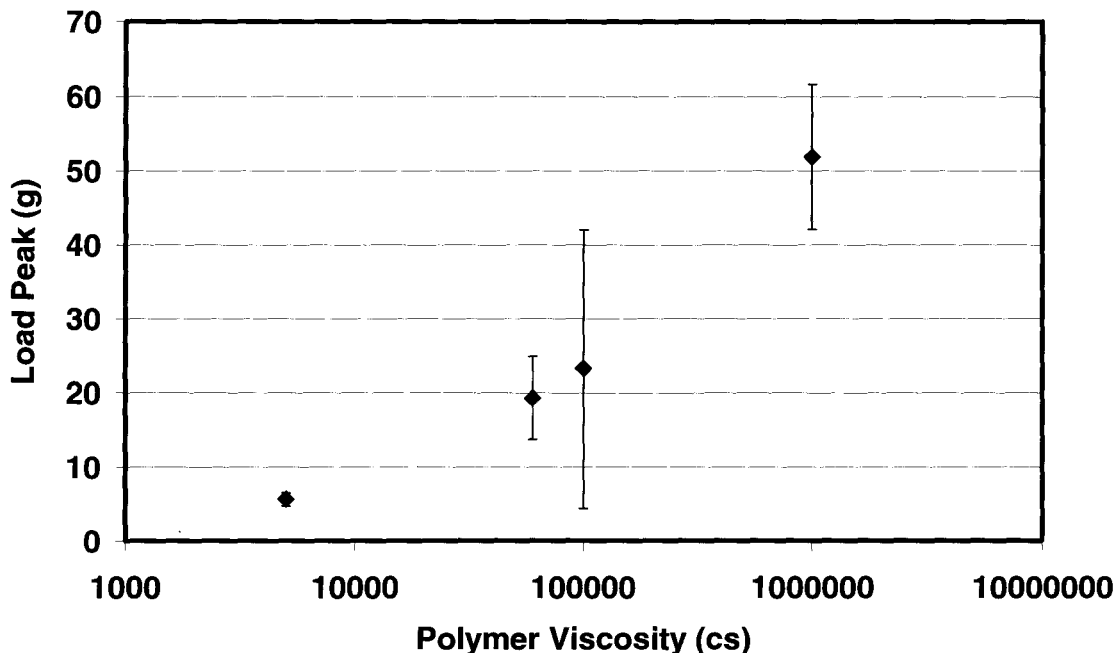


**Figure 35 – Tests done on the HMAT using # 7 probes showing the maximum load at different viscosities. These experiments were done using 0.15 mg PDMS and were pulled at 0.3 mm/s. The error bars are the standard deviation of 2, 4, 4 and 5 samples for the increasing viscosities.**

#### 4.2.4 The final tests

The final sets of tests were done using the hook and probe shown above in Figure 26 and Figure B.1.8 Appendix A.1. The probe box was altered so that cover was raised as much as possible to reduce tilting of the probes, and the cover itself was constructed by taking a spare well plate and drilling small holes in each well so that we could be sure that they were exactly in line with the sample wells (Figure 25). The first test using this configuration was promising (Figure 36). There is statistically significant difference between the two measurements. Subsequent tests again revealed a logarithmic trend (Figure 37). As expected, as the viscosity of the polymer increases, so does the adhesive strength.

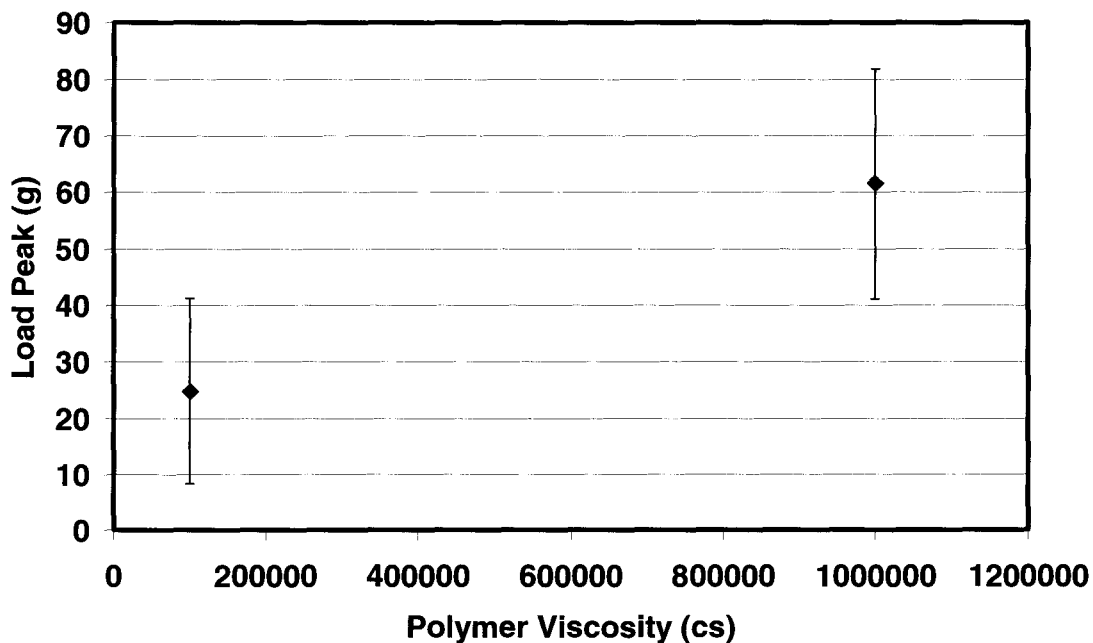


Figure 36 – Tests done on the HMAT using the final probes showing the maximum load at different viscosities. These experiments were done using 0.25 mg PDMS and were pulled at 0.3 mm/s. The error bars are the standard deviation of 5 samples for both data points

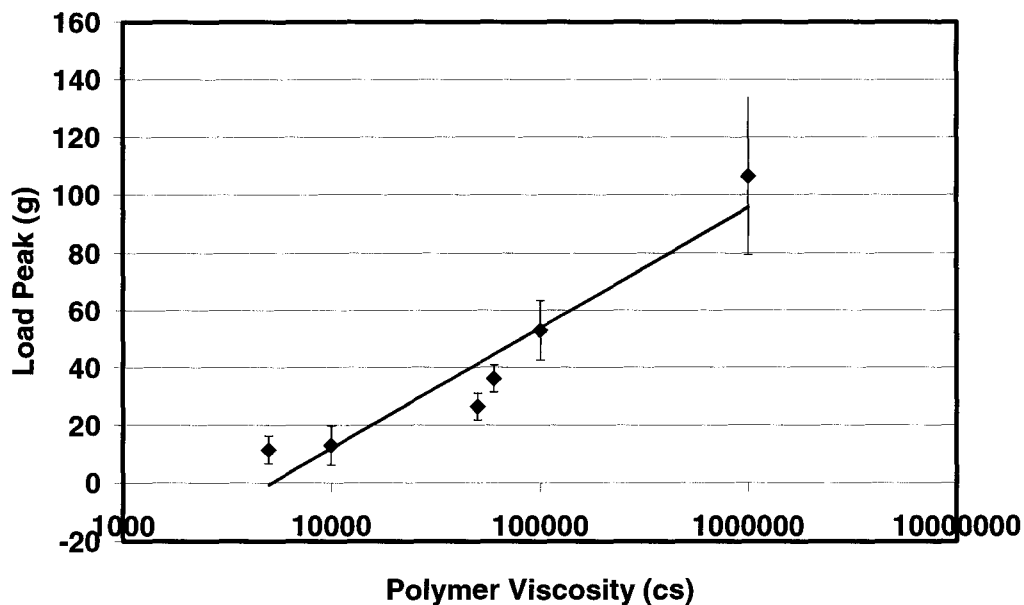


Figure 37 – Tests done on the HMAT using the final probes showing the maximum load at different viscosities. These experiments were done using 0.375 mg PDMS and were pulled at 0.3 mm/s. The error bars are the standard deviation of 7, 8, 7, 5, 7 and 7 samples for the increasing viscosities.

These tests showed that the final form of the HMAT gives good results with relatively small standard deviations that are acceptable for a test that is simply used for an initial screening of the polymer. The probes are easy to place and pull out and could be easily mass-produced by injection moulding or machining the flat caps to be glued to the capillary tubes.

## 5 Conclusion

At the conclusion of this project the HMAT was constructed and is able to perform 48 adhesion tests consecutively at about 30 s per test for a total of 24 min. The design utilized the rapid serial idea. The tests are rapid, automatic and less than half a gram of adhesive is needed. After many attempts, the final probes met the design requirements in that they are easy to place and pull out and could be easily mass-produced. Likewise, a probe box was found that ensures that the probes are as normal to the wells as possible while not hindering the actual tests. The tests on PDMS show that repeatability is still an issue as the standard deviations of the force are about 20% of the mean value. However, this machine is only designed to be used for primary screening, so accuracy is not as critical as it would be for later tests that would and should be performed on the adhesives that give the best results. Nonetheless, further work should be done to find better ways of preparing the samples. Further work could be focused on surface chemistry by changing the chemistry of the glass probes and/or the PS well plates in order to study the change in adhesion to well defined surfaces.

- <sup>1</sup> L.H. Sperling, Introduction to Physical Polymer Science, John Wiley & Sons, Bethlehem Pennsylvania, 1986
- <sup>2</sup> R. Pelton, Interfacial Engineering 4Z03 course notes, 2003
- <sup>3</sup> A. V. Pocius, Adhesion and Adhesives Technology, An Introduction 2<sup>nd</sup> Edition, Hanser Gardner Publications Inc, Ohio, 2002
- <sup>4</sup> K. L. Johnson, K. Kendal, A. D. Roberts, *Procedures of the Royal Society of London A*, 1971, 324, 301-313
- <sup>5</sup> K. Kendall, Molecular Adhesion and its Applications, Kluwer Academic/Plenum Publishers, New York, 2001
- <sup>6</sup> A. Falsafi, P. Deprez, F. S. Bates, M. Tirrell, *Journal of Rheology*. 1997, 41(6)
- <sup>7</sup> M. Rundlöf, M. Karlsson, L. Wagberg, E. Poptoshev, M. Rutland, P. Claesson, *Journal of Colloid and Interface Science*, 2000, 230, 441-447
- <sup>8</sup> M. Chaudhury, T. Weaver, C. Y. Hui, E. J. Kramer, *Journal of Applied Physics*, 1996, 80(1), 30-37
- <sup>9</sup> A. W. Adamson, Physical Chemistry of Surfaces Fifth Edition, John Wiley & Sons, U.S., 1990
- <sup>10</sup> A. Baszkin, L. Ter-Minassian-Saraga, *Polymer*, 1978, 11, 1083
- <sup>11</sup> J. Vlachopoulos, Courseware for 4X03 – Introduction to Plastics Processing, McMaster University, 2001
- <sup>12</sup> P. G. Schultz and X-D Xiang, *Current Opinion in Solid State & Materials Science*, 1998, 3, 153-158
- <sup>13</sup> E. W. McFarland, W. Henry Weinberg, *TIBTech*, 1999, 17, 107-115
- <sup>14</sup> R. Hoogenboom, M. A. R. Meier, U. S. Schubert, *Macromolecular Rapid Communications*, 2003, 24, 15-32
- <sup>15</sup> E. J. Amis, *Nature Materials*, Feb 2004, 3, 83-84
- <sup>16</sup> R. Iden, W. Schrof, J. Haderler, S. Lehmann, *Macromolecular Rapid Communications*, 2003, 24, 63-72
- <sup>17</sup> R. A. Potyrailo, *Macromolecular Rapid Communications*, 2004, 25, 77-94
- <sup>18</sup> A. J. Crosby, A. Karim, E. J. Amis, *Journal of Polymer Science Part B: Polymer Physics*, 2003, 41, 883-891
- <sup>19</sup> R. A. Potyrailo, R. J. Wroczynski, J. E. Pickett, M. Rubensztajn, *Macromolecular Rapid Communications*, 2003, 24 No1, 124-130
- <sup>20</sup> K. S. Lam, S. E. Salmon, E. M. Hersh, V. J. Hruby, W. M. Kazmierski, R. J. Knapp, *Nature*, Nov 1991, 354, 82-84
- <sup>21</sup> J.-L. Sormana, J. C. Meredith, *Material Research Innovations*, 2003, 7, 295-301
- <sup>22</sup> J.-B. D. Green, *Analytica Chimica Acta*, 2003, 496, 267-277
- <sup>23</sup> M. B. Kossuth, D. A. Hajduk, C. Fritag, J. Varni, *Macromolecular Rapid Communications*, 2004, 25, 243-248
- <sup>24</sup> C. Stafford, NIST Combinatorial Methods Center, <http://polymers.msel.nist.gov/combi/High-Throughput-Methods-Evaluation-Adhesive-Performance.html>, Last visited Oct 26 2004
- <sup>25</sup> A. Tuchbreiter, J. Marquardt, B. Kappler, J. Honerkamp, M. O. Kristen, R. Mühlaupt, *Macromolecular Rapid Communications*, 2003, 24, 47-62

# APPENDIX A - LabView Program



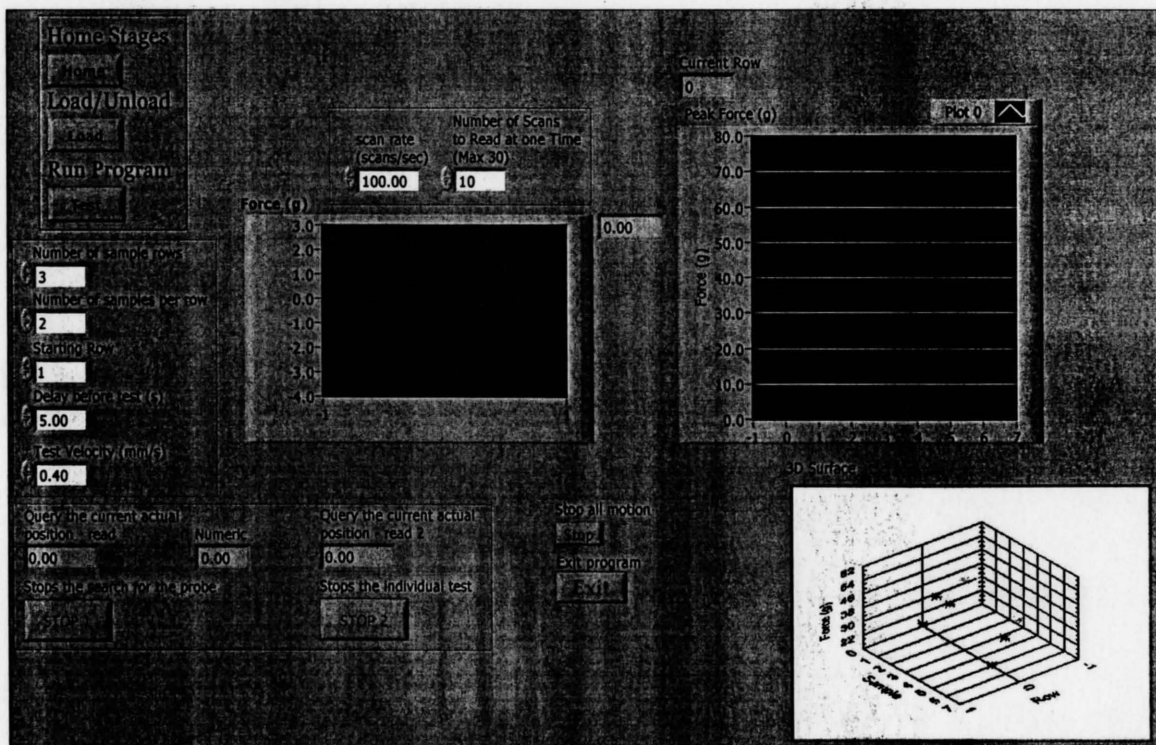
100g load cell long hook2, pause, t-probe, distance, every (C:\BACKUP\100g load cell long hook2, pause, t-probe, distance, every other row, one calibration.vi  
Last modified on 30/01/2005 at 12:20 PM  
Printed on 30/01/2005 at 12:23 PM

## Connector Pane



## 100g load cell long hook2, pause, t-probe, distance, every ot

## Front Panel





100g load cell long hook2, pause, t-probe, distance, every ( (

C:\BACKUP\100g load cell long hook2, pause, t-probe,  
distance, every other row, one calibration.vi

Last modified on 30/01/2005 at 12:20 PM

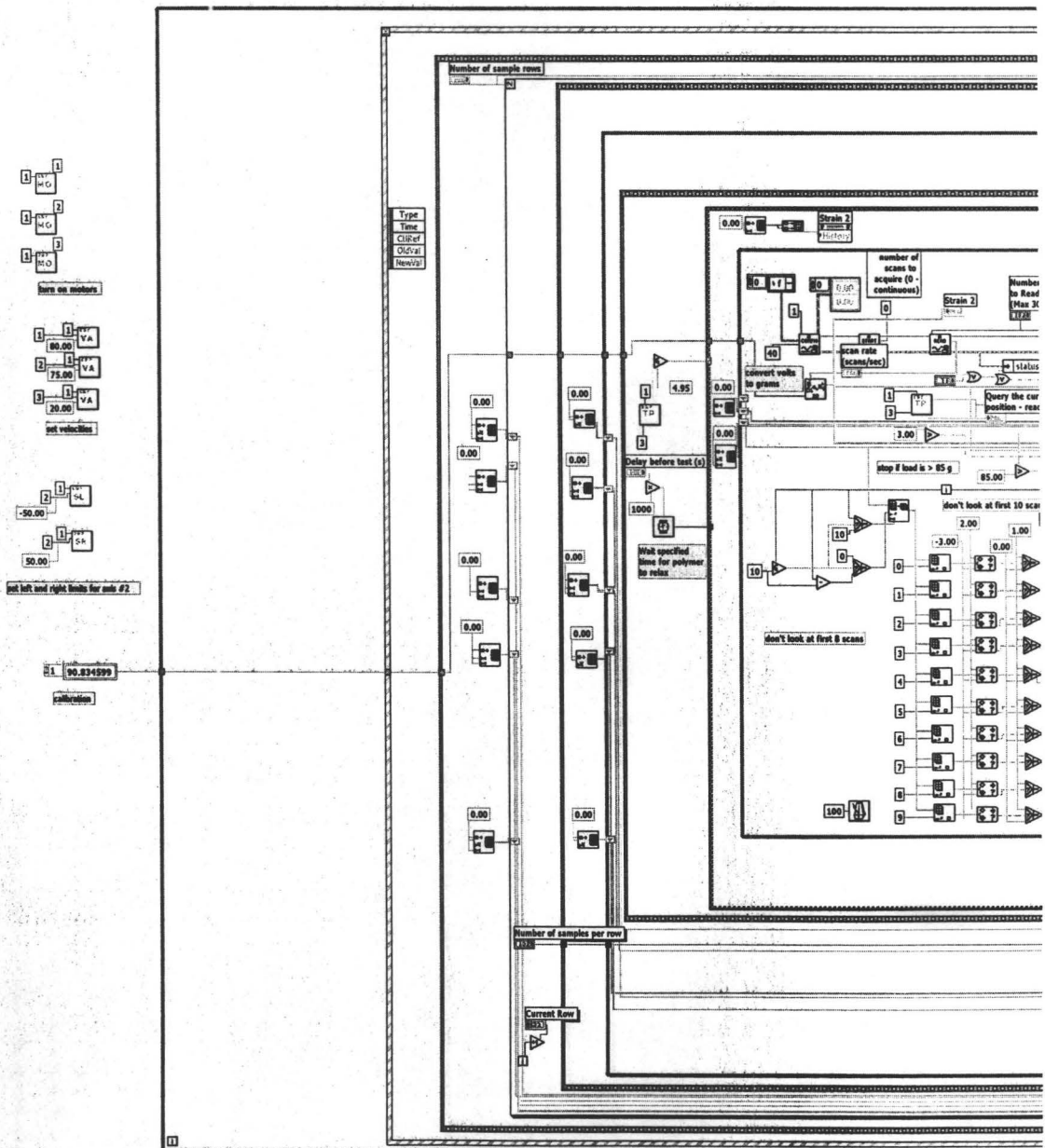
Printed on 30/01/2005 at 12:23 PM

**her row, one calibration.vi**



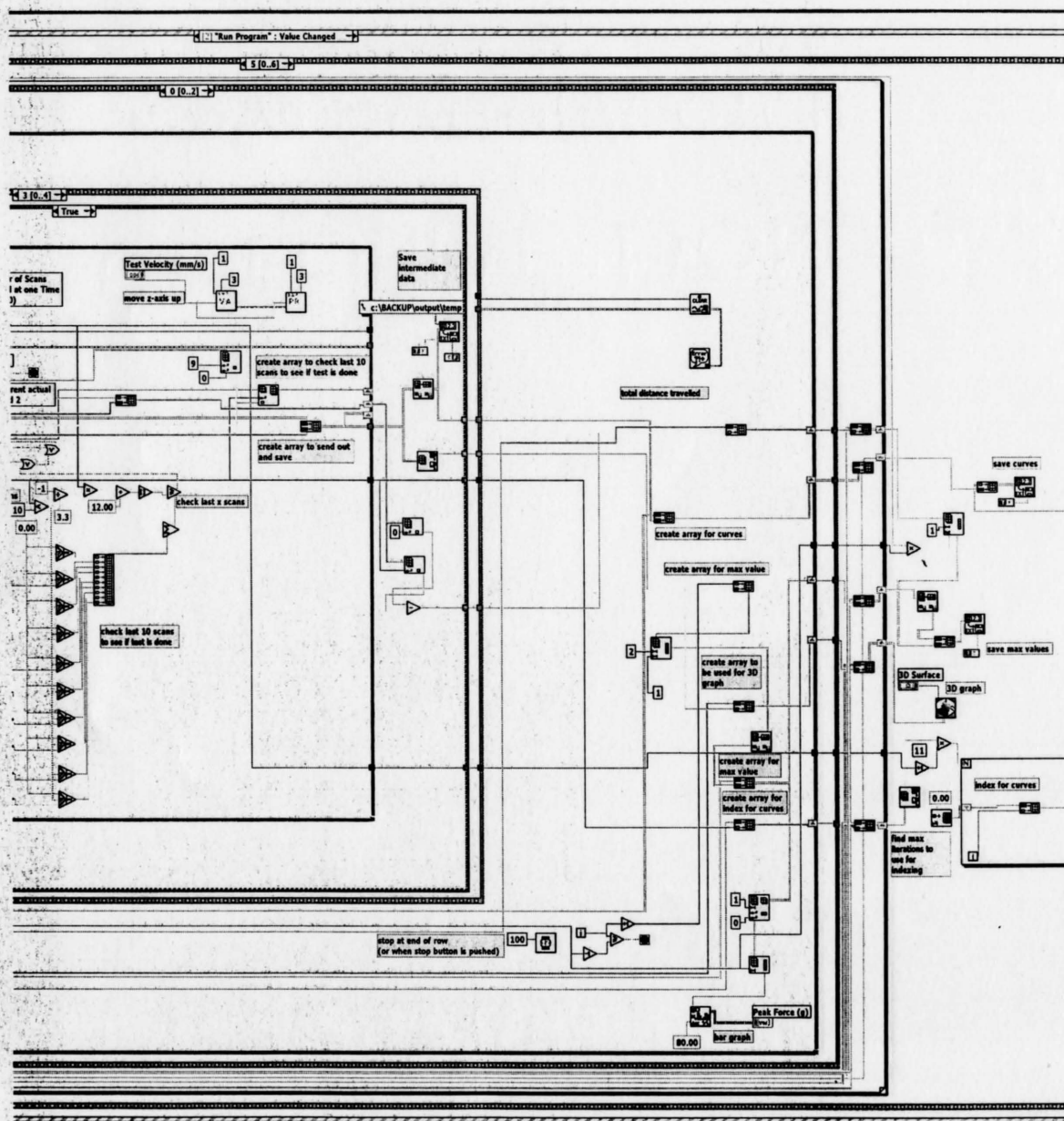
100g load cell long hook2, pause, t-probe, distance, every (   
 C:\BACKUP\100g load cell long hook2, pause, t-probe,   
 distance, every other row, one calibration.vi   
 Last modified on 30/01/2005 at 12:20 PM   
 Printed on 30/01/2005 at 12:23 PM

Block Diagram



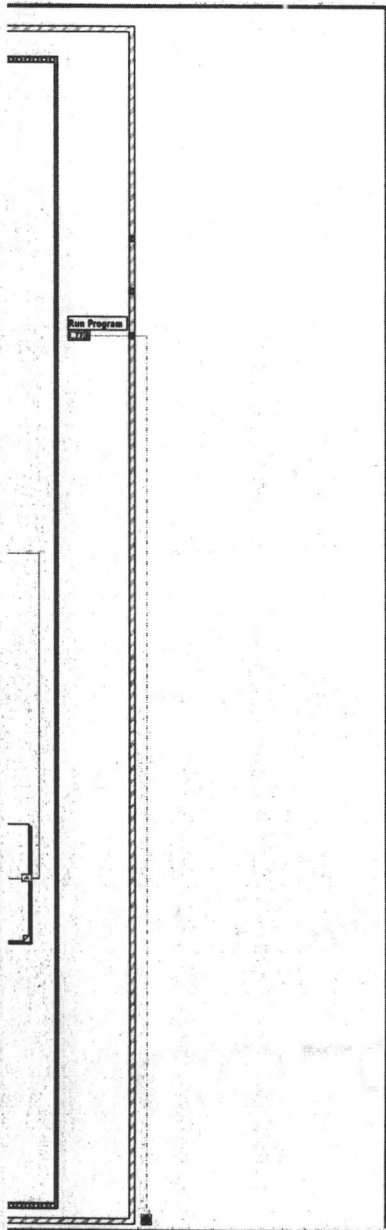


100g load cell long hook2, pause, t-probe, distance, every (   
 C:\BACKUP\100g load cell long hook2, pause, t-probe,   
 distance, every other row, one calibration.vi   
 Last modified on 30/01/2005 at 12:20 PM   
 Printed on 30/01/2005 at 12:23 PM





100g load cell long hook2, pause, t-probe, distance, every ( (C:\BACKUP\100g load cell long hook2, pause, t-probe, distance, every other row, one calibration.vi  
Last modified on 30/01/2005 at 12:20 PM  
Printed on 30/01/2005 at 12:23 PM



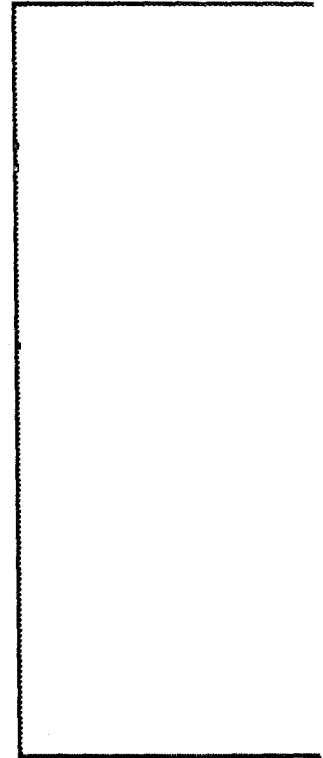


100g load cell long hook2, pause, t-probe, distance, every ( (

C:\BACKUP\100g load cell long hook2, pause, t-probe,  
distance, every other row, one calibration.vi

Last modified on 30/01/2005 at 12:20 PM

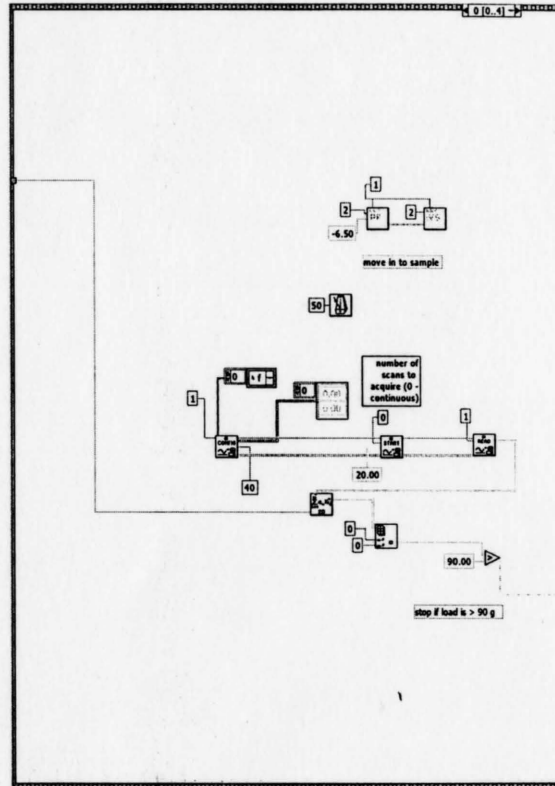
Printed on 30/01/2005 at 12:23 PM





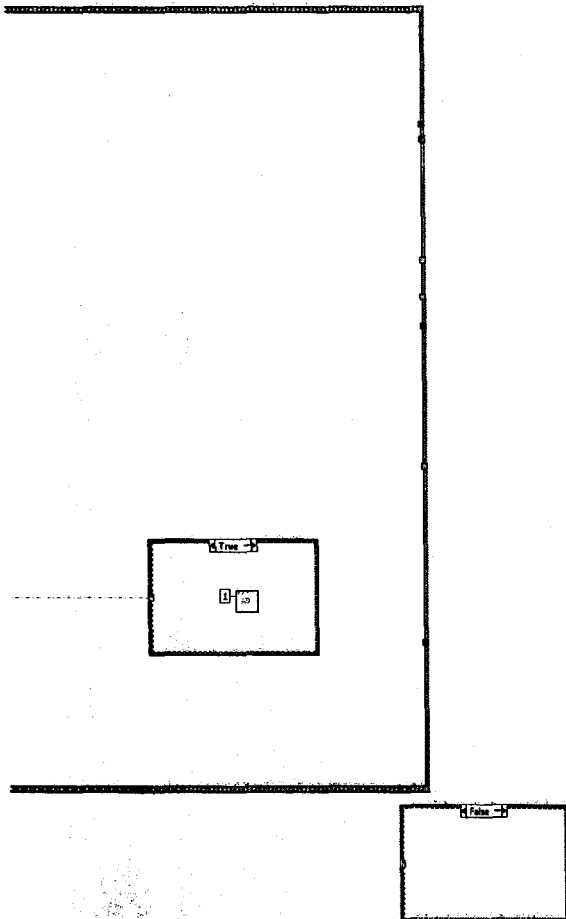


100g load cell long hook2, pause, t-probe, distance, every (C:\BACKUP\100g load cell long hook2, pause, t-probe, distance, every other row, one calibration.vi  
Last modified on 30/01/2005 at 12:20 PM  
Printed on 30/01/2005 at 12:23 PM



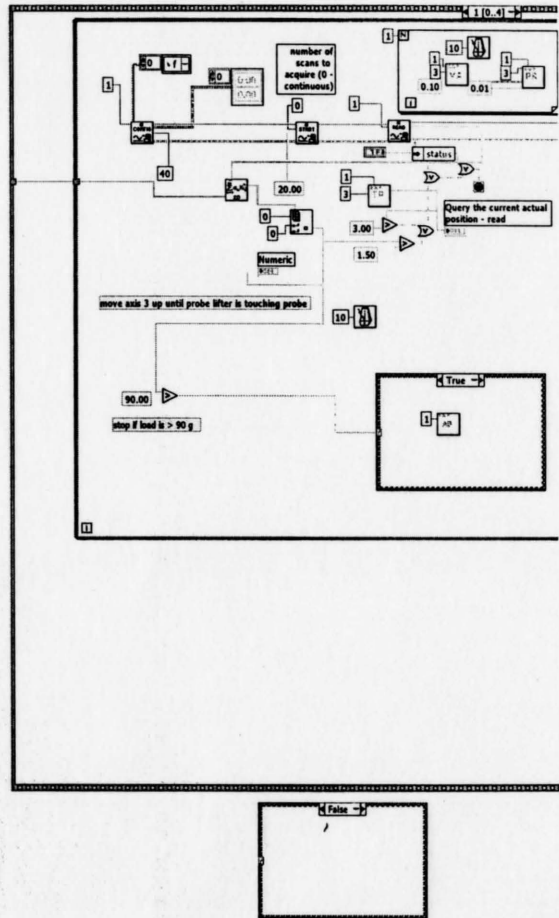


100g load cell long hook2, pause, t-probe, distance, every (C:\BACKUP\100g load cell long hook2, pause, t-probe, distance, every other row, one calibration.vi  
Last modified on 30/01/2005 at 12:20 PM  
Printed on 30/01/2005 at 12:23 PM





100g load cell long hook2, pause, t-probe, distance, every  
C:\BACKUP\100g load cell long hook2, pause, t-probe,  
distance, every other row, one calibration.vi  
Last modified on 30/01/2005 at 12:20 PM  
Printed on 30/01/2005 at 12:23 PM

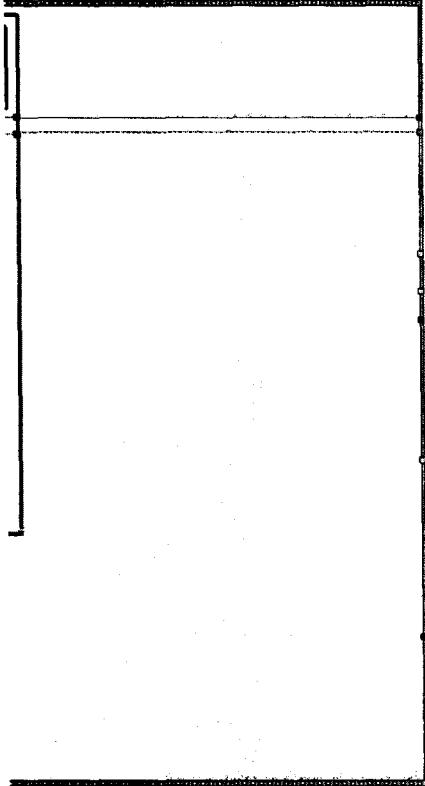




100g load cell long hook2, pause, t-probe, distance, every  
C:\BACKUP\100g load cell long hook2, pause, t-probe,  
distance, every other row, one calibration.vi

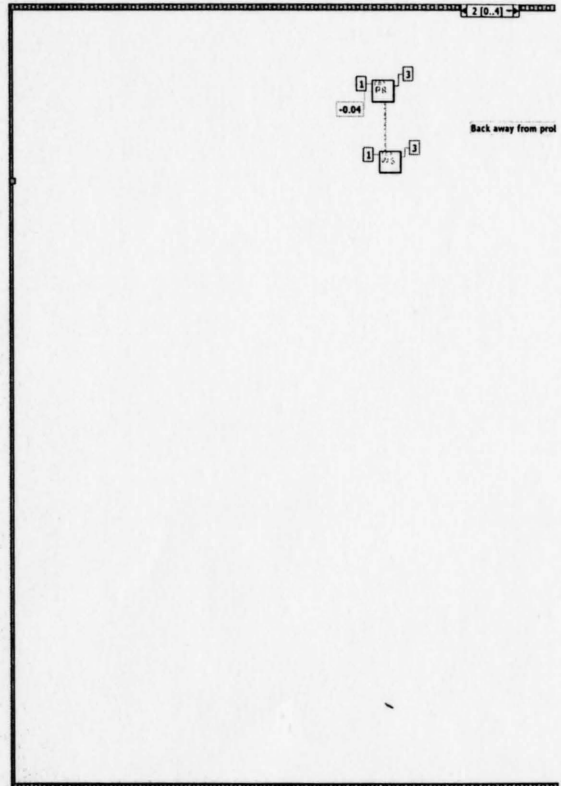
Last modified on 30/01/2005 at 12:20 PM

Printed on 30/01/2005 at 12:23 PM



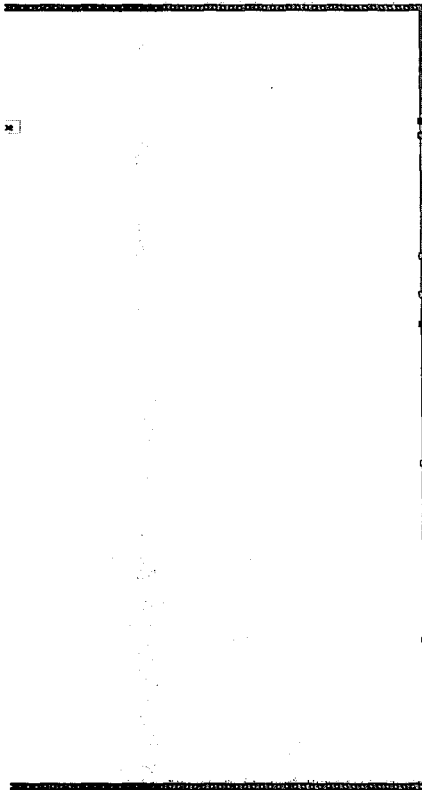


100g load cell long hook2, pause, t-probe, distance, every  
C:\BACKUP\100g load cell long hook2, pause, t-probe,  
distance, every other row, one calibration.vi  
Last modified on 30/01/2005 at 12:20 PM  
Printed on 30/01/2005 at 12:23 PM



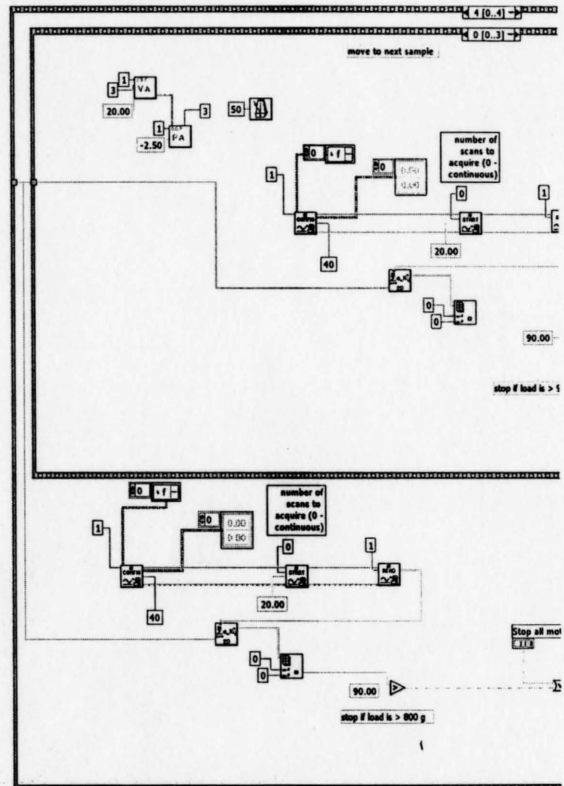


100g load cell long hook2, pause, t-probe, distance, every  
C:\BACKUP\100g load cell long hook2, pause, t-probe,  
distance, every other row, one calibration.vi  
Last modified on 30/01/2005 at 12:20 PM  
Printed on 30/01/2005 at 12:23 PM



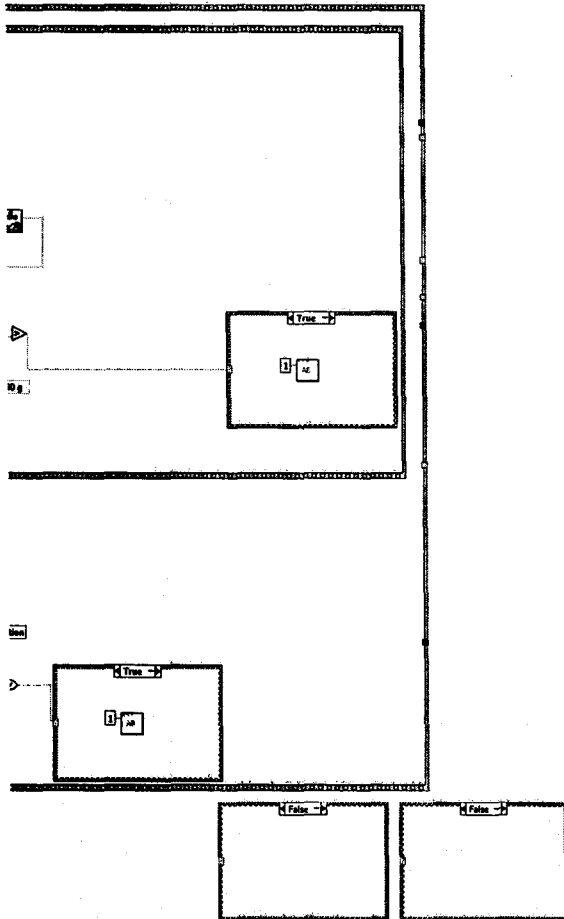


100g load cell long hook2, pause, t-probe, distance, every  
C:\BACKUP\100g load cell long hook2, pause, t-probe,  
distance, every other row, one calibration.vi  
Last modified on 30/01/2005 at 12:20 PM  
Printed on 30/01/2005 at 12:23 PM



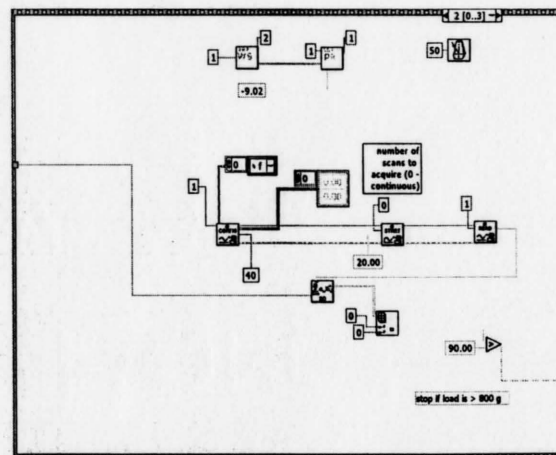
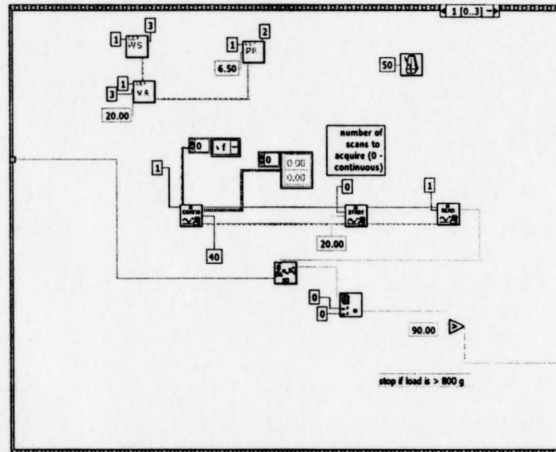


100g load cell long hook2, pause, t-probe, distance, every  
C:\BACKUP\100g load cell long hook2, pause, t-probe,  
distance, every other row, one calibration.vi  
Last modified on 30/01/2005 at 12:20 PM  
Printed on 30/01/2005 at 12:23 PM



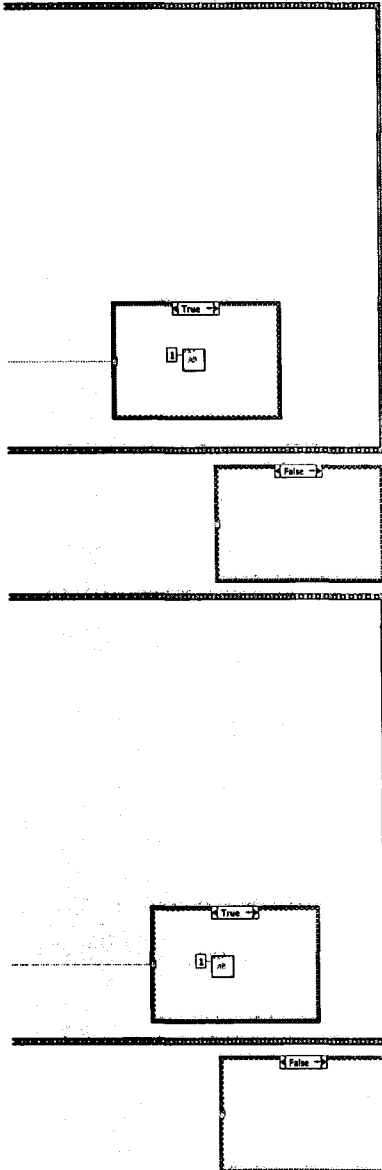


100g load cell long hook2, pause, t-probe, distance, every  
C:\BACKUP\100g load cell long hook2, pause, t-probe,  
distance, every other row, one calibration.vi  
Last modified on 30/01/2005 at 12:20 PM  
Printed on 30/01/2005 at 12:23 PM





100g load cell long hook2, pause, t-probe, distance, every  
C:\BACKUP\100g load cell long hook2, pause, t-probe,  
distance, every other row, one calibration.vi  
Last modified on 30/01/2005 at 12:20 PM  
Printed on 30/01/2005 at 12:23 PM

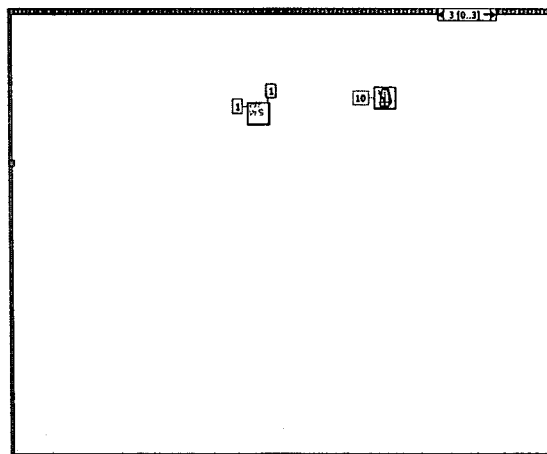




100g load cell long hook2, pause, t-probe, distance, every  
C:\BACKUP\100g load cell long hook2, pause, t-probe,  
distance, every other row, one calibration.vi

Last modified on 30/01/2005 at 12:20 PM

Printed on 30/01/2005 at 12:23 PM



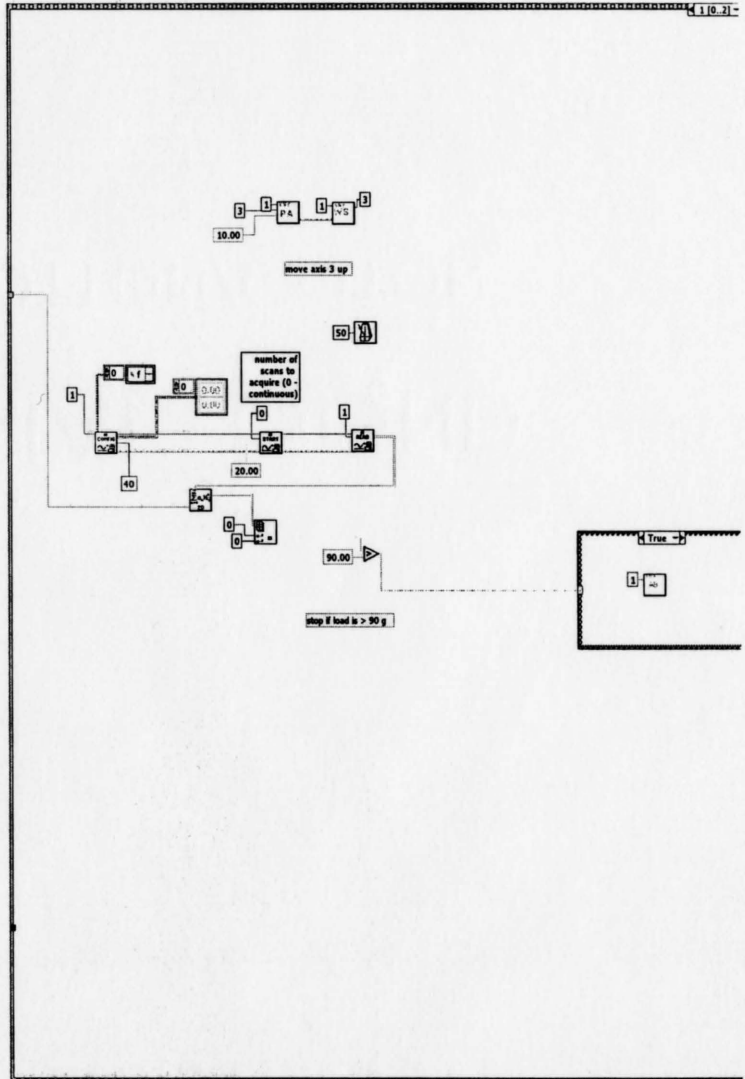


100g load cell long hook2, pause, t-probe, distance, every  
C:\BACKUP\100g load cell long hook2, pause, t-probe,  
distance, every other row, one calibration.vi  
Last modified on 30/01/2005 at 12:20 PM  
Printed on 30/01/2005 at 12:23 PM



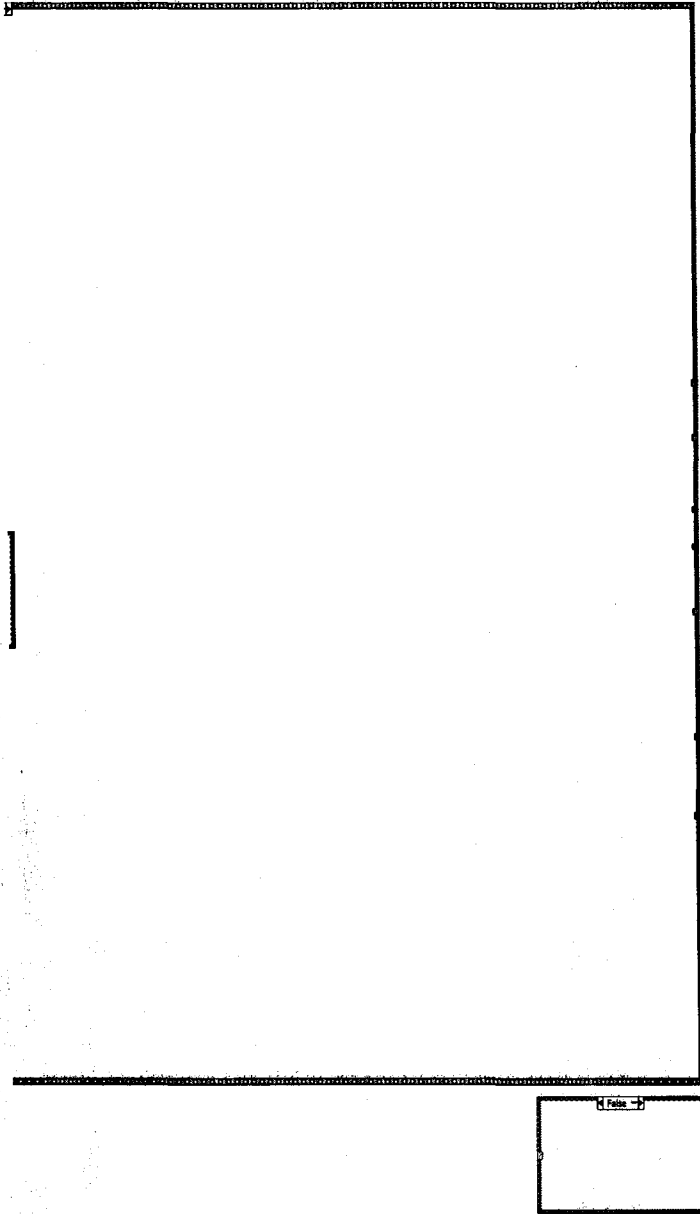


100g load cell long hook2, pause, t-probe, distance, every  
C:\BACKUP\100g load cell long hook2, pause, t-probe,  
distance, every other row, one calibration.vi  
Last modified on 30/01/2005 at 12:20 PM  
Printed on 30/01/2005 at 12:23 PM



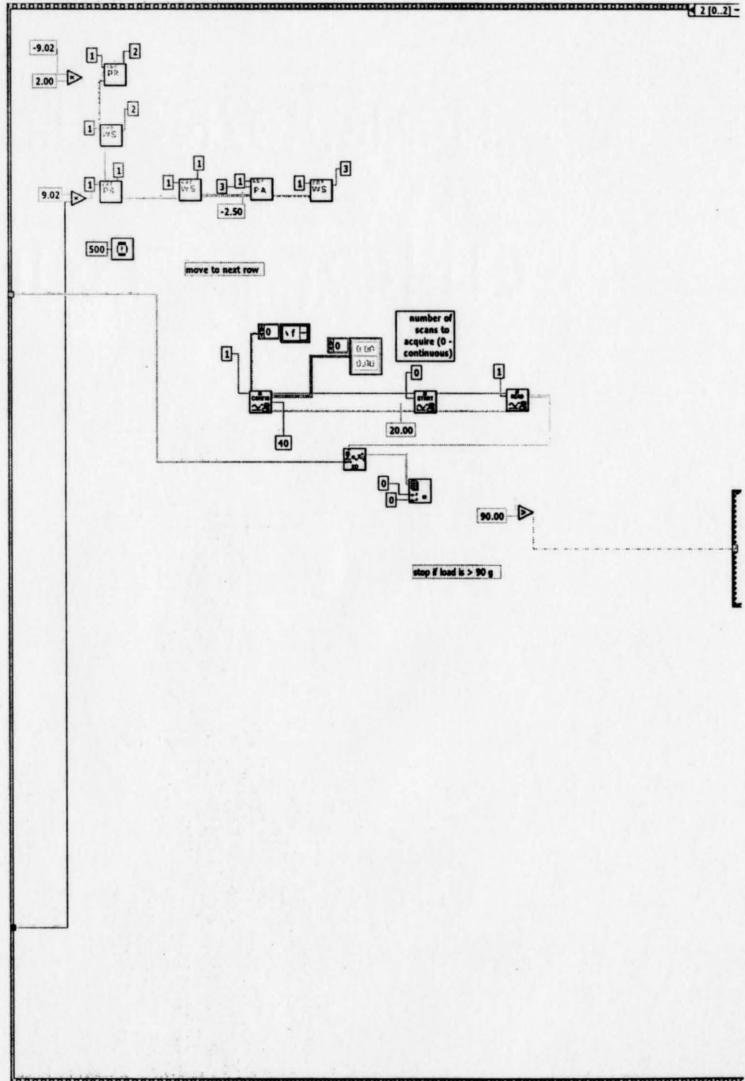


100g load cell long hook2, pause, t-probe, distance, every  
C:\BACKUP\100g load cell long hook2, pause, t-probe,  
distance, every other row, one calibration.vi  
Last modified on 30/01/2005 at 12:20 PM  
Printed on 30/01/2005 at 12:23 PM



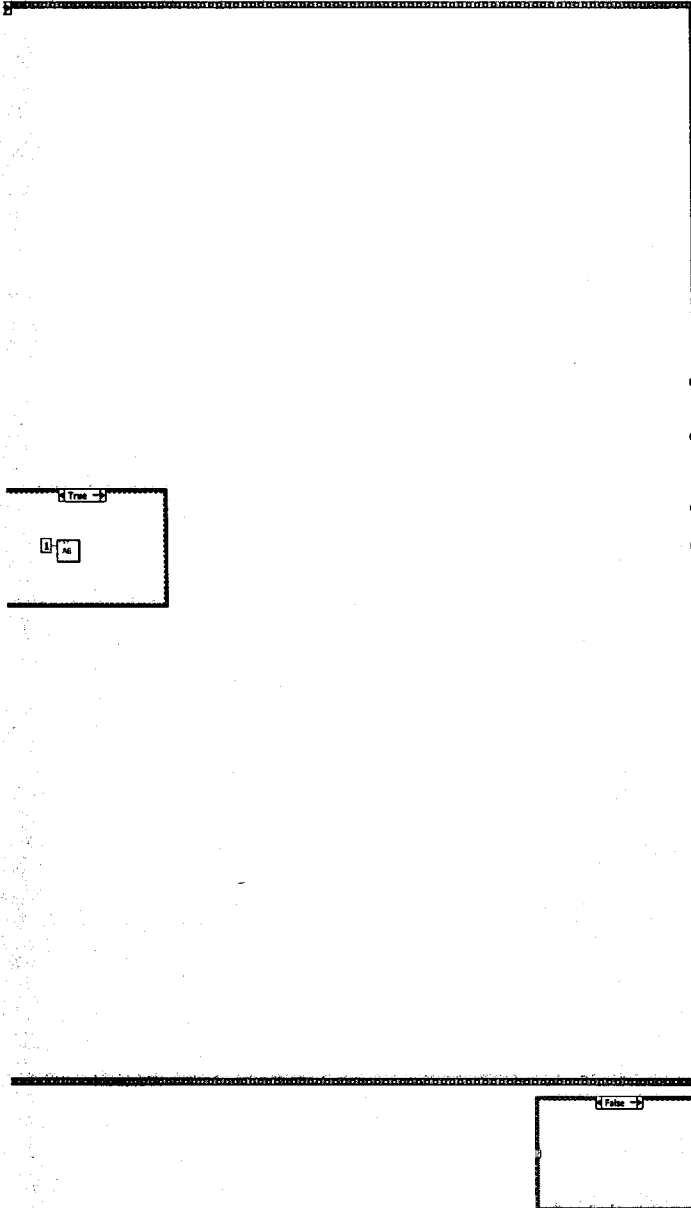


100g load cell long hook2, pause, t-probe, distance, every  
C:\BACKUP\100g load cell long hook2, pause, t-probe,  
distance, every other row, one calibration.vi  
Last modified on 30/01/2005 at 12:20 PM  
Printed on 30/01/2005 at 12:23 PM



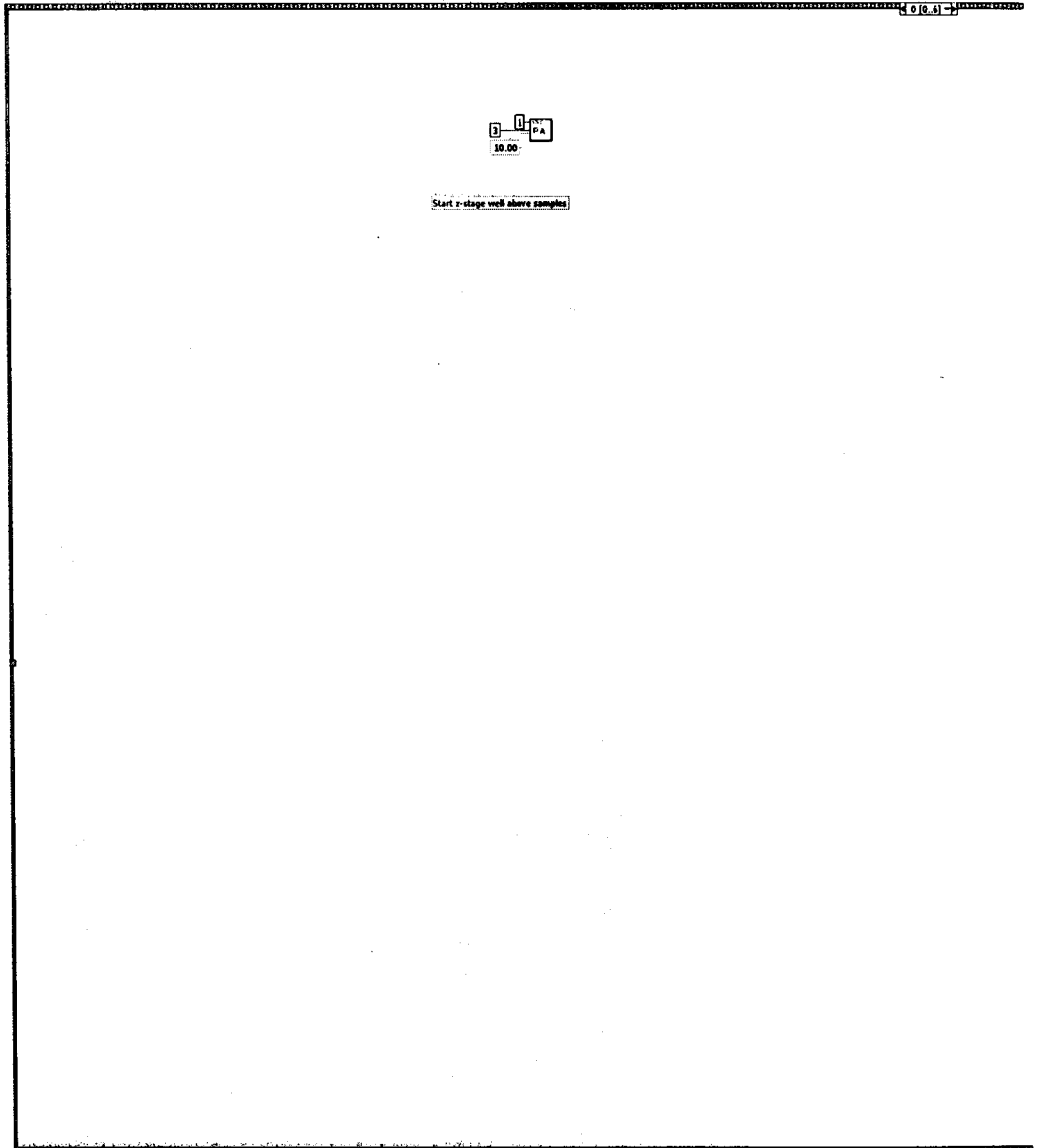


100g load cell long hook2, pause, t-probe, distance, every  
C:\BACKUP\100g load cell long hook2, pause, t-probe,  
distance, every other row, one calibration.vi  
Last modified on 30/01/2005 at 12:20 PM  
Printed on 30/01/2005 at 12:23 PM



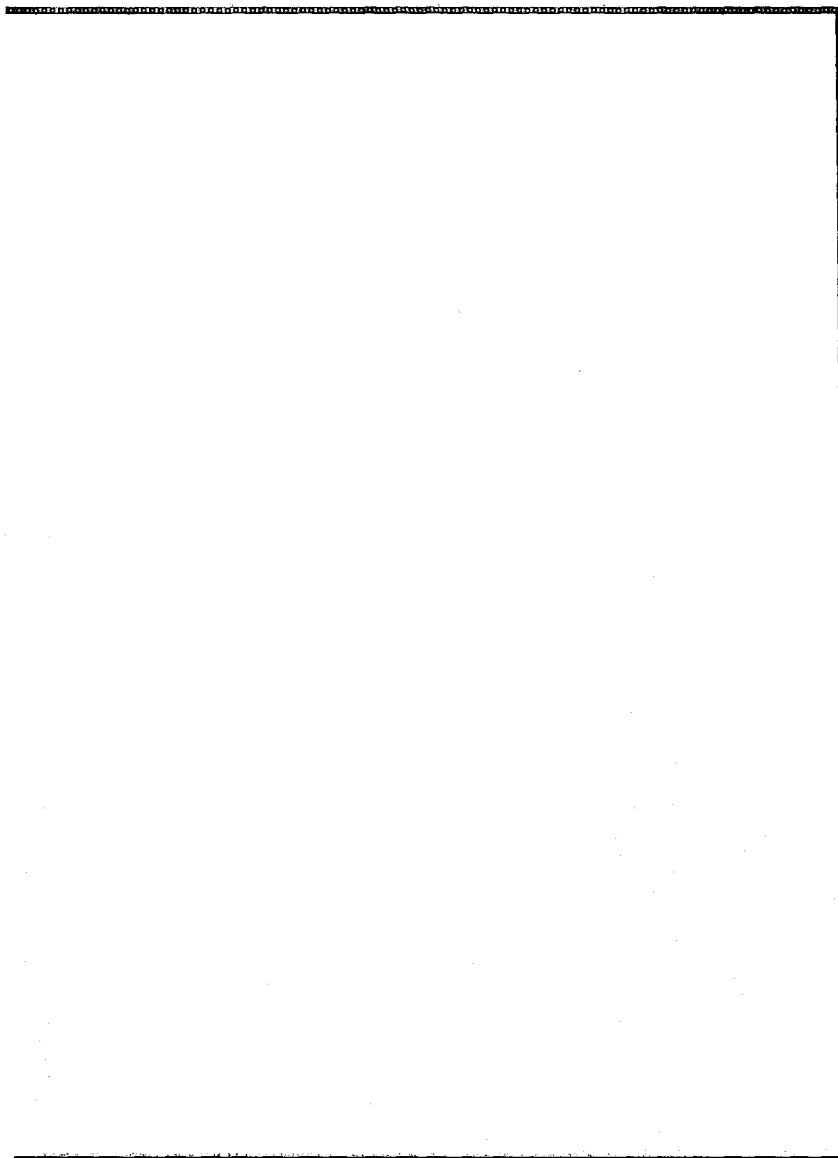


100g load cell long hook2, pause, t-probe, distance, every  
C:\BACKUP\100g load cell long hook2, pause, t-probe,  
distance, every other row, one calibration.vi  
Last modified on 30/01/2005 at 12:20 PM  
Printed on 30/01/2005 at 12:23 PM



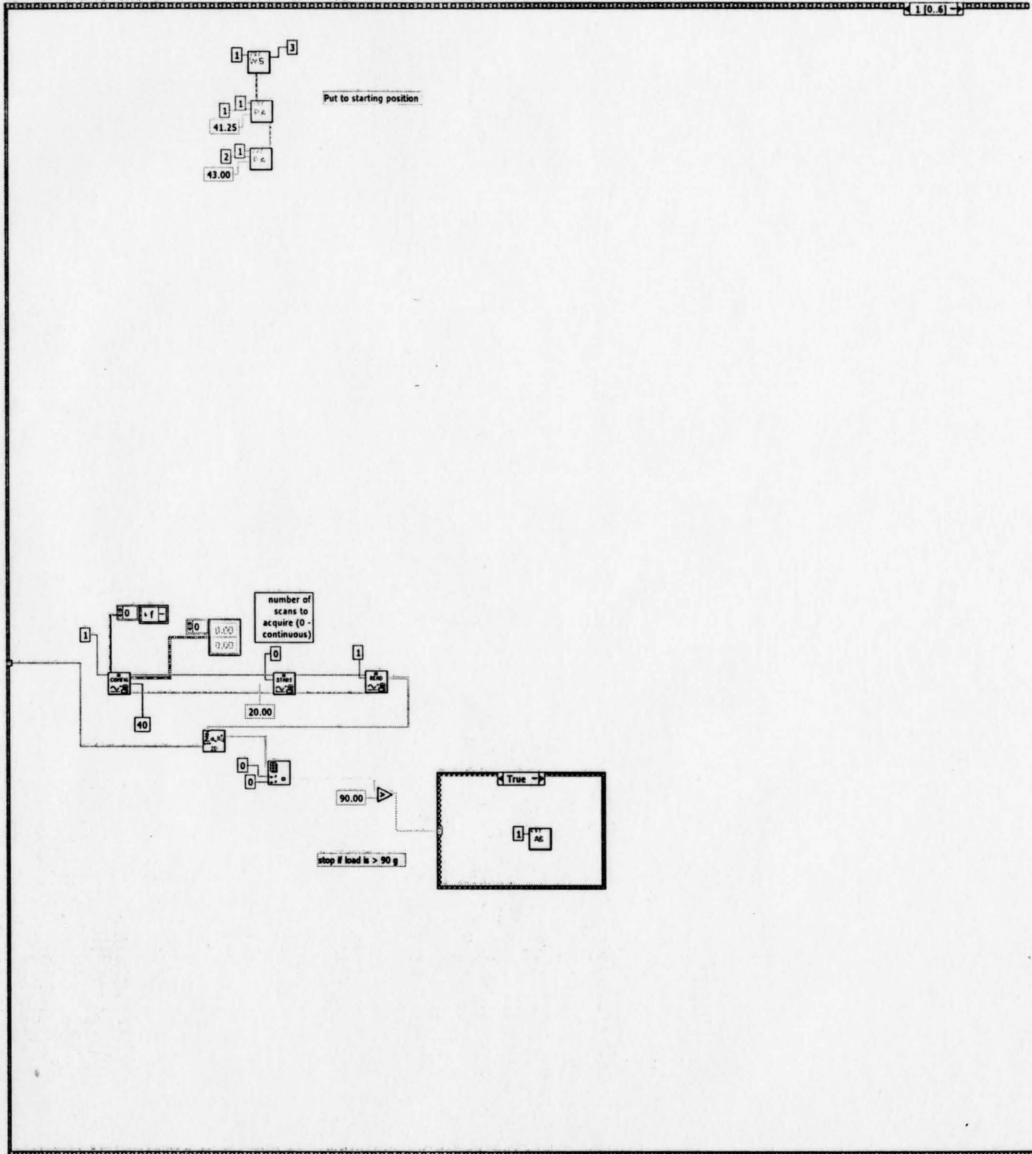


100g load cell long hook2, pause, t-probe, distance, every  
C:\BACKUP\100g load cell long hook2, pause, t-probe,  
distance, every other row, one calibration.vi  
Last modified on 30/01/2005 at 12:20 PM  
Printed on 30/01/2005 at 12:23 PM



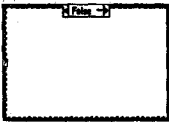
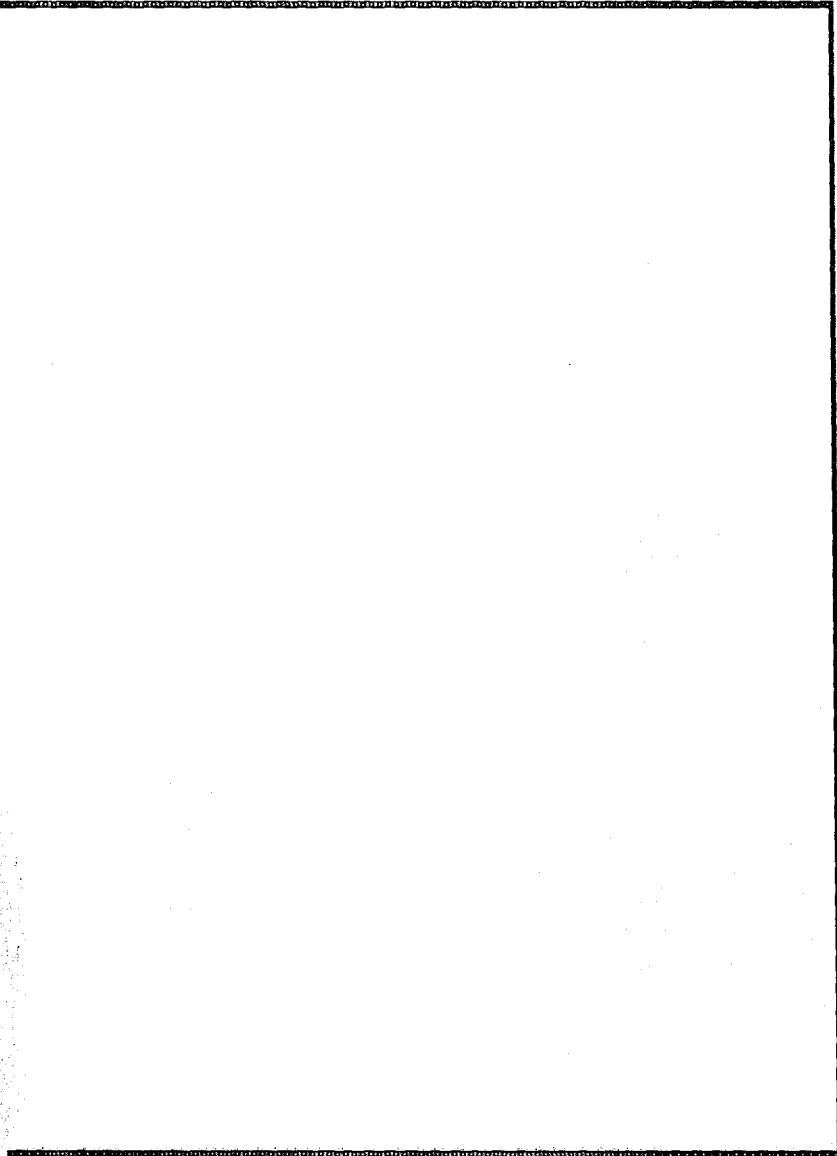


100g load cell long hook2, pause, t-probe, distance, every  
C:\BACKUP\100g load cell long hook2, pause, t-probe,  
distance, every other row, one calibration.vi  
Last modified on 30/01/2005 at 12:20 PM  
Printed on 30/01/2005 at 12:23 PM



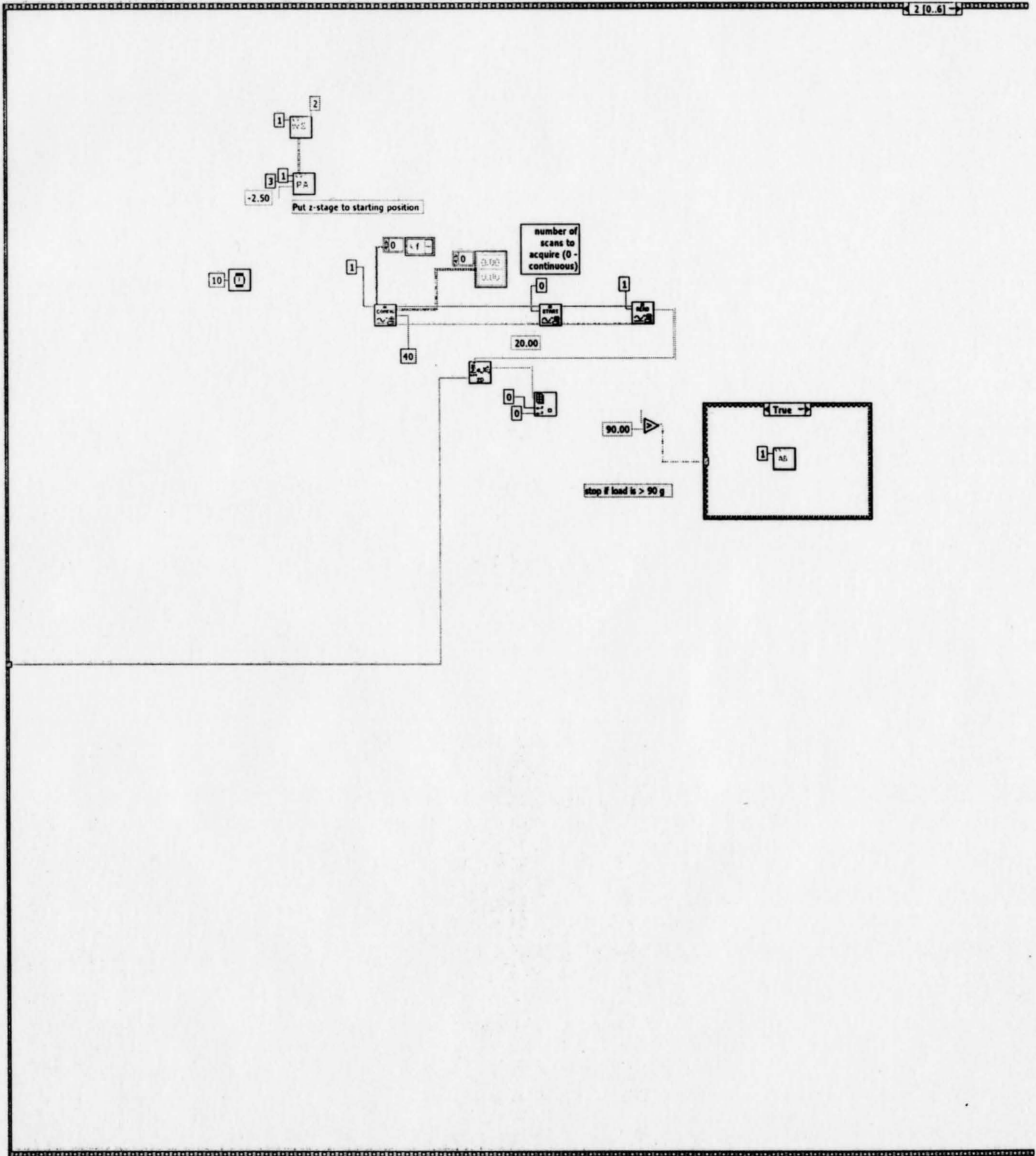


100g load cell long hook2, pause, t-probe, distance, every  
C:\BACKUP\100g load cell long hook2, pause, t-probe,  
distance, every other row, one calibration.vi  
Last modified on 30/01/2005 at 12:20 PM  
Printed on 30/01/2005 at 12:23 PM





100g load cell long hook2, pause, t-probe, distance, every  
C:\BACKUP\100g load cell long hook2, pause, t-probe,  
distance, every other row, one calibration.vi  
Last modified on 30/01/2005 at 12:20 PM  
Printed on 30/01/2005 at 12:23 PM



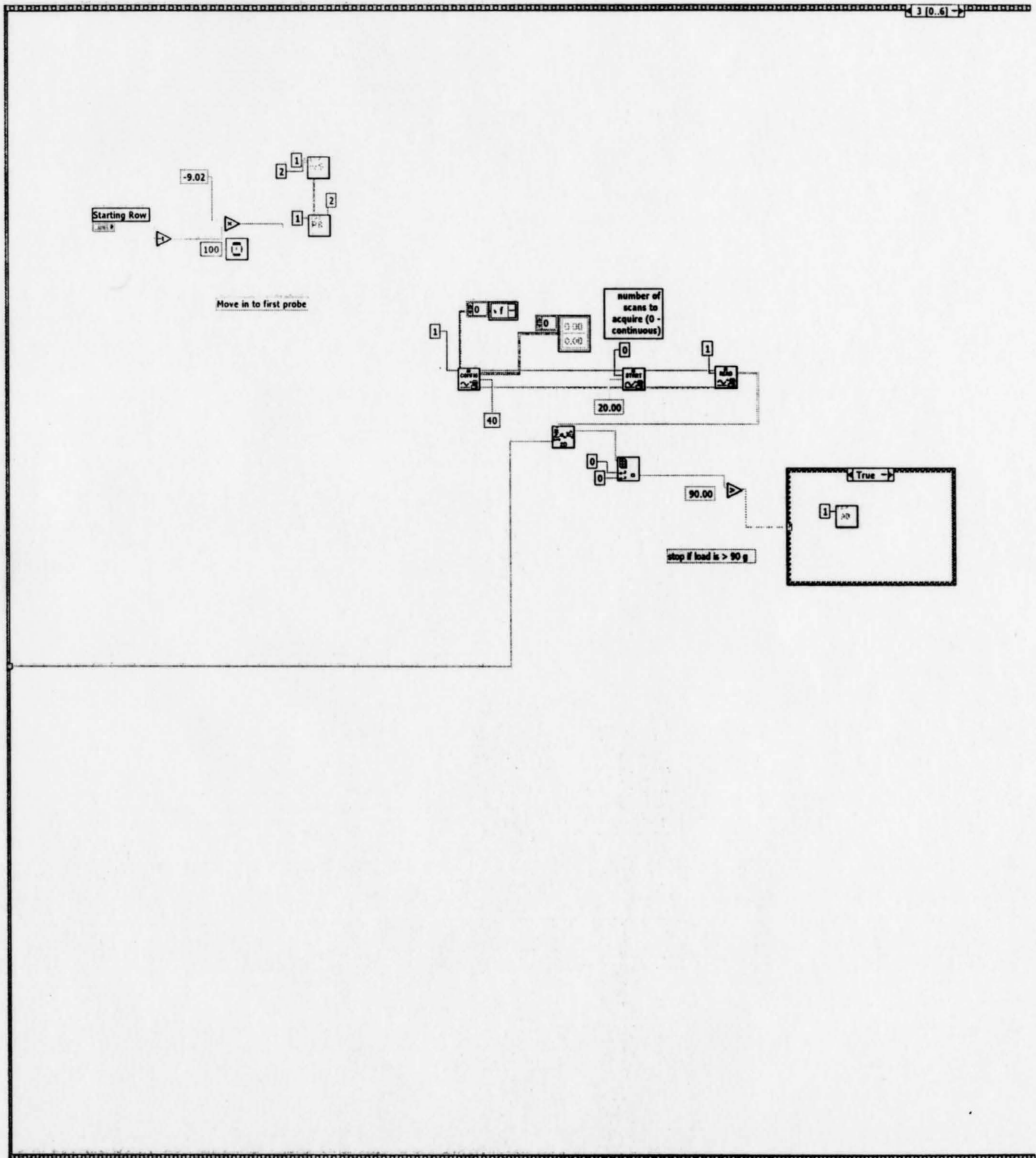


100g load cell long hook2, pause, t-probe, distance, every  
C:\BACKUP\100g load cell long hook2, pause, t-probe,  
distance, every other row, one calibration.vi  
Last modified on 30/01/2005 at 12:20 PM  
Printed on 30/01/2005 at 12:23 PM





100g load cell long hook2, pause, t-probe, distance, every  
C:\BACKUP\100g load cell long hook2, pause, t-probe,  
distance, every other row, one calibration.vi  
Last modified on 30/01/2005 at 12:20 PM  
Printed on 30/01/2005 at 12:23 PM



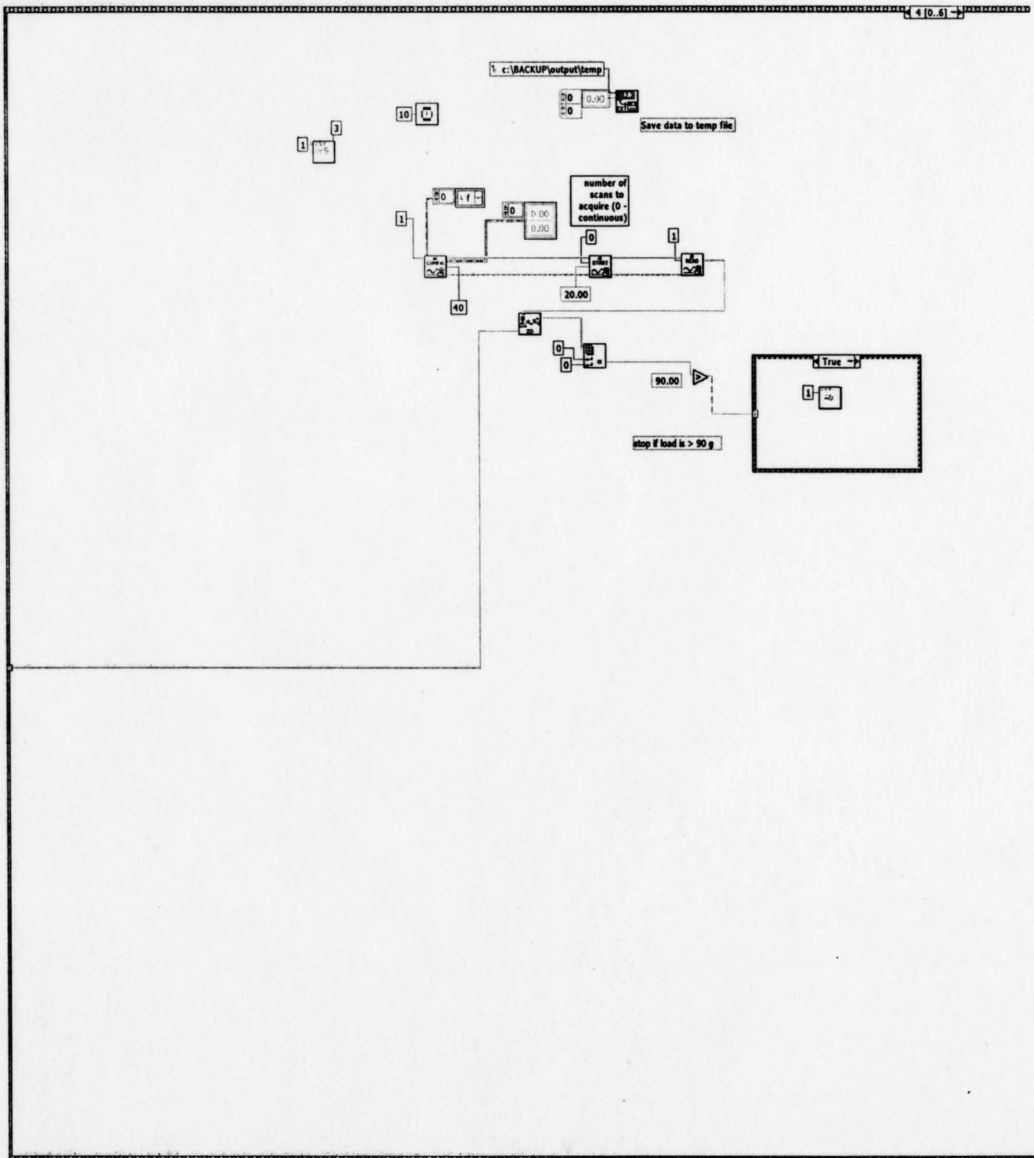


100g load cell long hook2, pause, t-probe, distance, every  
C:\BACKUP\100g load cell long hook2, pause, t-probe,  
distance, every other row, one calibration.vi  
Last modified on 30/01/2005 at 12:20 PM  
Printed on 30/01/2005 at 12:23 PM



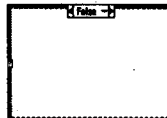


100g load cell long hook2, pause, t-probe, distance, every  
C:\BACKUP\100g load cell long hook2, pause, t-probe,  
distance, every other row, one calibration.vi  
Last modified on 30/01/2005 at 12:20 PM  
Printed on 30/01/2005 at 12:23 PM



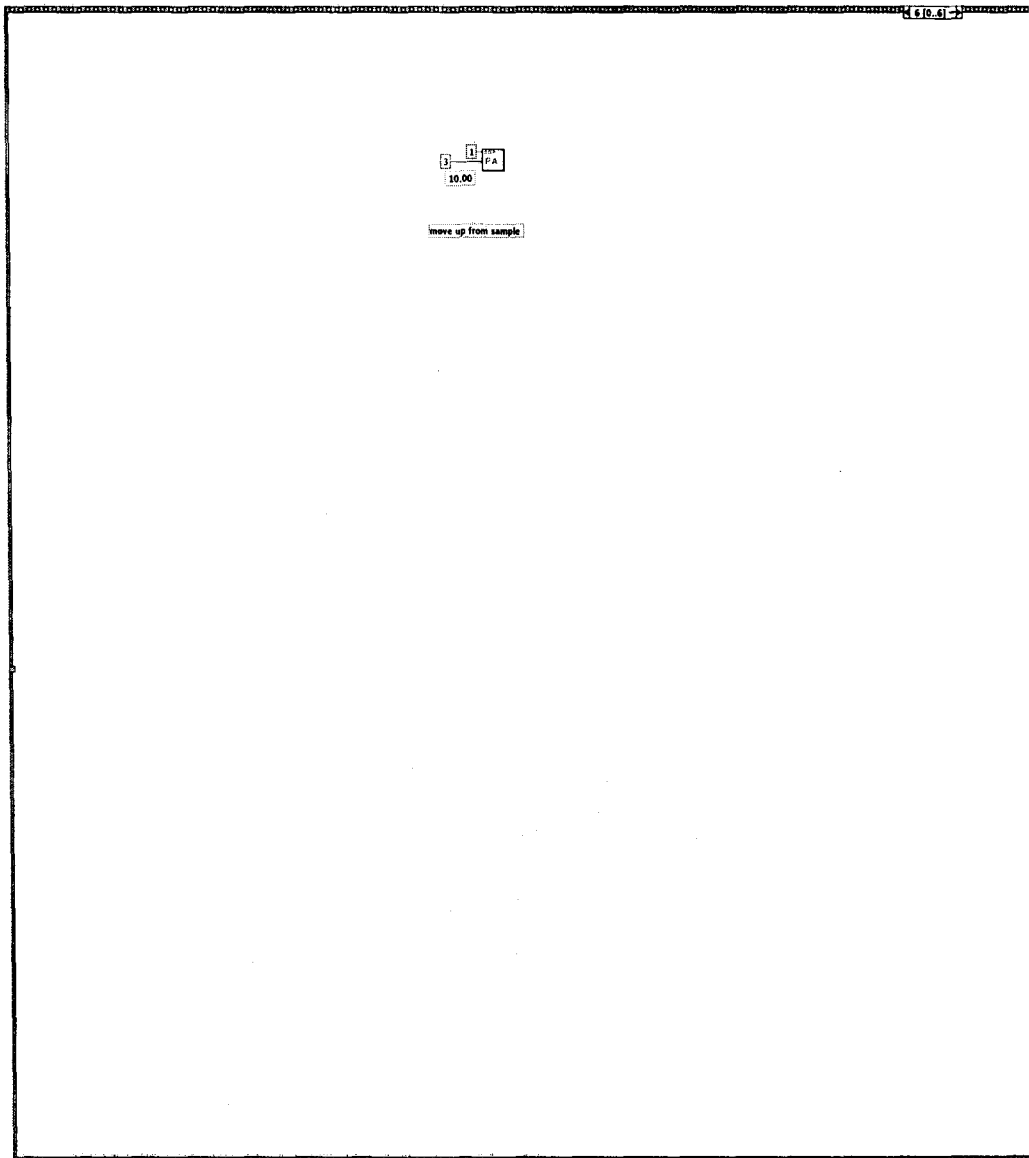


100g load cell long hook2, pause, t-probe, distance, every  
C:\BACKUP\100g load cell long hook2, pause, t-probe,  
distance, every other row, one calibration.vi  
Last modified on 30/01/2005 at 12:20 PM  
Printed on 30/01/2005 at 12:23 PM



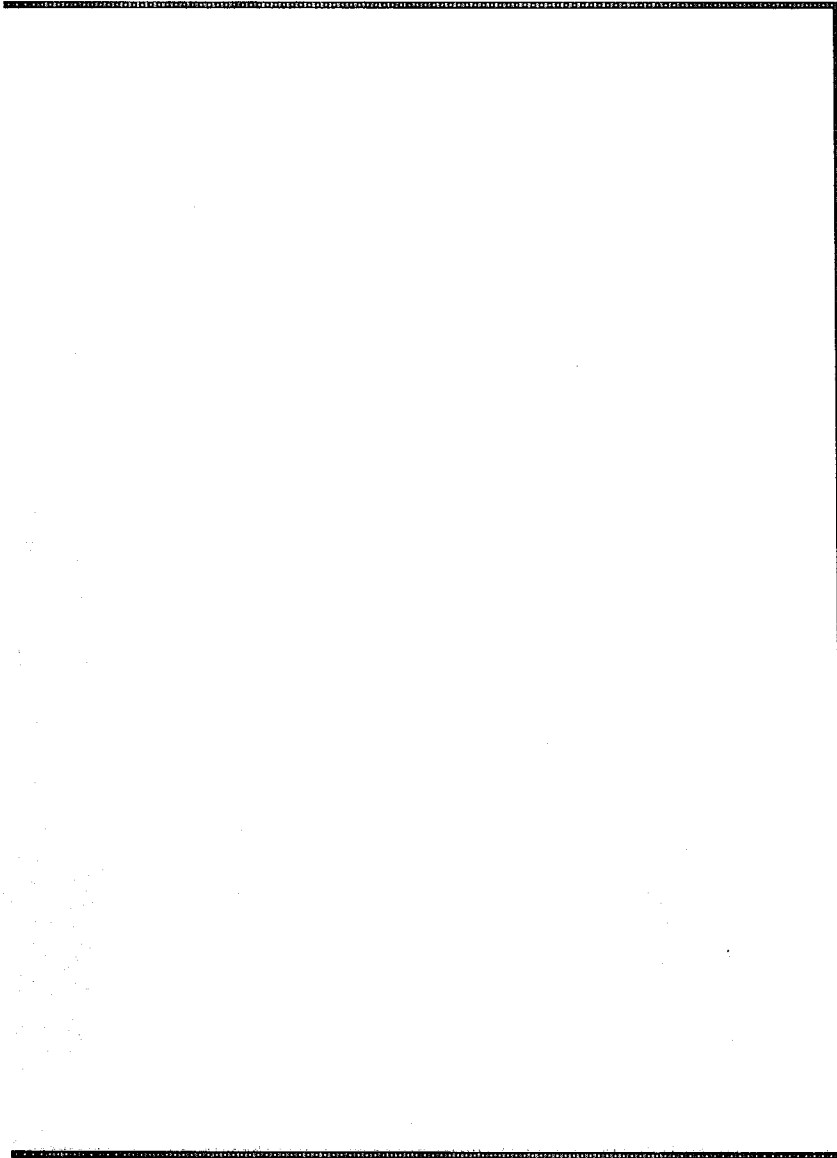


100g load cell long hook2, pause, t-probe, distance, every  
C:\BACKUP\100g load cell long hook2, pause, t-probe,  
distance, every other row, one calibration.vi  
Last modified on 30/01/2005 at 12:20 PM  
Printed on 30/01/2005 at 12:23 PM



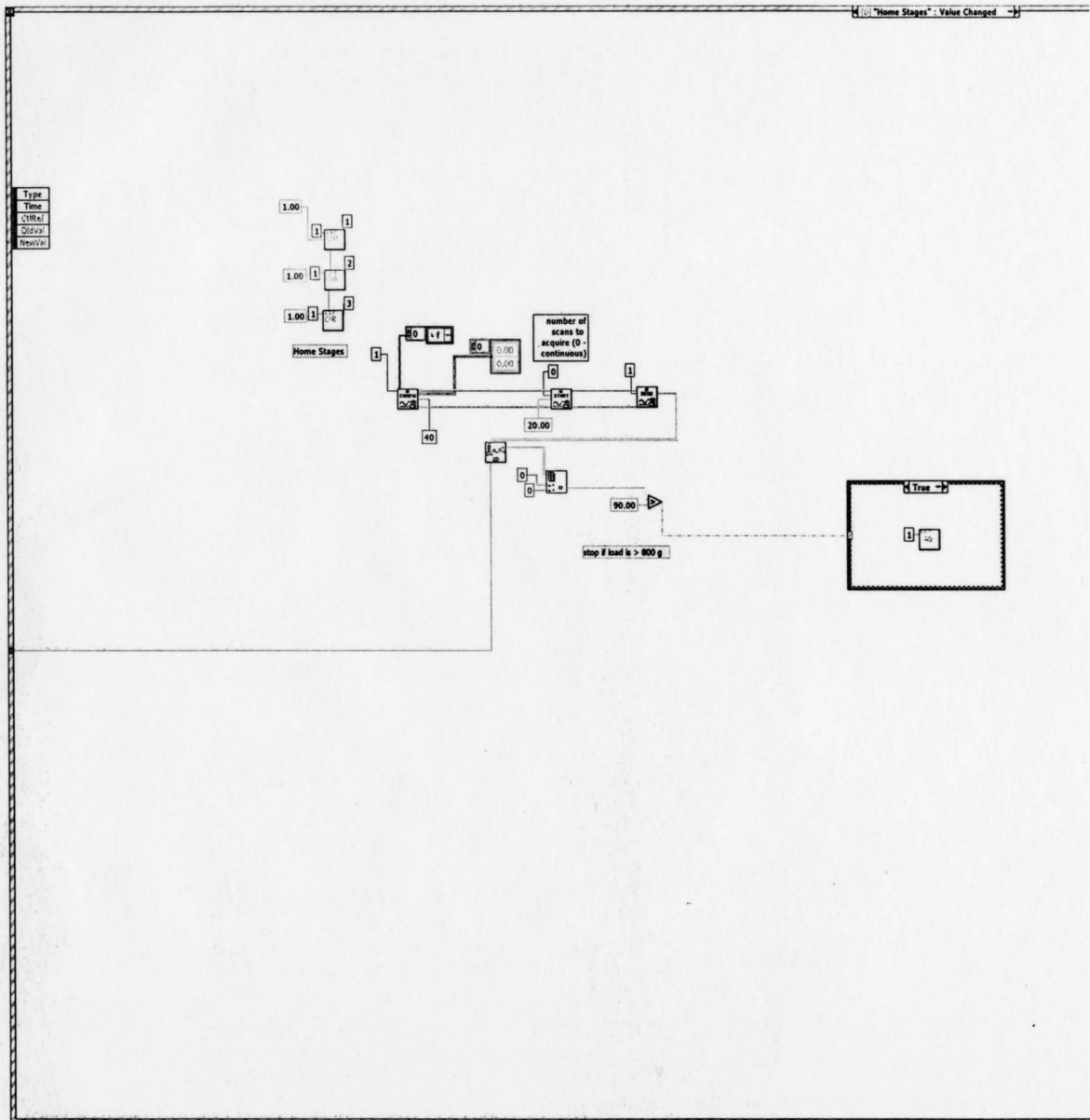


100g load cell long hook2, pause, t-probe, distance, every  
C:\BACKUP\100g load cell long hook2, pause, t-probe,  
distance, every other row, one calibration.vi  
Last modified on 30/01/2005 at 12:20 PM  
Printed on 30/01/2005 at 12:23 PM



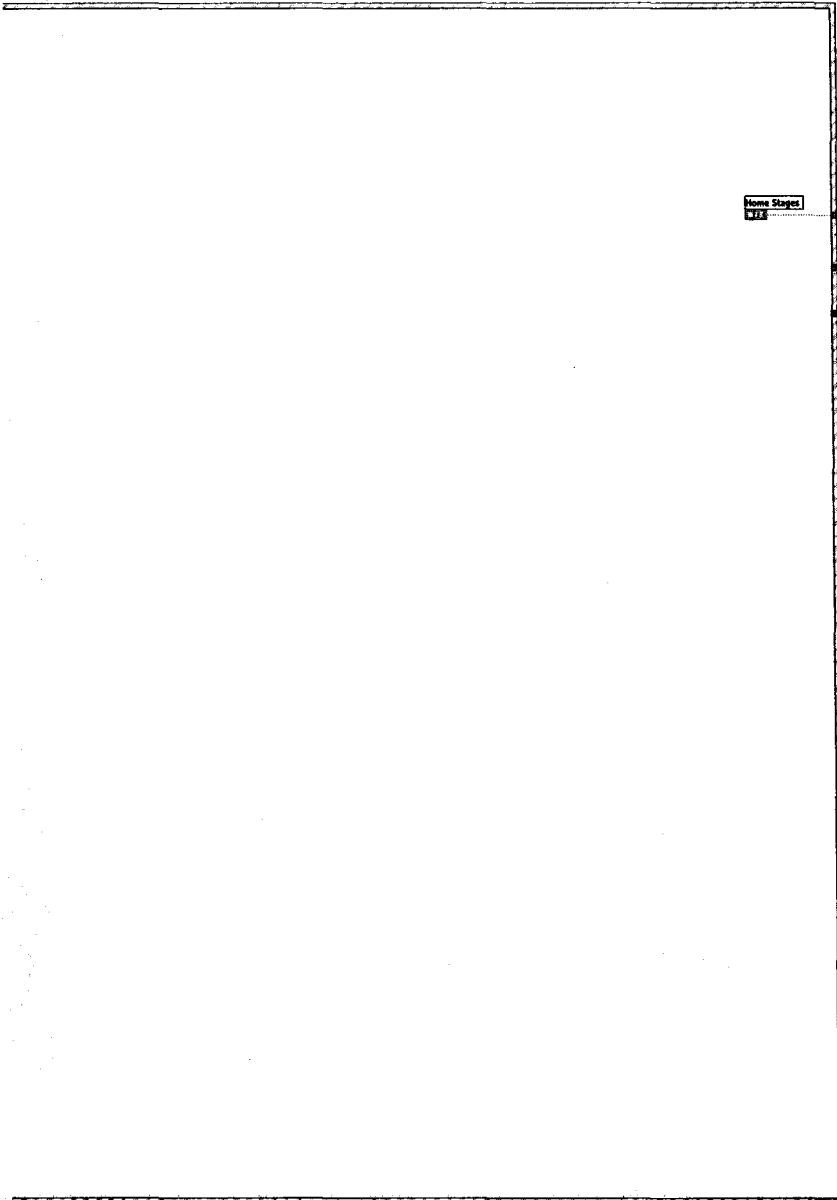


100g load cell long hook2, pause, t-probe, distance, every  
C:\BACKUP\100g load cell long hook2, pause, t-probe,  
distance, every other row, one calibration.vi  
Last modified on 30/01/2005 at 12:20 PM  
Printed on 30/01/2005 at 12:23 PM



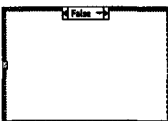


100g load cell long hook2, pause, t-probe, distance, every  
C:\BACKUP\100g load cell long hook2, pause, t-probe,  
distance, every other row, one calibration.vi  
Last modified on 30/01/2005 at 12:20 PM  
Printed on 30/01/2005 at 12:23 PM



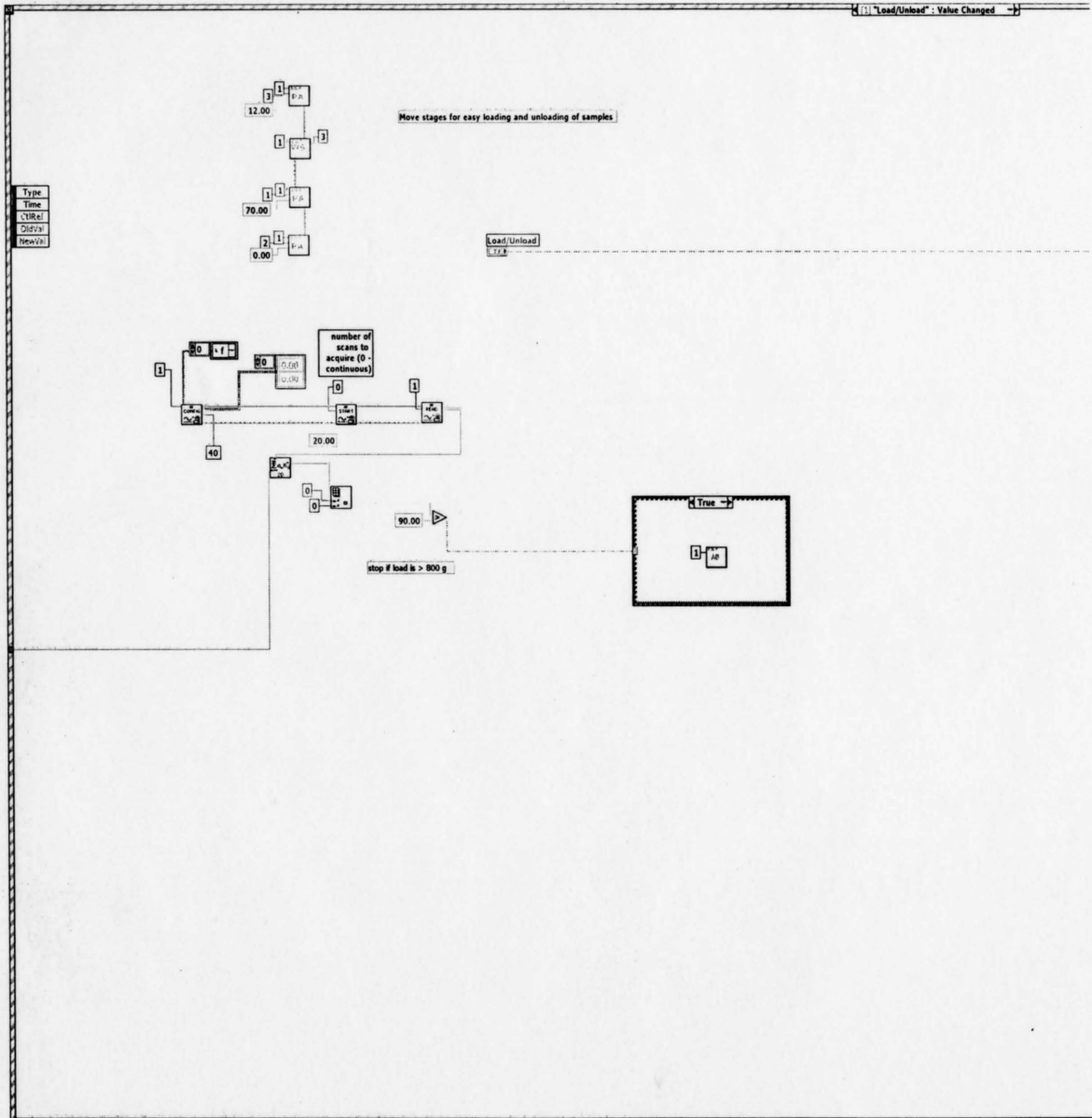
Home Stage  
1/1

False



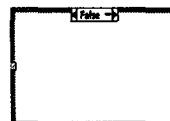
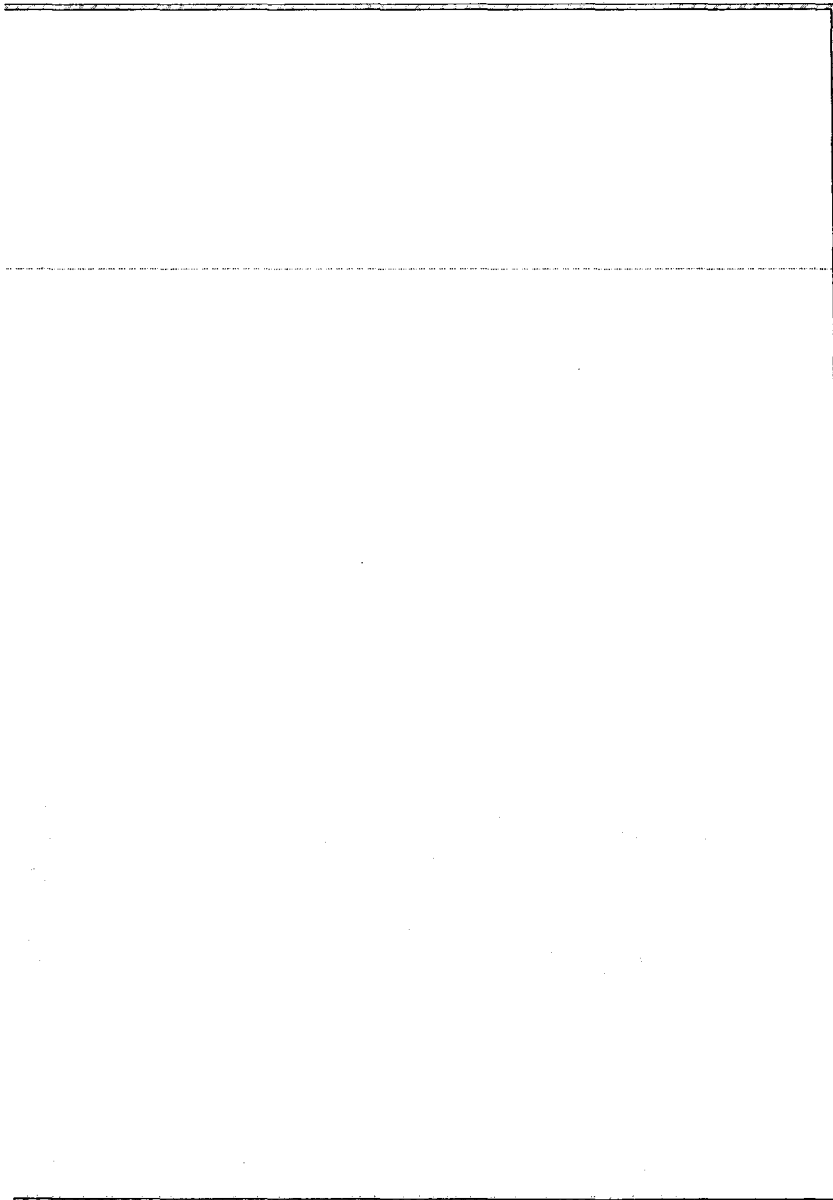


100g load cell long hook2, pause, t-probe, distance, every  
C:\BACKUP\100g load cell long hook2, pause, t-probe,  
distance, every other row, one calibration.vi  
Last modified on 30/01/2005 at 12:20 PM  
Printed on 30/01/2005 at 12:23 PM



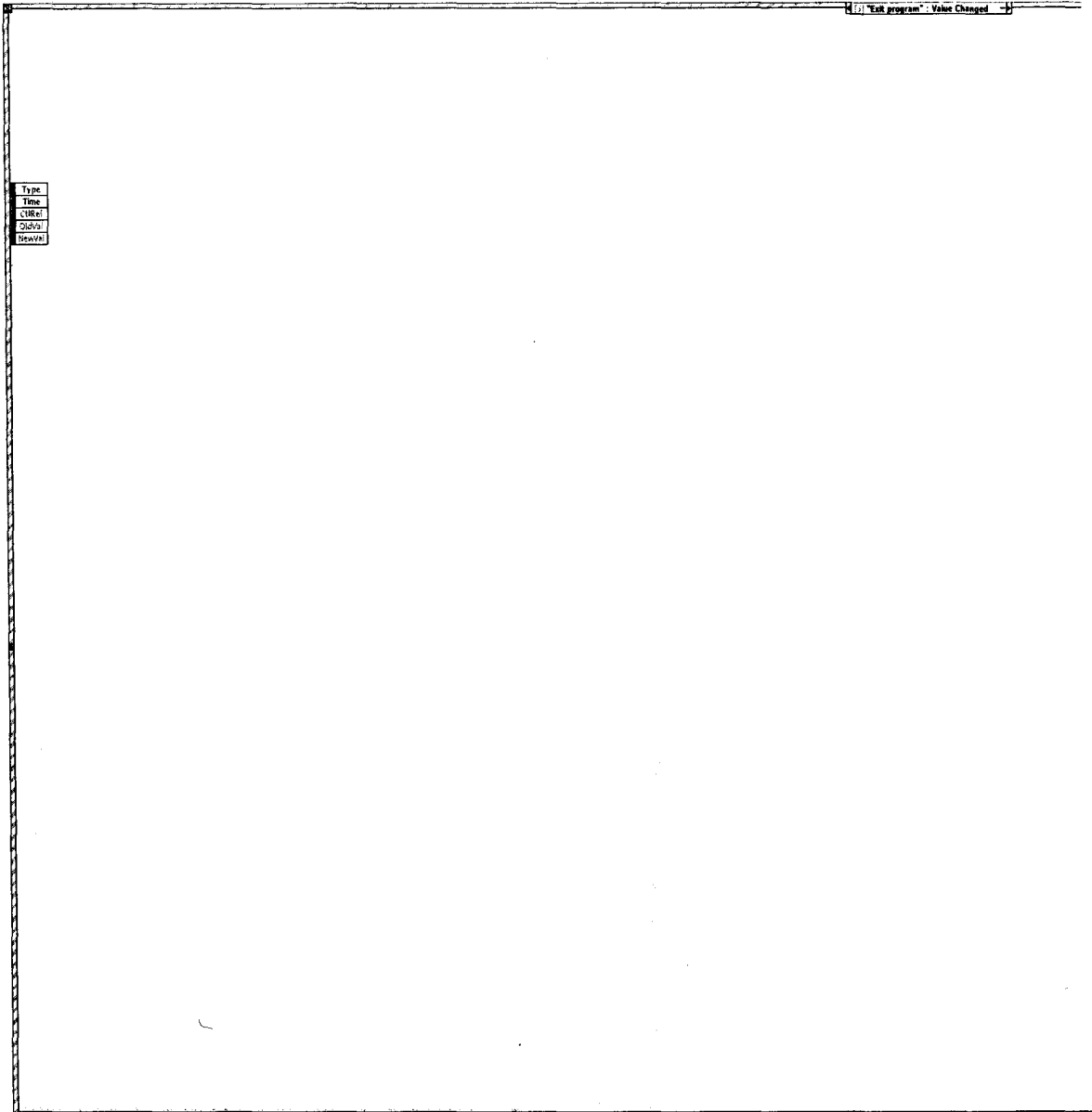


100g load cell long hook2, pause, t-probe, distance, every  
C:\BACKUP\100g load cell long hook2, pause, t-probe,  
distance, every other row, one calibration.vi  
Last modified on 30/01/2005 at 12:20 PM  
Printed on 30/01/2005 at 12:23 PM



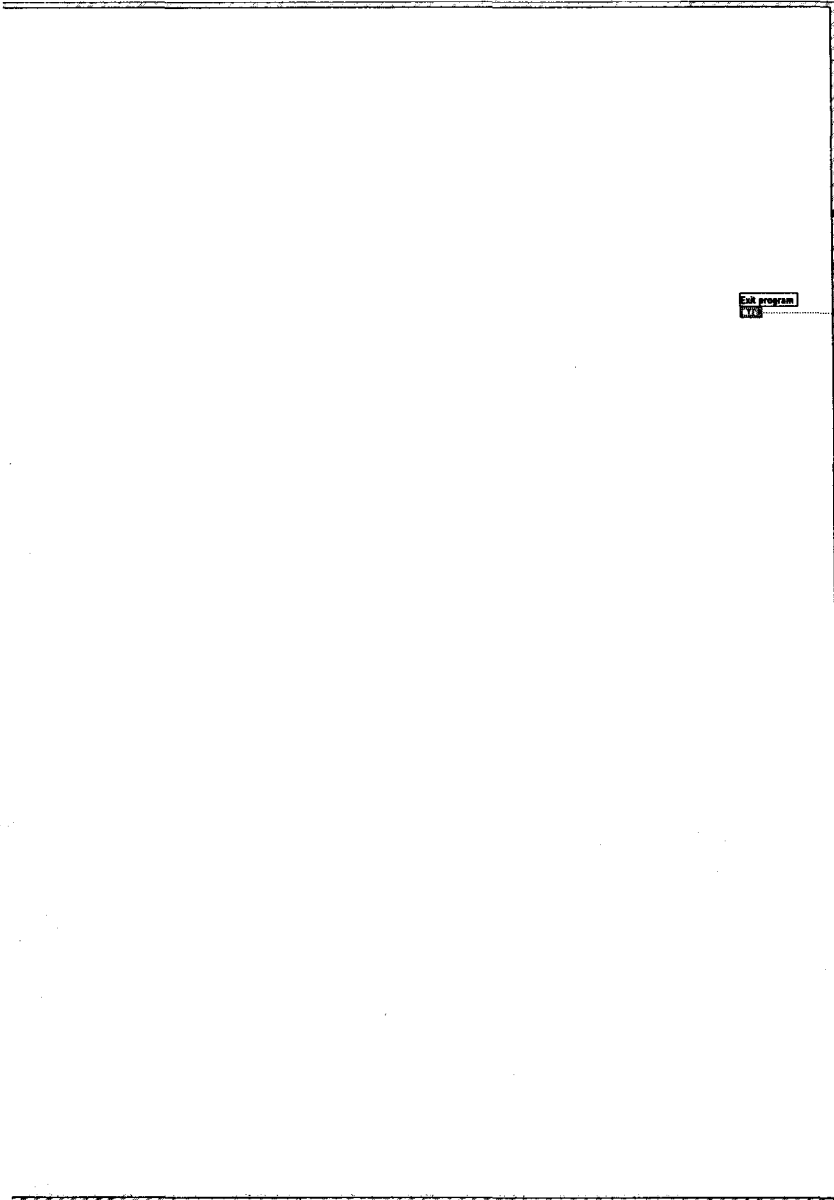


100g load cell long hook2, pause, t-probe, distance, every  
C:\BACKUP\100g load cell long hook2, pause, t-probe,  
distance, every other row, one calibration.vi  
Last modified on 30/01/2005 at 12:20 PM  
Printed on 30/01/2005 at 12:23 PM





100g load cell long hook2, pause, t-probe, distance, every  
C:\BACKUP\100g load cell long hook2, pause, t-probe,  
distance, every other row, one calibration.vi  
Last modified on 30/01/2005 at 12:20 PM  
Printed on 30/01/2005 at 12:23 PM



## **APPENDIX B.1 – Probes**

Throughout the course of these experiments the probes went through a number of transformations shown in Figure B.1.1 to Figure B.1.8. The first probes were constructed out of 5mm glass beads and a plastic tab (Figure B.1.1). The second probes were simply the glass beads on their own (Figure B.1.2). Probe #3 was made by a glass blower at McMaster University by cutting a 5mm diameter glass dowel into 5cm segments and rounding the ends (Figure B.1.3). Probe #4 was constructed by taking the glass rods and gluing a wire loop to one end (Figure B.1.4). Probe #5 was made by taking a 1.75mm diameter capillary tube with one closed end and bending the other end to make a hook (Figure B.1.5). Probe #6 was made by again taking the glass rods, but this time gluing two pieces of wire with eye loops at the end to the top, and then connecting them with a piece of suture string (Figure B.1.6). Probe #7 was made by taking a capillary tube and gluing onto it a small 5mm section perpendicular to the tube (Figure B.1.7). Finally, probe #8 was the last and current form. It was made by taking a capillary tube and gluing a flat head to the top (Figure B.1.8).

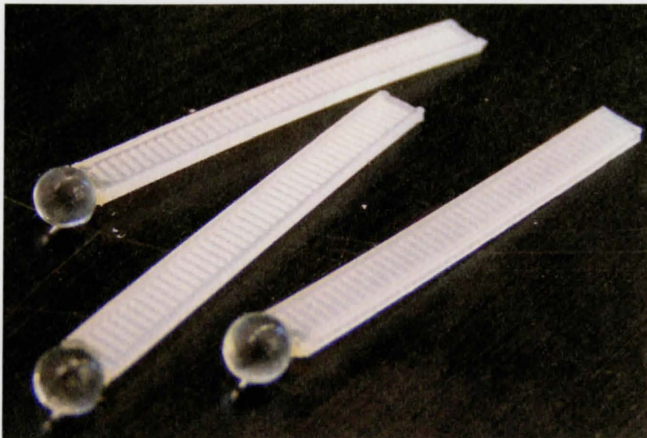


**Figure B.1.1 – Probe #1 – The first probes. They were made using a 5mm diameter glass bead with a plastic tab glued onto them**



**Figure B.1.2 – Probe #2 – The 5mm glass beads on their own**



**Figure B.1.3 – Probe #3. 5mm diameter glass rods with a rounded tip**

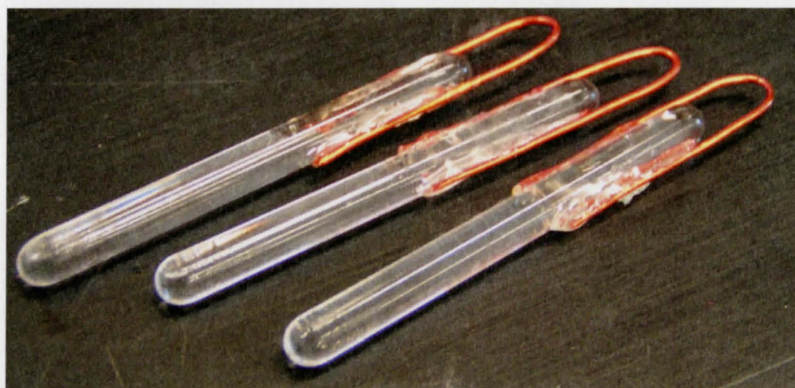


**Figure B.1.4 – Probe #4. 5mm diameter glass rods with a rounded tip and a wire loop glued to the top**

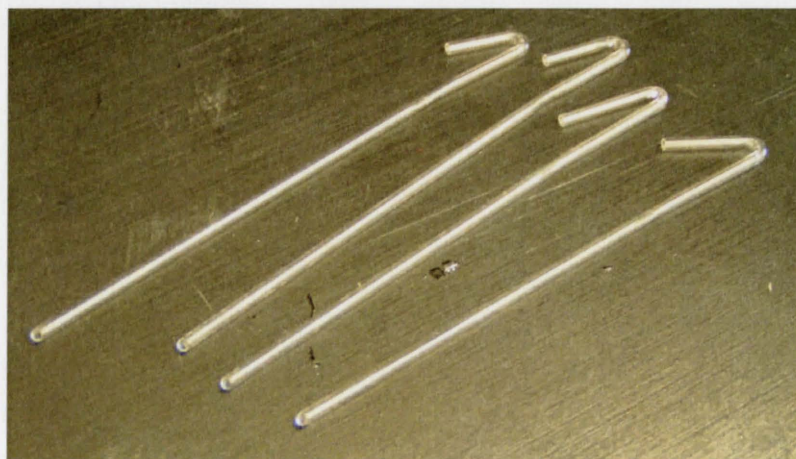


**Figure B.1.5 – Probe #5. 1.75mm diameter capillary tubes with one closed end and the other end bent to form a hook**



**Figure B.1.6 – Probe #6. 5mm diameter glass rods with a rounded tip and suture string tied across the top**

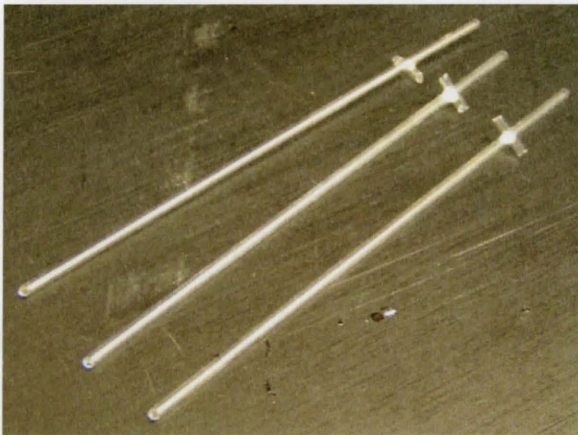


**Figure B.1.7 – Probe #7. Capillary tube with a small piece of glass glued perpendicular to the tube in a 't' shape.**



**Figure B.1.8 – Probe #8. The final form of the probe. A capillary tube with a flat head glued to the top for easy lifting**

## APPENDIX B.2 – Hooks

The hooks changed as the probes changed in order to best lift the probes. Probes number 1 and 3 did not require a separate hook, but used the clamp on the Instron (Figure B.2.1 and Figure B.2.2). After moving off of the Instron to the constructed adhesion tester, probes number 4, 5 and 6 used a simple hook (Figure B.2.3). Probe number 7 required a hook that could lift equally on both sides, so a fork shaped hook was made (Figure B.2.4). Finally, a fork-type hook was machined for use with the final probes (Figure B.2.5).

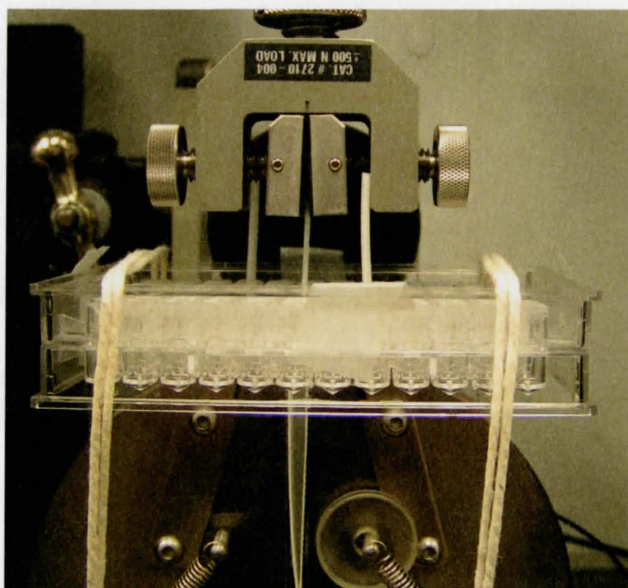


Figure B.2.1 – The first set-up on the Instron. Probe #1 is placed in the well and the clamp on the Instron is used to pull it out

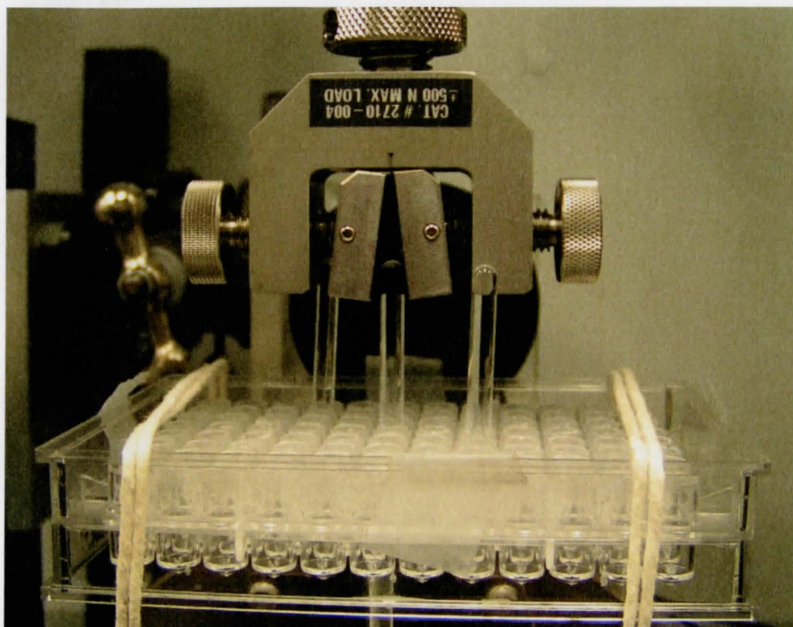


Figure B.2.2 – Probe #3 also utilized the existing clamp for the experiment

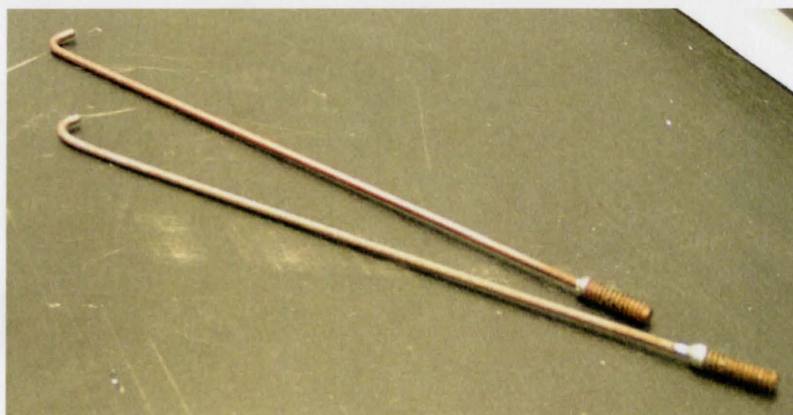


Figure B.2.3 – A hook used to perpendicularly lift probes # 4, 5 and 6.



Figure B.2.4 – The fork shaped hook used for probe #7.



**Figure B.2.5 – The final form of the probe lifter**